UNIVERSITY OF BELGRADE

FACULTY OF MEDICINE

Aleksa M. Janović

MICROSTRUCTURAL ADAPTATION
OF BONE TISSUE
OF THE FACIAL SKELETON
TO THE DISTRIBUTION
OF OCCLUSAL LOAD
IN DENTULOUS SUBJECTS
AND ITS ROLE IN THE DEVELOPMENT
OF THE FACIAL FRACTURES

Doctoral Dissertation

Belgrade, 2014

УНИВЕРЗИТЕТ У БЕОГРАДУ

МЕДИЦИНСКИ ФАКУЛТЕТ

Алекса М. Јановић

МИКРОСТРУКТУРНА АДАПТАЦИЈА КОШТАНОГ ТКИВА ФАЦИЈАЛНОГ СКЕЛЕТА НА ДИСТРИБУЦИЈУ ОКЛУЗАЛНОГ ОПТЕРЕЋЕЊА КОД ОСОБА СА ПУНИМ ЗУБНИМ НИЗОМ И ЊЕНА УЛОГА У НАСТАНКУ ПРЕЛОМА ФАЦИЈАЛНОГ СКЕЛЕТА

докторска дисертација

Београд, 2014

PhD advisor:

Professor Dr. Marija Đurić

University of Belgrade – Faculty of Medicine

Members of the evaluation committee:

1. Prof. Dr. Slobodan Nikolić, University of Belgrade – Faculty of Medicine

2. Prof. Dr. Milovan Dimitrijević, University of Belgrade – Faculty of Medicine

3. Prof. Dr. Nenad Filipović, University of Kragujevac – Faculty of Mechanical Engineering

Date of public presentation: _____

Ментор:

Професор др Марија Ђурић

Универзитет у Београду – Медицински факултет

Чланови комисије за оцену и одбрану докторске дисертације:

1. професор др Слободан Николић, Универзитет у Београду – Медицински факултет – председник комисије

2. професор др Милован Димитријевић, Универзитет у Београду – Медицински факултет

3. професор др Ненад Филиповић, Универзитет у Крагујевцу – Факултет инжењерских наука

Датум јавне одбране дисертације: _____

Title of the doctoral dissertation:

MICROSTRUCTURAL ADAPTATION OF BONE TISSUE OF THE FACIAL SKELETON TO THE DISTRIBUTION OF OCCLUSAL LOAD IN DENTULOUS SUBJECTS AND ITS ROLE IN THE DEVELOPMENT OF THE FACIAL FRACTURES

Summary

Background

Occlusal forces have traditionally been explained to transfer through the facial skeleton along specific osseous trajectories known as buttresses. These regions were assumed as zones of strength due to their thick cortical bone structure, while the areas between the buttresses containing thin cortical bone were considered weak and fragile. However, recent studies revealed that both cortical and trabecular bone of the mid-facial skeleton of dentulous individuals exhibit remarkable regional variations in structure and elastic properties. These variations have been frequently suggested to result from the different involvement of cortical and trabecular bone in the transfer of occlusal forces, although there has been no study to link bone microarchitecture to the occlusal loading. Moreover, although the classical concept of buttresses has been extensively studied by mechanical methods, such as finite element (FE) analysis, there is still no direct evidence for occlusal load distribution through the cortical and trabecular bone compartments individually. Additionally, relatively less scientific attention has been paid to the investigation of bone structure along Le Fort fracture lines that have traditionally been assumed as weak areas at which the mid-facial skeleton commonly fractures after injury. Papers published so far in this field focused mainly on the epidemiology and the role of injury mechanism in the fracture development, without considering the structural basis of increased bone fragility along the Le Fort fracture lines.

Hypotheses

Our hypotheses were the following:

- both cortical and trabecular bone participate in the occlusal load distribution through the mid-facial skeleton,

- certain bone areas in both osseous compartments are subjected to higher occlusal loading than others,

- both compact and trabecular bone exhibit regional variations in microarchitecture as a result of different occlusal loads to which they are subjected during mastication,

- increased bone fragility along Le Fort fracture lines is due to weak cortical and trabecular bone microarchitecture in biomechanical terms.

Material and methods

In order to investigate the mechanical behavior of the mid-facial skeleton during mastication, we developed a three-dimensional computer model of a young adult male skull from images obtained by computed tomography. The model included: compact bone, trabecular bone, teeth, all hollow structures within the mid-facial skeleton, and jaw-closing muscles. Biting and clenching were simulated on the model using finite element method, and effective Von Mises stress (VMS), compressive and tensile component of principal stress, and displacement were analyzed. These stresses were also measured at the specific points in cortical and trabecular bone of the model along and between the buttresses. Stresses measured in the cortical bone were compared with the results of a recently published study from Prado et al. (2013), who simulated mastication on a similar skull model composed only of cortical bone.

Bone specimens were detached from the corresponding sites on the same dry skull and their microarchitecture was analyzed by micro-computed tomography. For the investigation of bone microarchitecture in relation to the occlusal stress, bone specimens were classified into high stress or low stress group based on the magnitude of VMS experienced during mastication. Further, we analyzed bone microarchitecture in relation to the Le Fort fracture lines, namely, in bone specimens detached from these lines vs. bone specimens located away from the fracture lines.

Results and conclusions

Simulation of masticatory activities in this study showed that both cortical and trabecular bone participate in the distribution of occlusal forces. In the cortical bone, occlusal forces distributed along five vertical (pared nasomaxillary, pared zygomaticomaxillary buttress, nasal septum) and two horizontal (frontal, zygomatic) buttresses, with the highest stress and displacement registered along the nasomaxillary buttress. We also observed that trabecular bone in the anterior maxilla was under significantly lower stress when compared to the cortical bone, whereas both osseous compartments in the posterior maxilla showed similar stress. This finding indicates that cortical bone has a priority in the distribution of occlusal loads through the anterior maxilla, while both cortical and trabecular bone in the posterior maxilla are equally involved in performing this task.

Comparative analysis of stress registered in our model and in the model of Prado et al. (2013) showed similar distribution of VMSs through the cortical bone, but with much lower values registered in our model. Significant differences were detected in the distribution and the magnitude of the principal stresses. Concerning that the model of Prado et al. (2013) was composed only of cortical bone, our findings suggest that FE analysis of stress may be significantly affected if the skull is modeled without trabecular bone.

Our results of bone microstructural analysis clearly demonstrated that the mid-facial skeleton in the investigated skull exhibits regional variations in cortical and trabecular bone microarchitecture that could be a consequence of an adaptation process to different occlusal stress.

Cortical bone microarchitecture in the regions subjected to high occlusal stress showed a tendency toward greater thickness and density, lower porosity, and greater pore separation. Correlation analysis between microarchitectural parameters revealed that an increase in cortical thickness is accompanied by a significant increase in bone volume tissue density and pore separation. Additionally, the analysis also indicated that an increase in cortical porosity in the mid-facial skeleton is based on the pore enlargement.

More pronounced differences in bone microarchitecture between the groups were detected in trabecular bone, which had significantly greater bone volume fraction

(BV/TV), trabecular thickness (Tb.Th), and tissue volume density (TV.Dn) in the high stress group. Considering that trabecular bone BV/TV and Tb.Th are usually the first to change during the alteration of loading, our results support their high sensitivity to the changes in occlusal stress. Additionally, correlation analysis revealed that trabecular bone significantly increases its BV/TV and TV.Dn in response to increased VMS and compressive stress, which could reflect a possible mechanism of facial bone adaptation to increased occlusal loading.

Only slight differences in cortical and trabecular bone microarchitecture were found between the sites of Le Fort fractures and other parts of the mid-facial skeleton. Namely, bone along Le Fort fracture lines showed tendency toward thinner and more porous cortical bone with larger pores, while trabeculae at the same sites had different shape and connectivity density that were not statistically significant. We detected significantly higher degree of anisotropy of trabecular bone at the Le Fort lines, which indicates that trabeculae are orientated in the direction of the habitual loading, e.g. occlusal forces. Given that such trabecular network is able to withstand forces resulting from mastication, it may be less resistant to unusual loads such as horizontally directed mechanical forces. Regardless of this finding, there was no clear evidence of weaker bone microarchitecture in biomechanical terms in the mid-facial skeleton along Le Fort fracture lines.

Keywords: bone, mid-facial skeleton, buttresses, microarchitecture, finite element analysis, occlusal loading, Le Fort fracture.

Scientific field: Medicine
Specific scientific field: Skeletal biology

Наслов докторске дисертације:

МИКРОСТРУКТУРНА АДАПТАЦИЈА КОШТАНОГ ТКИВА ФАЦИЈАЛНОГ СКЕЛЕТА НА ДИСТРИБУЦИЈУ ОКЛУЗАЛНОГ ОПТЕРЕЋЕЊА КОД ОСОБА СА ПУНИМ ЗУБНИМ НИЗОМ И ЊЕНА УЛОГА У НАСТАНКУ ПРЕЛОМА ФАЦИЈАЛНОГ СКЕЛЕТА

Резиме

Увод

      Према традиционалном објашњењу, пренос оклузалног оптерећења кроз кости лица током жвакања обавља се дуж специфичних путања унутар кости званих трајекторије или „батреси". Ови делови костију лица сматрани су јаким зонама јер их изграђује кортикална кост велике дебљине, док су делови кости смештени између трајекторија сматрани слабим и фрагилним због њихове танке кортикалне грађе. Међутим, недавним истраживањима је откривено да и кортикална и трабекуларна кост средњег масива лица код особа са пуним зубним низом показују значајне регионалне варијације у грађи и еластичним својствима. Ове се варијације често сматрају адаптацијом кортикалне и трабекуларне кости на различито оптерећење у преносу оклузалних сила током жвакања, иако повезаност микроархитектуре кости и оклузалног оптерећења до сада није испитивана код људи. Штавише, иако је класични концепт преноса оклузалног оптерећења дуж трајекторија интензивно проучаван механичким методама, као што је метод коначних елемената, још увек није испитано на који начин се оклузалне силе преносе појединачно кроз кортикалну и трабекуларну кост. Значајно мању научну пажњу је привлачило испитивање грађе костију лица дуж Le Fort линија које су традиционално сматране најчешћим местима прелома костију фацијалног скелета узрокованих механичким силама. Досадашње студије у овој области су биле фокусиране углавном на епидемиолошка истраживања и улогу механизма повреде у настанку ових прелома, док структурна основа повећане фрагилности кости дуж Le Fort линија није испитивана.

Хипотезе

Наше хипотезе су биле:

- да и кортикална и трабекуларна кост фацијалног скелета учествују у преносу оклузалних сила током жвакања,

- да и кортикална и трабекуларна кост у одређеним деловима фацијалног скелета трпе веће оптерећење током жвакања у односу на друге регионе,

- да кортикална и трабекуларна кост показују регионалне варијације у микроархитектури које су последица њихове адаптације на различито оклузално оптерећење током жвакања, и

- да лоша микроархитектура кости у биомеханичком смислу доприноси повећаној фрагилности фацијалног скелета дуж Le Fort линија.

Материјал и методе

У циљу испитивања механичког понашања костију средњег масива лица током жвакања, направљен је тродимензионални компјутерски модел лобање млађе одрасле особе мушког пола на основу снимака начињених апаратом за компјутеризовану томографију. Модел је садржао: кортикалну кост, трабекуларну кост, зубе, све шупљине унутар костију средњег масива лица, и мишиће за жвакање. На моделу је симулиран процес грижења и стискања зуба методом коначних елемената (finite element method) и анализирани су ефективни (von Mises) напони, компресивна и затезна компонента главних напона, и померања унутар модела. Наведени напони су мерени у моделу на одређеним местима у кортикалној и трабекуларној кости, дуж трајекторија и између њих. Измерени напони у кортикалној кости су упоређени са резултатима недавно објављене студије аутора Prado и сар. (2013), који су симулирали жвакање на сличном компјутерском моделу лобање израђеном само од кортикалне кости.

Са исте лобање за коју смо направили компјутерски модел узети су узорци кости, чија је микроархитектура анализирана применом микро-компјутеризоване томографије. Да би се испитала повезаност оклузалних сила и микроархитектуре кости, узорци су класификовани у две групе у зависноси од тога да ли трпе висок или низак напон током жвакања. У циљу даље анализе микроархитектуре кости у

односу на Le Fort линије прелома, сви узорци су поређени на основу тога да ли су узети са места ових линија или не.

Резултати и закључци

Симулација процеса жвакања је показала да и кортикална и трабекуларна кост учествују у преносу оклузалних сила кроз кости средњег масива лица. Оклузалне силе су се преносиле кроз кортикалну кост дуж пет вертикалних трајекторија (парна носновилична, парна јагодичновилична, и носна преграда) и две хоризонталне трајекторија (чеона, јагодична), при чему су највећи напони и померања регистровани дуж носновиличне трајекторије. Такође је уочено да је трабекуларна кост у делу фацијалног скелета изнад предњих зуба под значајно мањим напоном у односу на кортикалну кост, док су у оба сегмента кости у делу фацијалног скелета изнад бочних зуба регистроване сличне вредности напона. Овај налаз сугерише да кортикална кост у предњем делу фацијалног скелета има важнију улогу у преносу оклузалних сила, док су у бочној регији кортикална и трабекуларна кост подједнако ангажоване у обављању овог задатка.

Упоредна анализа напона регистрованих у кортикалној кости у нашем моделу и у моделу аутора Prado и сар. (2013) показала је да је у оба случаја дистрибуција von Mises напона у кортикалној кости слична, али су интензитети напона у нашем моделу били нижи. Значајне разлике између модела су примећене у дистрибуцији и интензитету компресивне и затезне компоненте главних напона. Имајући у виду да је компјутерски модел лобање аутора Prado и сар. (2013) био израђен само од кортикалне кости, овај налаз указује на то да резултати анализе напона могу бити значајно промењени уколико у модел лобање није укључена и трабекуларна кост.

Резултати структурне анализе кости су јасно показали да кости средњег масива лица показују регионалне разлике у микроархитектури кортикалне и трабекуларне кости, које могу бити одраз њихове адаптације на различито оклузално оптерећење.

Кортикална кост на местима која трпе веће оптерећење током жвакања је показала склоност ка већој дебљини и густини, мањој порозности, и већој раздвојености пора. Корелативна анализа између параметара је откила да је

повећање дебљине кортикалне кости праћено значајним повећањем њене густине и раздвојености пора. Поред тога, показано је и да се повећање порозности кортикалне кости фацијалног скелета дешава на рачун повећања величине пора.

Израженије разлике су откривене у микроархитектури трабекуларне кости, која је имала значајно већи волумен и дебљину трабекула у групи која трпи веће оклузално оптерећење током жвакања. Будући да се ови параметри често први мењају током промена оптерећења на кост, наши резултати такође говоре у прилог њихове велике осетљивости на интензитет оклузалног оптерећења. Поред тога, корелативна анализа је показала да са порастом напона у кости значајно расте волумен и густина трабекуларне кости, што може да укаже на могући механизам микроструктурне адаптације костију лица на повећано оклузално оптерећење.

Сасвим мале разлике у микроархитектури кортикалне и трабекуларне кости забележене су између места Le Fort линија прелома и других делова фацијалног скелета. Наиме, кости лица дуж Le Fort линија имале су нешто тању и порознију кортикалну кост са већим порама, док су трабекуле у овим деловима фацијалног скелета биле другачије по облику и међусобно повезање. Регистрован је значајно већи степен анизотропије трабекуларне кости на местима Le Fort линија, што указује на то да је већина трабекула орјентисана у правцу дејства сила које на њих делују током уобичајених активности, тј. жвакања. Будући да је оваква трабекуларна мрежа способна да се одупре дејству оклузалних сила, она је истовремено мање отпорна на дејство сила из других праваца, нпр. механичке силе хоризонталног правца. Упркос овом налазу, наши резултати нису јасно указали на то да је микроархитектура кости дуж Le Fort линија прелома лошија у биомеханичком смислу у односу на друге делове фацијалног скелета.

Кључне речи: кост, фацијални скелет, трајекторије, микроархитектура, метод коначних елемената, оклузално оптерећење, Le Fort фрактуре.

Научна област: медицина

Ужа научна област: биологија скелета (остеологија)

TABLE OF CONTENTS

1. INTRODUCTION

1.1. The facial skeleton: an anatomical perspective

The facial skeleton is made up of fifteen irregular bones joined in a multifunctional unit that assists in the processes of deglutition, respiration, speech, housing the sensory organs, and many others. Some of the facial bones, such as the maxilla and mandible, contain teeth and/or air-filled cavities (paranasal sinuses) which make their morphology more complex.

Like other skeletal sites, the facial bones consist of compact (or cortical) bone and spongy (or trabecular) bone. Cortical bone covers the surfaces of the bones and air-filled cavities, while trabecular bone occupies the space beneath cortical bone layer. Given that majority of the facial bones consist only of thin cortical bone and the fact that only few bones contain significant amounts of trabecular bone makes the facial skeleton unique in terms of morphology and architecture.

1.2. Classic concept of occlusal load transfer

Early descriptions of the facial skeleton architecture were made at the beginning of the 20th century, when few researchers observed that certain regions of the mid-facial skeleton consist of a very thick cortical bone that have a form of vertical and horizontal pillars (Le Fort, 1901; Testut, 1911; Cryer, 1916). These osseous pillars were assumed to act as stress trajectories or "buttresses" that ensure structural integrity of the mid-facial skeleton during mastication by transferring occlusal forces from the teeth to the cranial base and vault (Cryer, 1916). Cryer (1916) originally described six vertical and three horizontal buttresses of the mid-facial skeleton (Figure 1). Three paired vertical buttresses (nasomaxillary, zygomaticomaxillary, and pterygomaxillary) had been suggested to transfer most of the occlusal load (Figure 1A). The *nasomaxillary* or *anterior buttress* was suggested to transfer occlusal forces from the anterior teeth upward around the piriform aperture to the frontal process of the maxilla and the frontal bone. The *zygomaticomaxillary* or *middle buttress* was assumed to dissipate occlusal

forces from the premolars and the anterior molar(s) toward the frontal and temporal bone following the frontal and the temporal process of the zygomatic bone, respectively. The *pterygomaxillary* or *posterior buttress* was suggested to distribute the loads from the posterior molars(s) to the cranial base over the posterior maxillary wall and the pterygoid processes of the sphenoid bone. The osseous part of the nasal septum (Figure 1B), which was initially assumed to support the main vertical buttresses (Cryer, 1916), had been recently proposed as the seventh vertical or *sagittal buttress* that is equally important in the distribution of occlusal loads (Pollock, 2012).
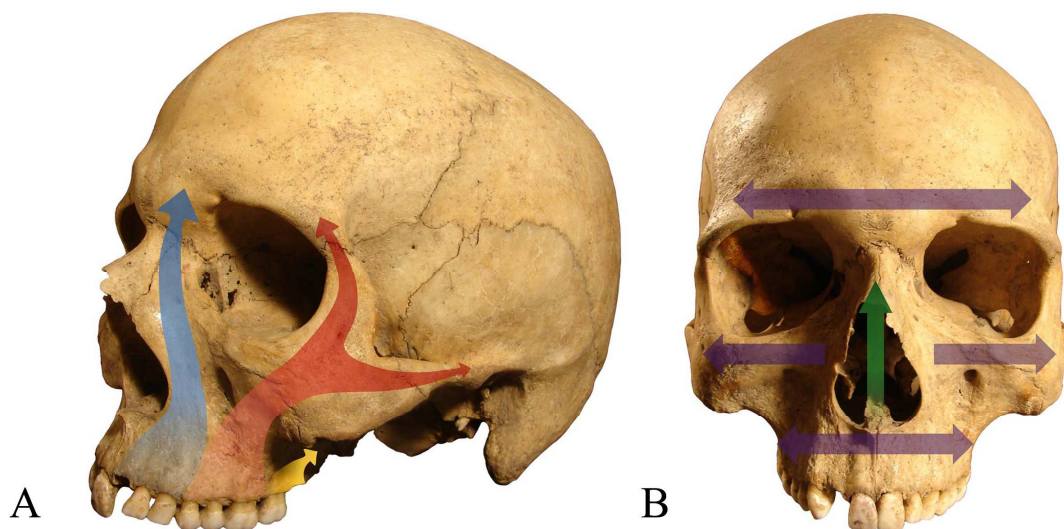
*Figure 1. Buttresses of the mid-facial skeleton: **A**. the **nasomaxillary buttress** (blue arrow), the **zygomaticomaxillary buttress** (red arrow), and the **pterygomaxillary buttress** (yellow arrow); **B**. the **sagittal buttress** (green arrow), the **frontal buttress** (upper violet arrow), the **zygomatic buttress** (middle violet arrows), and the **maxillary buttress** (lower violet arrow).*

Classical theory of the occlusal load distribution also proposed three horizontal buttresses (Figure 1B) to be indirectly involved in performing this task by interconnecting the vertical buttresses at different levels (Cryer, 1916; Sicher and Tandler, 1928). The maxillary buttress consists of the alveolar processes and the hard palate that make a platform from which all vertical buttresses ascend. The zygomatic

buttress includes infraorbital rims, and the body and the temporal processes of the zygomatic bones, and thus connects the anterior and the middle vertical buttresses. The same vertical buttresses are also connected at the level of the supraorbital rims and the region of glabella, which constitute the frontal buttress. Beside their role in the stabilization of the vertical buttresses, horizontal buttresses were suggested to support the mid-facial skeleton mechanically against horizontally oriented impacts to the face (Cryer, 1916; Sicher and Tandler, 1928; Rowe and Williams, 1985).

Testut (1911) and Cryer (1916) suggested that distribution of occlusal loads occurs only through the cortical bone along buttresses, while the remaining parts of the mid-facial skeleton between the buttresses were assumed not involved in this process due to their thin cortical bone structure (Testut, 1911; Cryer, 1916).

1.3. Investigations of the occlusal load transfer by mechanical methods

1.3.1. Strain gauge analysis

The mechanical behavior of the mid-facial skeleton during mastication was extensively studied in dry human skulls using strain sensitive transducers, also known as strain gauges (Endo, 1965; 1966; 1970). When attached to the bone surface, these electronic devices were able to register microdeformations of cortical bone in response to artificial tooth loading. During such experiments, Endo (1965; 1966; 1970) found mainly compressive deformations on the cortical bone surface along the vertical buttresses and simultaneous tensile deformations in the region of the horizontal buttresses. Although the highest strains were detected in the cortical bone of the alveolar process just above the loaded teeth (Endo, 1965), its magnitude was significantly higher around the anterior teeth than around the molars (Endo, 1965). Moreover, Endo found that loading of the anterior teeth causes much higher strains at any point in cortex of the mid-facial skeleton than posterior teeth loading (Endo, 1965).

The contribution of the masseter and/or temporalis muscle action to the deformation of the facial skeleton was also investigated by strain gauge technique. It was found that isolated action of both muscles causes similar pattern of bone

deformations in the upper third of the facial skeleton with the only difference in the strain magnitude (Endo, 1970). Namely, bone strains in response to the masseter action were predominantly tensile, whereas isolated action of the temporalis muscle caused mainly compressive bone deformations at the same sites (Endo, 1970).

1.3.2. Photoelastic models of the skull

Recently, the distribution of occlusal forces was analyzed in three-dimensional (3D) models of the mid-facial skeleton by photoelastic technique of stress analysis. These models were created of a birefringent isotropic material, which could predict direction of occlusal force dissipation by "transforming internal stress into the visible light" (Alexandridis et al., 1981). Namely, when a beam of polarized light passes through the photoelastic material under loading, it will split into two beams showing the direction of the principal stress (Alexandridis et al., 1981; 1985). Beside the qualitative analysis, this technique also offered a semi quantitative assessment of the stress magnitude presented by different color intensity. Using 3D photoelastic models of the skull, Alexandridis et al. (1985) found uniform stress distribution along the three main vertical buttresses. The highest stress was observed in the alveolar process. Similar to Endo's findings of significantly lower principal strains in the posterior vs. anterior maxilla (Endo, 1965), Alexandridis et al. (1981; 1985) also described much lower occlusal stress in the region of the pterygomaxillary buttress.

Although strain gauge data and photoelastic models revealed important data related to the mechanical behavior of cortical bone during occlusal loading, neither the contribution of all masticatory muscles nor the role of trabecular bone in the occlusal force distribution were possible to assess by these techniques.

1.3.3. Finite element analysis

More recent application of computer modeling in the field of dental biomechanics, e.g. 3D finite element analysis (FEA), appeared the most promising for clarifying the pattern of occlusal load distribution through the mid-facial bones (Tanne et al., 1988). Using this technique, it became possible to create computer models of

geometrically complex structures composed of materials with different elastic properties, such as the skull, and to perform both qualitative and quantitative analyses of stress and strain within each material during various loading conditions. However, the advantages of FEA were used only partially by a few studies that investigated occlusal load transfer without a comprehensive evaluation of the mid-facial biomechanics. Moreover, these studies provided conflicting results that, in some cases, differed significantly from the theory of buttresses and/or strain gauge data. The first 3D FEA of the skull showed nearly uniform distribution of occlusal stress through the cortical bone of the mid-facial skeleton during simulation of clenching (Gross et al., 2001). The same authors also reported that von Mises stress (VMS) resulted from biting simulation splits above the loaded tooth in the "V"-like form and dissipates in the direction different from buttresses (Gross et al., 2001). By contrast, Cattaneo et al. (2003) described that the distribution of VMS during the first and second molar biting follows the route of the zygomaticomaxillary buttress. More recently, Prado et al. (2012; 2013) measured VMS at the specific points along the proposed vertical buttresses during the loading of the canine, anterior molars, and posterior molars, respectively, and concluded that occlusal stress distributes unevenly through the mid-facial skeleton.

In addition to inconsistent results reported in previous FE studies, the anatomy of the mid-facial skeleton models had been frequently oversimplified. The models were usually created only of cortical bone (Gross et al., 2001; Prado et al., 2012; Prado et al., 2013) neglecting the fact that trabecular bone within the maxilla and the zygomatic bone might participate in the distribution of occlusal forces. Only Cattaneo et al. (2003) included trabecular bone in the model, but the occlusal load distribution was analyzed only in cortical bone. The authors generally focused on the investigation of the main vertical buttresses, while the mechanical behavior of the nasal septum and the horizontal buttresses during habitual masticatory activities had been rarely reported. Bone elastic properties and the magnitude of force applied to the teeth, accurate selection of which is crucial for FEA (Strait et al., 2005; Gröning et al., 2012), differed significantly from the experimentally calculated values in healthy dentate individuals. Moreover, these studies did not provide direct evidence for occlusal stress distribution, particularly through the cortical and trabecular bone compartments individually.

1.4. Relationship between facial bone structure and occlusal loading

Bone is a dynamic tissue that changes its structure in response to functional loading (Wolff, 1870; Skedros and Baucom, 2007). This concept known as "Wolff's law" had been extensively studied in the postcranial bones, especially in the proximal femur and the vertebrae. However, the role of the functional masticatory activities in the microstructural adaptation of the mid-facial bones has received little scientific consideration.

Recent studies in both animals and humans (Bresin et al., 1994; Bresin et al., 1999; Mavropoulos et al., 2004; Mavropoulos et al., 2005; Tanaka et al., 2007; Odman et al., 2008; Kingsmill et al., 2010) demonstrated that alterations in magnitude and/or direction of occlusal loading may cause remarkable changes in cortical and trabecular bone structure. Reduced occlusal loading in animals fed with soft food had been associated with thinner cortical bone (Bresin et al., 1999), highly mineralized cortical and trabecular bone (Tanaka et al., 2007), and decreased trabecular thickness (Tb.Th) and bone volume fraction (BV/TV) of trabecular bone (Bresin et al., 1994; Mavropoulos et al., 2004; Mavropoulos et al., 2005; Odman et al., 2008). Kingsmill et al. (2010) also reported that switch to a soft food diet in growing rats results in a greater mineralization density of the frontal bone. The altered bone structure was also detected in the frontal and zygomatic bone of edentulous human skulls (Dechow et al., 2010; Williams and Slice, 2014). Reduced occlusal loading following tooth loss causes thinning of cortical bone in the whole facial skeleton (Dechow et al., 2010), and also the change of trabecular shape within the zygomatic bone from plate-like to rod-like, thinning of trabeculae, reduced trabecular bone density, and more irregular arrangement of trabeculae (Kato et al., 2004; Yoshino et al., 2007). Although these studies had been largely restricted to the alveolar bone assessing its local biomechanical response to the occlusal loading, they strongly suggest that facial skeleton acts as a functional unit and that investigations of functional bone adaptation should include the whole mid-facial skeleton instead of a single region.

Moreover, recent studies of the mid-facial bone structure also revealed remarkable regional variations in cortical and trabecular bone architecture in dentulous individuals (Peterson and Dechow, 2003; Peterson et al., 2006; Park et al., 2008). Thin

cortical bone placed between the buttresses was found to be generally denser in comparison to areas containing thick cortical bone (Peterson and Dechow, 2003; Peterson et al., 2006). Regional variations in density of both cortical and trabecular bone were also detected on CT images in dentulous patients (Park et al., 2008). Beside structural differences, the elastic modulus of the cortical bone also varied significantly across the dentulous maxilla (Peterson et al., 2006). These studies focused only on mapping the inter-site variations in architecture and mechanical properties of the mid-facial bones, even though such variations were suggested to reflect different involvement of bone in the transfer of occlusal forces (Peterson et al., 2006). There has been no comprehensive study of the regional variations of the mid-facial bone microarchitecture in relation to the occlusal load distribution.

1.5. Investigation of the mid-facial fractures

The maxillo-facial fractures are among the most common injuries in trauma patients (Hardt and Kuttenberger, 2010). The leading causes of the facial injuries are traffic accidents, sport-related injuries and daily life activities, which account for almost 90% of all maxillo-facial fractures (Steidler et al., 1980; Kahnberg and Göthberg, 1987; Rakocevic, 1993; Alvi et al., 2003; Gassner et al., 2003; Hardt and Kuttenberger, 2010; Venugopal et al., 2010). Although the facial bone fractures can affect an individual from early childhood to old age, they are most commonly diagnosed in the third decade of life (Dimitroulis and Eyre, 1991; Rakocevic, 1993; Gassner et al., 2003; Lee, 2009). Epidemiological studies also suggested clear male predominance in the overall craniofacial trauma (Steidler et al., 1980; Gassner et al., 2003; Hardt and Kuttenberger, 2010; Venugopal et al., 2010; Zandi et al., 2011).

1.5.1. Zones of weakness in the mid-facial skeleton

It has been traditionally explained that fractures of the mid-facial skeleton occur in the regions where bone has a weaker structure in biomechanical terms. Early anatomical descriptions of the facial bone architecture assumed thin cortical bone located between the buttresses as zones of weakness (Testut, 1911; Cryer, 1916). Based

on the strain gauge data, Endo (1965) assigned the part of the maxilla above the anterior teeth as a weak area due to the highest strains registered in this region during tooth loading. However, Le Fort (1901) was more precise in defining the zones of weakness within the mid-facial skeleton. By performing a series of experiments on cadaveric skulls, this author recognized characteristic locations in the maxilla and associated bones at which fractures most commonly occur after contusion and compressive blows to the face (Le Fort, 1901). Le Fort originally described three "areas of inherent weakness and comminution" (Le Fort, 1901), which became widely accepted classification scheme of the mid-facial fractures in both basic sciences and clinical practice (Figure 2).
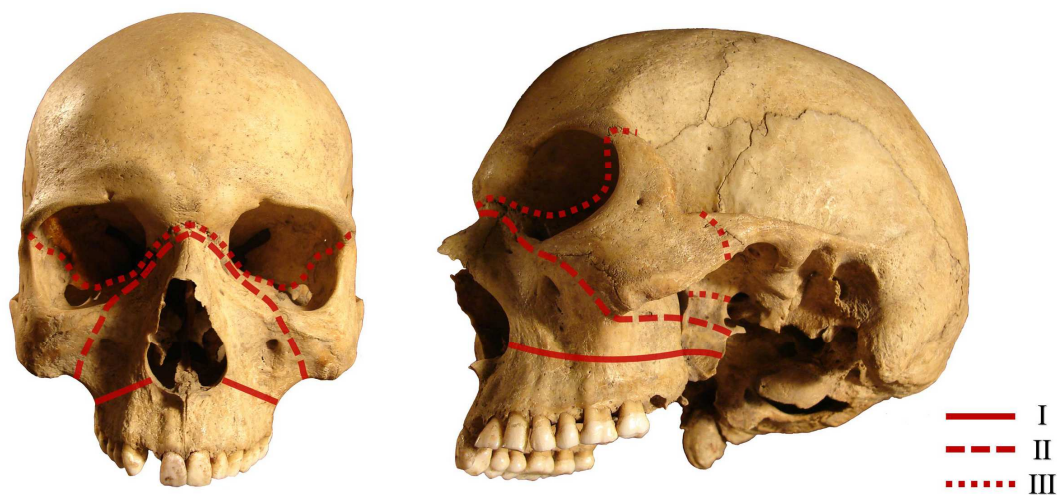
Figure 2. Lines of weakness in the mid-facial skeleton suggested by Le Fort

The first area, known as Le Fort I fracture line, extends from the lateral aspect of the piriform aperture through the maxilla above the apices of the tooth roots including the pterygoid plates (Figure 2). Le Fort II fracture line starts from the nasofrontal suture or below it, progresses through the frontal process of the maxilla and the lacrimal bone to the inferior orbital wall and rim, passes downward and outward along the anterior surface of the maxilla under the zygomatic bone, progress across the pterygomaxillary junction to the pterygoid process (Figure 2). Le Fort III fracture line extends from the nasofrontal and frontomaxillary sutures along the medial orbital wall, passes over the

orbital floor and its lateral wall involving the zygomaticofrontal suture and the zygomatic arch (Figure 2).

1.5.2. The role of the bone-related factors in the Le Fort fracture development

Although Le Fort suggested that bone architecture is important in the fracture development (Le Fort, 1901), it remained almost unexplored to what extent bone-related factors contribute to the increased fragility along Le Fort lines. In the last decades, many authors assessed bone fracture tolerance by measuring the minimum force needed to cause a fracture in a single facial bone. The nasal bones were found to be the weakest in the facial skeleton with a fracture tolerance ranging between 342.5 N and 850 N (Swearingen, 1965; Nahum, 1975; Cormier et al., 2010). Other bones, such as the maxilla and zygomatic bone, were more tolerable to mechanical forces resisting up to 1801 N (Swearingen, 1965; Schneider and Nahum, 1972; Nahum, 1975; Allsop et al., 1988; Yoganandan et al., 1991; Hardt and Kuttenberger, 2010).

Recent studies that investigated age-related bone fractures at postcranial skeletal sites suggest that bone structure and geometry play a significant role in the fracture development (Beck et al., 1990; Nakamura et al., 1994; Duboeuf et al., 1997; Michelotti and Clark, 1999; Partanen et al., 2001; Gnudi et al., 2004; Pulkkinen et al., 2006; Kaptoge et al., 2008; Djonic et al., 2011). Age-related deterioration in bone structure and composition that happen at all hierarchical levels of bone organization leads to a reduction in bone strength and the consequent increase in fracture risk (Lundeen et al., 2000; Cui et al., 2008; Chen et al., 2010; Djuric et al., 2010; Bernhard et al., 2013; Djonic et al., 2013; Milovanovic et al., 2014). Furthermore, regional heterogeneity in cortical and trabecular bone microarchitecture that result from differential stress and strain distribution through the bone was frequently used to explain why bone is more susceptible to fracture in certain parts than in others (Burr et al., 1997; Ciarelli et al., 2000; Legrand et al., 2000; Homminga et al., 2002; Robling et al., 2002; Gong et al., 2005; Warden et al., 2005; Ruff et al., 2006; Stauber and Müller, 2006; Eckstein et al., 2007; Hulme et al., 2007; Djuric et al., 2010; Wegrzyn et al., 2010; Milovanovic et al., 2012). However, there has been no study to assess microstructural properties of the mid-facial bones along Le Fort fracture lines.

2. RESEARCH HYPOTHESES

Our hypotheses were that:

1. both cortical and trabecular bone participate in the transfer of occlusal forces through the mid-facial skeleton,

2. distribution of occlusal forces through the mid-facial skeleton is not uniform, and that certain bone areas in both cortical and trabecular bone experience higher occlusal loads during habitual masticatory activities than others,

3. both compact and trabecular bone exhibit regional variations in microarchitecture as a result of different occlusal stress experienced during mastication,

4. increased bone fragility along Le Fort fracture lines in the mid-facial skeleton is due to weak cortical and trabecular bone microarchitecture in biomechanical terms.

3. RESEARCH GOALS

The aims of our research were the following:
1. to develop an improved 3D computer model of the mid-facial skeleton and to simulate biting and clenching using finite element analysis (FEA),
2. to clarify the distribution of occlusal forces through the cortical and trabecular bone of the mid-facial skeleton during biting and clenching, through qualitative and quantitative analyses of stress and displacement,
3. to analyze microstructural properties of cortical and trabecular bone by micro-computed tomography (micro-CT) in those regions of the mid-facial skeleton for which computer simulation (FEA) shows that are subjected to high and low occlusal stress,
4. to compare quantitative microstructural parameters of cortical and trabecular bone between regions of the mid-facial skeleton subjected to high and low stress and to explore whether these parameters are associated with adaptation of the mid-facial skeleton to the occlusal loads,
5. to analyze microstructural properties of cortical and trabecular bone of the mid-facial skeleton by micro-CT along Le Fort fracture lines,
6. to compare quantitative microstructural parameters of cortical and trabecular bone between areas of Le Fort fracture lines and other parts of the mid-facial skeleton and to assess whether these parameters are associated with a greater bone fragility in the region of Le Fort fractures.

4. MATERIAL AND METHODS

4.1. Finite element analysis

Finite element (FE) method is a numerical technique that is widely used in engineering to predict mechanical behavior of geometrically complex objects under various loading conditions. The technique is based on the principle of dividing the whole object into small parts of the same geometry, known as finite elements, which are interconnected by number of nodes. Displacement of elements and nodes resulting from loading can be calculated, if the mechanical properties of the tested object and finite elements are known. The obtained values of nodal displacement are used to calculate stress and strain of the object by numerous mathematical equations.

In FE analysis, stress is commonly reported in effective von Mises stress and principal stress. Von Mises stress (VMS) reflects the overall stress state in the object, but it cannot define the type of stress, e.g. compression or tension. This can be expressed by principal stress, which negative values indicate compression, whereas positive values characterize tensile stress. The distribution of stress in the tested object is commonly illustrated by different colors. In the case of VMS, red areas on the object signify high stress, while blue areas indicate low stress (Figure 3A). Similar is for principal stress: areas under tension are presented in red color, whereas areas under compression are in blue (Figure 3B).
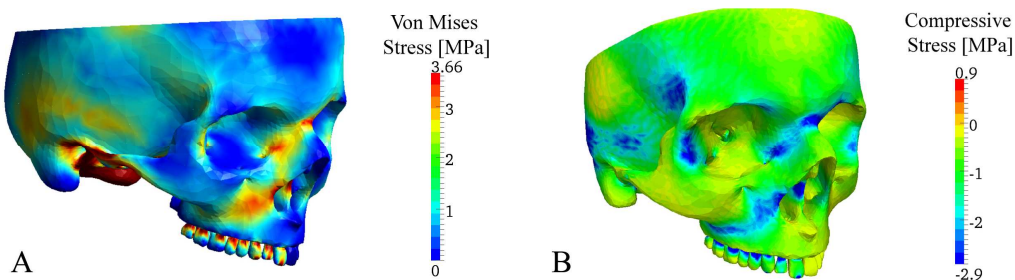
Figure 3. *Distribution of von Mises stress (**A**) and compressive stress (**B**) in the skull model obtained by finite element analysis.*

Concerning that FE analysis is performed on the computer model of the desired object, more realistic representation of its geometrical details will provide more accurate results. For complex objects, it is also possible to model more than one material and to assess their mechanical behavior individually. Additionally, certain variables are also needed to be defined during the modeling procedure in order to make the FE analysis possible. These include:

- material properties of each material that constitute the model (defined by Young's modulus and Poisson's ratio), and

- selection of boundary conditions (the site(s) on the tested object where the force will be applied including its magnitude and direction; region(s) of the object where finite elements will be constrained and not displaced during loading).

Given that FE method is an approximation of a real condition, inaccurate selection of any of these variables could potentially influence the FEA results.

4.1.1. Development of computer model of the mid-facial skeleton

4.1.1.1. Selection of the dry human skull

A computer model of the mid-facial skeleton in our study was developed from CT images of a dry skull of a young adult Caucasian male (Figure 4A), which was selected from the skeletal collection stored at the Laboratory for Anthropology, Institute of Anatomy, School of Medicine, University of Belgrade. The skull was completely preserved with the fully dentate maxilla.

4.1.1.2. Scanning of the skull by computer tomography

The skull excluding mandible was scanned in a dry condition using clinical Computed Tomography (*Somatom Sensation 16,* Siemens, Munich, Germany). The CT imaging was performed at the Department of Radiology, School of Dentistry, University of Belgrade. The skull was positioned parallel to the Frankfurt plane.

Scanning was performed in a bone window with a voltage of 120 kV and a tube current of 40 mAs. A total of 179 axial sections were obtained with a single slice thickness of 0.75 mm (Figure 4B).

4.1.1.3. Extraction of bone and teeth from CT images

The development of 3D computer model of the mid-facial skeleton from CT images and FE analysis were performed at the Bioengineering Research and Development Center (BioIRC), Faculty of Engineering, University of Kragujevac. The CT images were imported into Mimics visualization software (version 10.1, Materialize, Leuven, Belgium) that allowed an accurate 3D representation of the mid-facial anatomy including variations in cortical thickness, location and volume of the trabecular bone, and all hollow structures within the facial bones. An automatic segmentation procedure based on thresholding and boolean operations were used to mark out and extract cortical bone, trabecular bone and teeth from CT images in individual models, and to join them together in the final computer model of the mid-facial skeleton (Figure 4C). First, bone areas were selected on each CT slice via automatic segmentation and extracted in a temporary skull model, which contained both cortical and trabecular bone. Hollow structures inside the skull, e.g. the paranasal sinuses, nasal and cranial cavity, were also created during this step. Part of the cranial vault above the attachment site of the temporalis muscle was excluded in order to keep only the region of interest and to reduce the time of analysis. By combining automatic and manual segmentation, cortical bone was marked out on CT images and extracted in an individual cortical bone model. This model was then subtracted from the temporary skull model by means of boolean operations in order to leave parts of the mid-facial skeleton containing only trabecular bone. Given that the resolution of CT images was not sufficient for the precise 3D reconstruction of trabecular network, trabecular bone was modeled as a solid structure. The segmentation procedure was also used to select and extract teeth from CT images (Figure 4C). The periodontal ligament was not modeled due to its minor influence to the overall load transfer through the mid-facial skeleton (Cattaneo et al., 2003; Wood et al., 2011; Gröning et al., 2012).
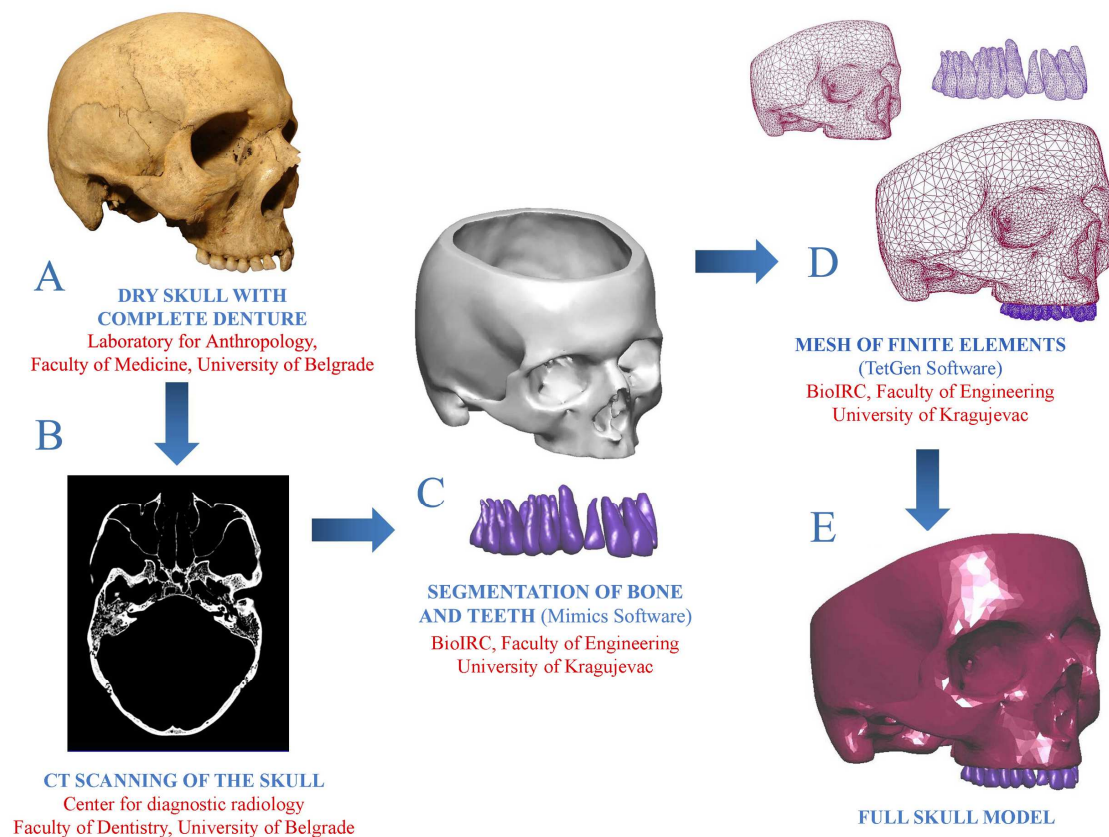
*Figure 4. Development of the computer model of the skull. **A**. Selected dry human skull; **B**. CT scan of the skull at the level of the zygomatic arches; **C**. Computer model of bone and teeth extracted from CT images; **D**. Mesh of finite elements; **E**. Full skull model.*

4.1.2. Creation of mesh of finite elements

After computer models of cortical bone, trabecular bone, and teeth were created, all tissues were divided into finite elements. Figure 4D shows a mesh of finite elements created within each tissue by TetGen software (Hang Si, WIAS, Berlin, Germany). We used linear tetrahedrons as finite elements with an average size of 0.25 mm, 1.0 mm, and 2.5 mm for cortical bone, trabecular bone, and teeth, respectively. The total number of finite elements and nodes representing each tissue is listed in Table 1.

Table 1*. Number of nodes and elements representing each tissue in the model*

Material	Nodes	Elements
Cortical bone	101271	182232
Trabecular bone	89545	144782
Teeth	59964	97126

4.1.3. Selection of material properties

Cortical bone, trabecular bone and teeth were assumed as isotropic, homogeneous, and linearly elastic materials. The dry skull was used only for an accurate representation of the mid-facial skeleton geometry, but the material properties of the dry bone were not assigned to any tissue in order to avoid possible influence on the FE results. Instead, Young's moduli of 9.1 GPa, 4.5 GPa, and 20 GPa were assigned to cortical bone, trabecular bone, and teeth, respectively. Unlike previous FE studies, Young's modulus assigned to cortical bone in our study is the mean value calculated experimentally for fresh facial bones (Peterson et al., 2006). Given that the elastic properties of fresh trabecular bone of the facial skeleton are lacking in the literature, Young's modulus of 4.5 GPa was drawn based on the suggestions of Al-Khafagy (2010). This author demonstrated that the relationship between cortical and trabecular bone material properties used in our study ensures stress distribution through both materials during FEA. The Young's modulus for teeth was the most frequently used value in the literature. The Poisson's ratio for all tissues was 0.3, because this is also the most frequently used value for bone and teeth in FE analysis (Hsu and Chang, 2010).

4.1.4. Selection of boundary conditions

First molar biting, canine biting, and clenching were simulated on the model by applying static vertical forces to the center of the tooth crown(s) in the direction of the tooth root axis.

The first molar and the canine biting were simulated respectively, because occlusal contacts during every chewing cycle occur most frequently between maxillary and mandibular first molars and canines on the chewing side (Ingervall, 1972). The first molar was loaded with the force of 400 N, which is the most frequently recorded bite force in the molar region in healthy young adults (Ferrario et al., 2004; Bakke, 2006). The canine was loaded with 160 N given that the force registered during canine biting in healthy young adults is around 40% of the force recorded in the molar region (Ferrario et al., 2004; Bakke, 2006).

Unilateral and bilateral clenching was simulated by applying forces to the half of the dental arch and to the full dental arch, respectively. These masticatory activities were chosen because every chewing cycle ends in the position of the maximum intercuspation that ensures the maximum contacts between the maxillary and mandibular teeth and subsequent uniform loading of all teeth and their supporting tissues (Lundeen and Gibbs, 1982; Mohamed and Christensen, 1985). During unilateral clenching, one (loaded) half of the dental arch was assumed as working side, while the opposite (unloaded) side was assumed as balansing side. A total force of 840 N applied during unilateral clenching was distributed along the dental arch as follows: molars were loaded together with 400 N, premolars were loaded with 280 N, while the force of 160 N was equally distributed between canine and incisors. The abovementioned force magnitude for premolars and anterior teeth were selected bearing in mind that bite forces generated by these teeth represent 70% and 40% of the bite force recorded in the molar region in healthy young adults, respectively (Kumagai et al., 1999; Ferrario et al., 2004; Bakke, 2006).

In the case of bilateral clenching, the full dental arch was loaded with the total force of 1176 N. Molars were loaded bilaterally with 560 N because this is the most frequently reported bite force in the molar region of healthy adults during bilateral clenching (Shiau and Wang, 1993; Tortopidis et al., 1998; Ferrario et al., 2004; Bakke,

2006). According to the data in the literature (Kumagai et al., 1999; Ferrario et al., 2004; Bakke, 2006), the magnitude of forces applied bilaterally to premolars (392 N) and anterior teeth (224 N) represented 70% and 40% of the bite force applied to molars.

During all simulations, the forces were applied continuously during one second with a gradual increase in magnitude until the abovementioned values were achieved.

Finite elements and nodes at the occipital condyles were constrained during all simulations.

4.1.5. Modeling of jaw-closing muscles

Simultaneously with teeth loading, additional forces were applied to the skull model at the insertion sites of the masseter, the temporalis, and the medial pterygoid muscle in order to simulate their action during biting and clenching. These muscles are mainly responsible for jaw closing and *in vivo* teeth loading during mastication. We used Hill's three component model to create the muscles and to determine the forces that they produce (Kojic et al., 1998; Stojanovic et al., 2007; Stojanovic, 2007). A number of rods representing each muscle were attached to the corresponding insertion areas on the skull (Figure 5). The mandibular attachment sites were computed as artificial areas in the space using previously reported 3D muscle coordinates (Van Eijden et al., 1997; Gross et al., 2001). The rods were composed of finite elements with the assigned elastic modulus of 0.8 MPa (Yamada, 1970). Additional parameters used for muscle modeling are displayed in Table 2. The length and cross sectional area of the rods corresponded to the physiological values reported by Van Eijden et al. (1997). According to Korioth and Hannam (1994), rods constituting each muscle were divided into two groups in order to simulate muscle pulling in more than one direction. Forces generated by each muscle portion are displayed in Table 2. The applied forces were distributed evenly over the skull insertion areas.

During molar and canine biting, muscle pulling was simulated on the loaded side of the dental arch. In the case of unilateral clenching, muscle forces were simulated bilaterally with the lower values on the opposite (unloaded) half of the dental arch.

Muscle forces had the same magnitude on both sides during the simulation of bilateral clenching.
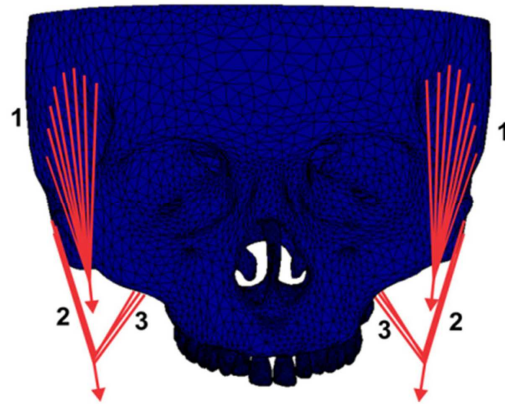
Figure 5. Modeling of the temporalis (1), masseter (2), and medial pterygoid muscle (3). Red lines illustrate rods that simulate muscle fibers, while arrows show direction of their action.

Table 2. Parameters used for modeling of the jaw-closing muscles

Muscle	Total muscle length [a] (mm)	Cross-sectional area [a] (cm^2)	Force [b] (N)
Masseter			
Superficial part	45.5	6.8	190.4
Deep part	25.5	3.5	81.6
Temporalis			
Anterior part	50.0	8.0	158.0
Posterior part	52.0	5.5	96.0
Medial pterygoid			
Anterior part	38.0	3.0	174.8
Posterior part	45.0	3.5	90.5

[a] – Data from Van Eijden et al. (1997); [b] – from Korioth and Hannam (1994).

4.1.6. Finite element analysis of stress

Effective von Mises stress (VMS) and compressive and tensile component of principal stress in cortical and trabecular bone of the model were analyzed qualitatively and quantitatively. Distribution and magnitude of VMS in both osseous compartments were assessed for all simulated masticatory activities, while distribution and magnitude of principal stress in the cortical and trabecular bone were evaluated for unilateral clenching.

In order to clarify which vertical buttress bears the most of the occlusal load during unilateral clenching, VMS and principal stress were measured at the specific sites along the nasomaxillary, zygomaticomaxillary, and pterygomaxillary buttress on the loaded side of the skull (Figure 6A-C). Magnitude of VMS and the maximum principal stress along the zygomaticomaxillary buttress was also compared with the results of previously reported FE study by Prado et al. (2013). These authors simulated mastication on the similar model of the mid-facial skeleton, but included only cortical bone. For comparative analysis, VMS and the maximum principal stress were measured at the same points in the cortical bone along the zygomaticomaxillary buttress, like in the abovementioned study (Figure 6D).
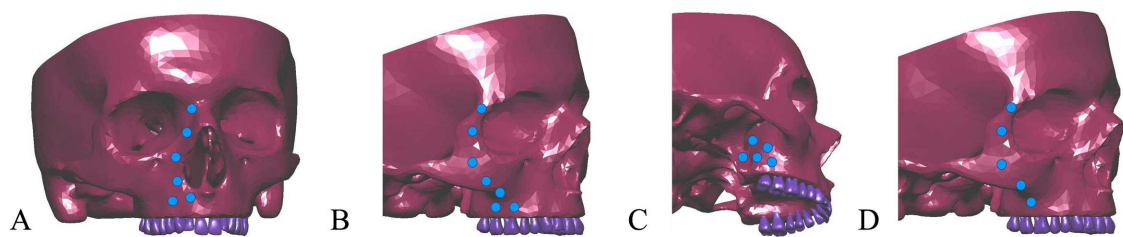
Figure 6. Measurement sites of VMS and principal stress in cortical bone along nasomaxillary (A), zygomaticomaxillary (B), and pterygomaxillary (C) buttress including measurement sites (D) used for comparative analysis with the study of Prado et al. (2013).

For the correlation analysis between occlusal stress and microarchitecture of the mid-facial bones, magnitude of VMS and principal stress were measured at the specific points in cortical and trabecular bone on the loaded side of the FE model during unilateral clenching. Twenty-five and thirteen measurement sites were selected in cortical and trabecular bone, respectively, bearing in mind location of buttresses proposed by the classical theory and the distribution of occlusal stress obtained during FEA. The VMS and principal stress were calculated within a small bone volume at each site with the radius of 1mm.

In the cortical bone, stress was measured at the following sites (Figure 7): along the alveolar process of the maxilla at the level of the apices of the tooth roots (point 1-5), 5 mm above the apices of the tooth roots (point 6-9), at the site where the posterior maxilla meets the pterygoid processes (point 10), in the body of the maxilla and the zygomatic bone along the buttresses (point 11-19) and between the buttresses (point 20-25).
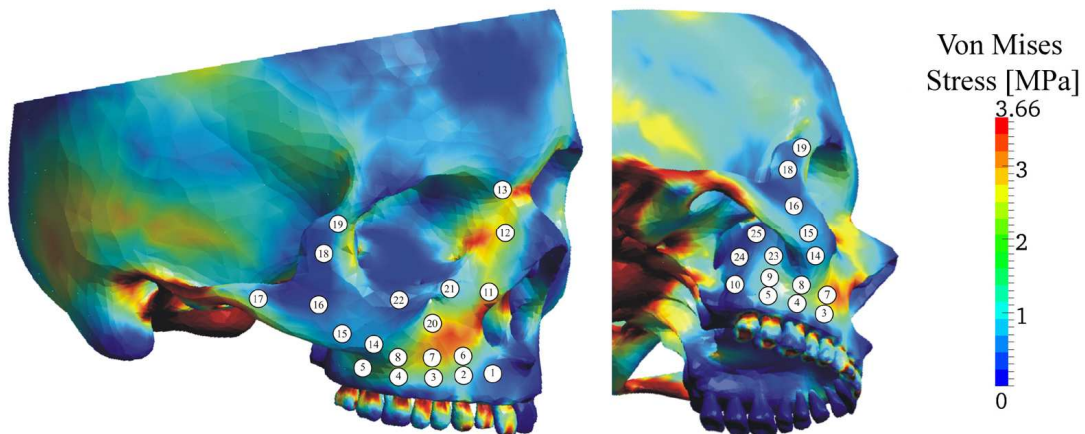
Figure 7. *Measurement sites of von Mises stress and principal stress in the cortical bone of the skull model.*

In the trabecular bone, VMS and principal stress were measured at the following sites (Figure 8): along the alveolar process of the maxilla at the level of the apices of the tooth roots (point 1-5), 5 mm above the apices of the tooth roots (point 6-8), in the frontal process of the maxilla (points 9 and 10), in the body of the zygomatic bone (point 11), in the temporal process of the zygomatic bone (point 12), and in the frontal process of the zygomatic bone (point 13).
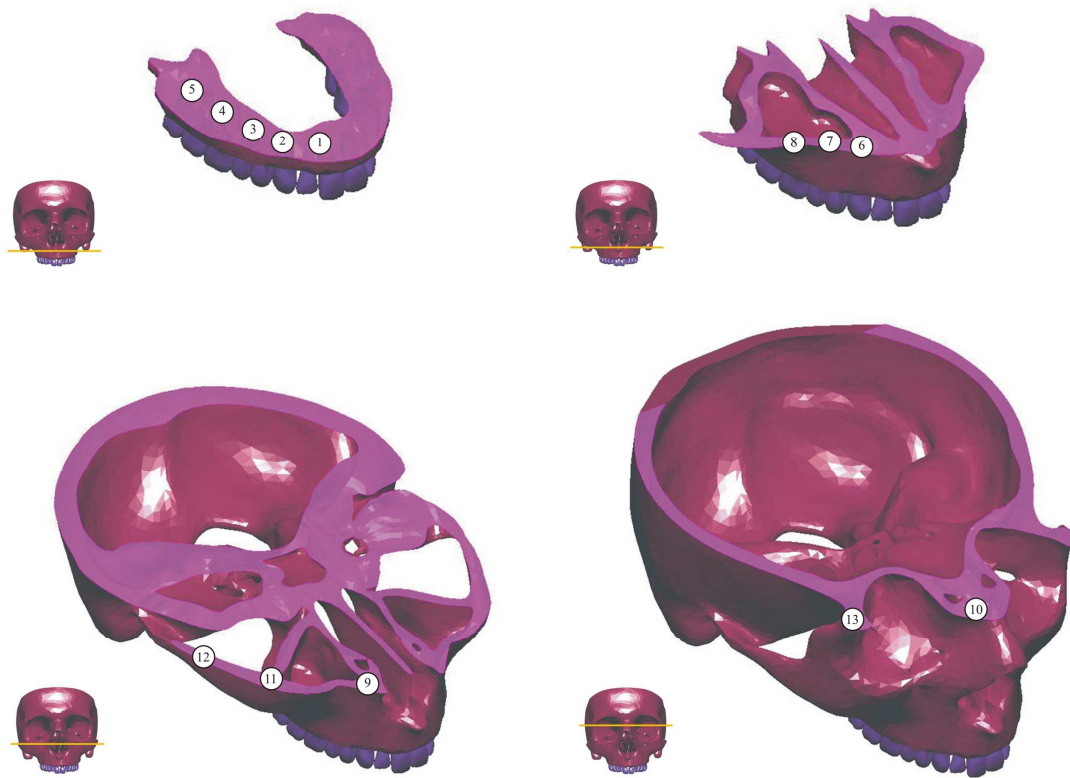
Figure 8. Measurement sites of von Mises stress and principal stress in the trabecular bone of the skull model.

4.1.7. Finite element analysis of effective displacement

Effective displacement depicts movement of the skull model in the space by calculating magnitude of displacement at the level of nodes. This parameter was analyzed qualitatively and semi quantitatively in the skull model during unilateral and bilateral clenching. Displacement was assessed along *x-axis* (medial/lateral movement), *y-axis* (superior/inferior movement), and *z-axis* (anterior/posterior movement). Similar to VMS and principal stress, the magnitude of effective displacement is illustrated by different colors. Red color indicates the greatest displacement, while areas in blue signify the lowest displacement.

4.2. Selection and preparation of bone specimens

Cortical and trabecular bone specimens were detached from the same dry skull for which computer model was developed.

Twenty-five cortical and thirteen trabecular bone specimens were detached from the sites of the maxilla and the zygomatic bone at which VMS and principal stress were measured during unilateral clenching (Figure 9). Bone specimens were excised using Low Speed Diamond Saw (SYJ-160, MTI). Cortical and trabecular bone specimens located at the same sites in the facial bones were excised together in order to avoid bone damage, but their microarchitecture was evaluated separately on micro-computed tomography.
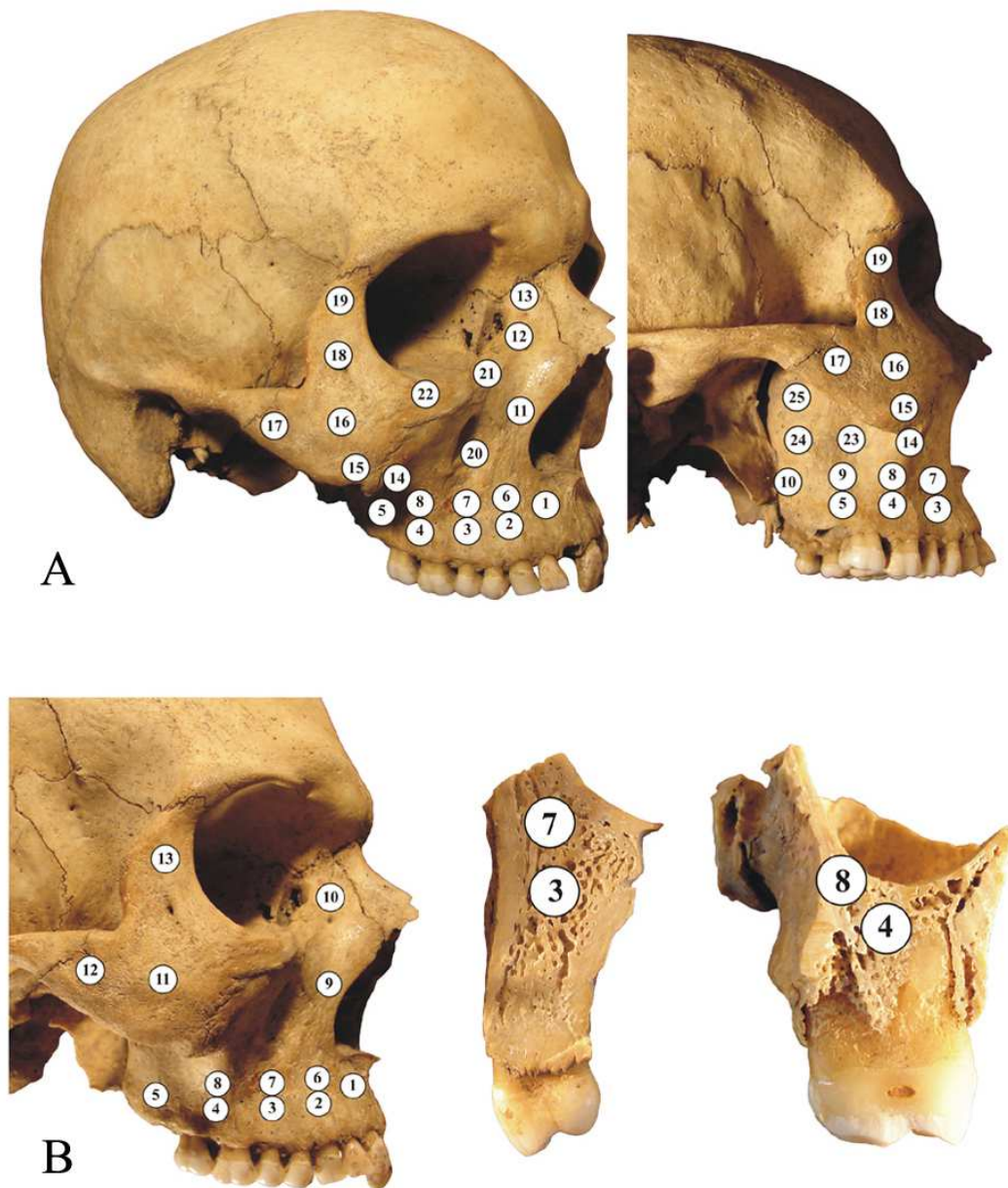
*Figure 9. Locations from which bone specimens were harvested. **A**. Cortical bone: along the alveolar process at the level of the apices of the tooth roots (1-5), along the alveolar process 5 mm above the apices of the tooth roots (6-9), the site where the posterior maxilla meets the pterygoid process (10), in the body of the maxilla and zygomatic bone along the buttresses (11-19) and between the buttresses (20-25); **B**. Trabecular bone: the alveolar process at the level of the apices of the tooth roots (1-5), 5 mm above the apices of the tooth roots (6-8), the frontal process of the maxilla (9,10), and the zygomatic bone (11-13).*

4.3. Classification of bone specimens

4.3.1. Classification of bone specimens for the analysis of bone microarchitecture in relation to occlusal stress

Cortical and trabecular bone specimens were classified into *high stress* or *low stress group* based on the observed tendency of calculated VMS to concentrate at the lower or higher level on the stress scale. Cortical bone specimens subjected to stresses above 2.25 MPa were classified into *high stress group*, while specimens from areas experiencing up to 1.49 MPa were classified into *low stress group* (Chart 1). Similarly, trabecular bone specimens that experienced stresses below 0.46 MPa and above 0.49 MPa were classified into *low stress* and *high stress group*, respectively.
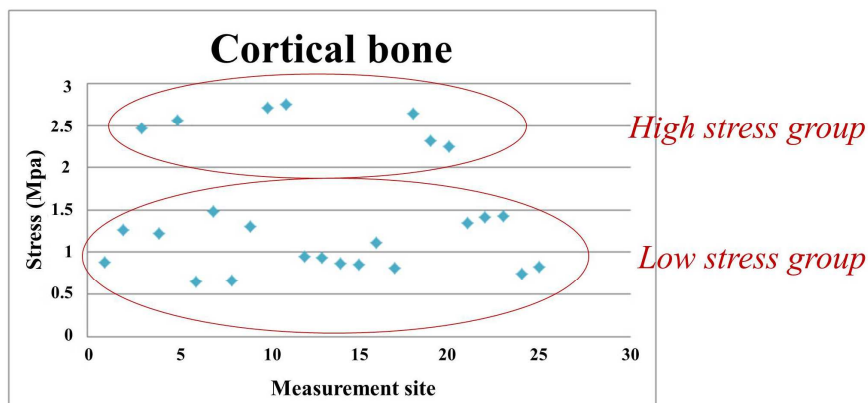
Chart 1. *Classification of cortical bone specimens based on von Mises stress values.*

4.3.2. Classification of bone specimens for the analysis of bone microarchitecture in relation to Le Fort fracture sites

For the analysis of bone microarchitecture in relation to Le Fort fracture sites, twenty-five cortical and thirteen trabecular bone specimens were reclassified based on their location in the mid-facial skeleton. Namely, cortical and trabecular bone

specimens located along Le Fort fracture lines were classified into *Le Fort group*, whereas specimens taken from the sites away from Le Fort fracture lines were classified into *Non-Le Fort group* (Figure 10).
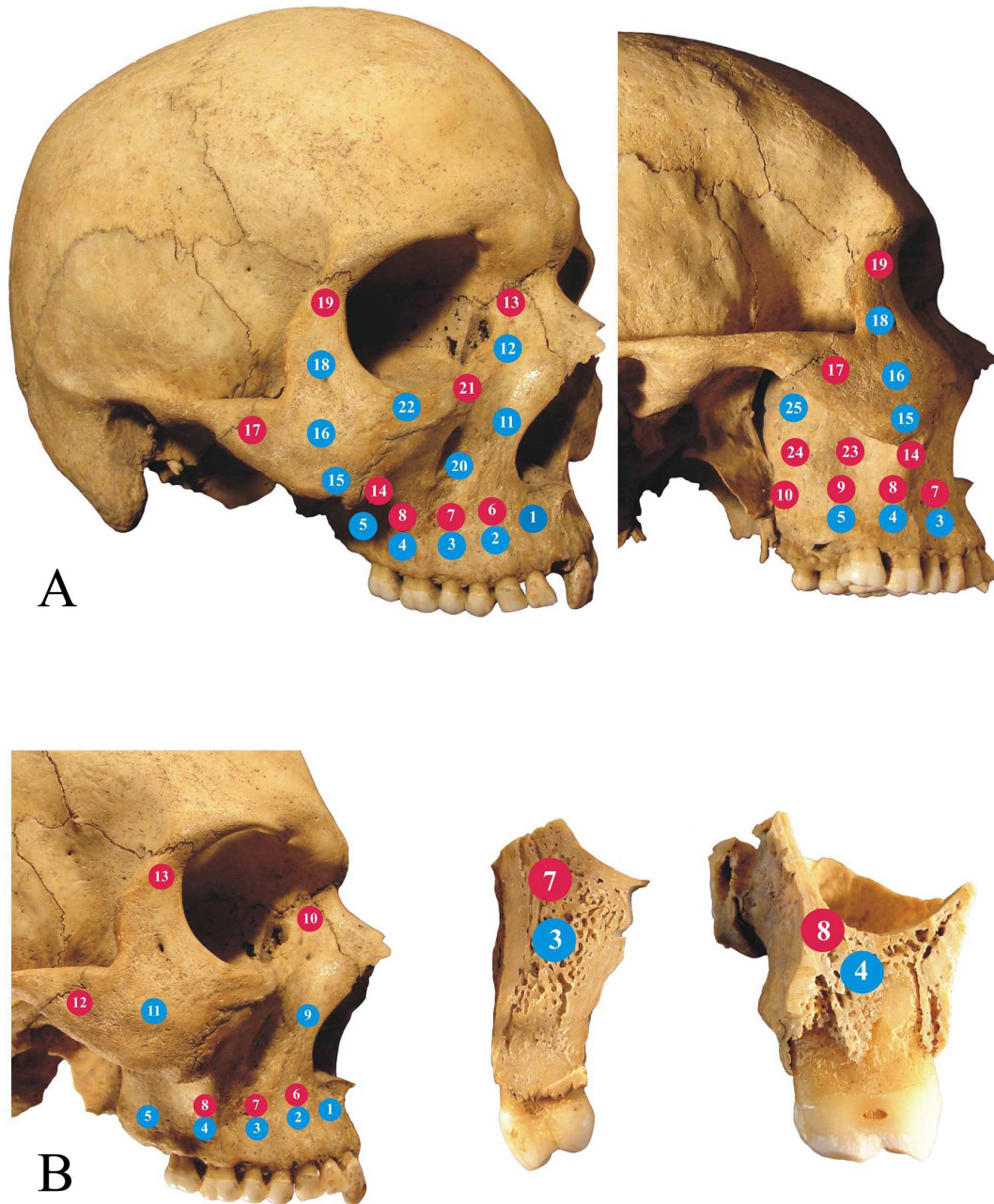
Figure 10. *Cortical (A) and trabecular (B) bone specimens classified into Le Fort group (red points) and Non-Le Fort group (blue points).*

4.4. Micro-computed tomography

Micro-computed tomography (micro-CT) is a high resolution imaging technique, which had recently become the "gold standard" for the assessment of bone architecture (Figure 11A). The principle of image acquisition by micro-CT is similar to clinical computed tomography. It also uses X-rays to scan the specimen and to visualize it in a number of 2D sections based on the X-ray attenuation data (Figure 11B,C). The 3D representation of the scanned specimen can be performed from 2D scans using image reconstruction algorithms (Figure 11D). Given that the thickness of each 2D section (voxel size) can be set to less than 10 µm, micro-CT is able to provide high resolution 3D reconstruction images of the scanned bone specimen and thus to visualize bone trabeculae precisely. On 2D images and 3D reconstruction images various morphometric parameters that characterize bone microarchitecture can be measured directly with software.
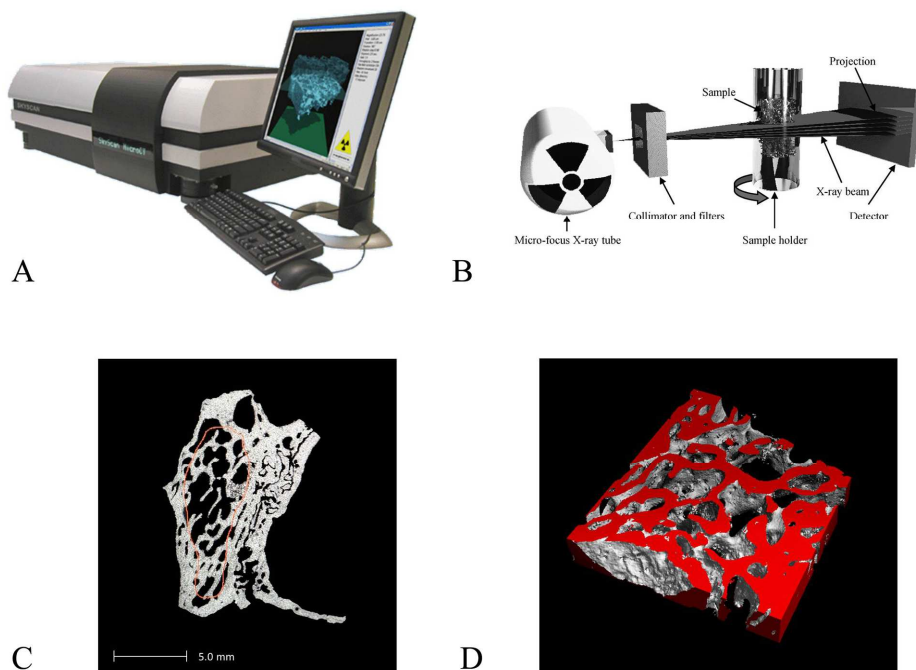
Figure 11. *A*. *Micro-computed tomography; **B**. principle of image acquisition (from the publication of Bouxsein et al., 2010); **C**. 2D section of trabecular bone specimen; **D**. 3D reconstruction image of the trabecular bone specimen.*

Micro-CT has several advantages over the other techniques for assessment of bone micromorphology (Bouxsein et al., 2010), such as histomorphometry:

- Allows direct measurement of bone morphology,
- Larger volume of interest can be analyzed,
- It is a non-destructive technique and the scanned bone specimen can be used for further analysis, e.g. mechanical testing,
- Comparison of X-ray attenuation in the bone with that of hydroxyapatite standards allows calculation of bone tissue mineralization.

4.4.1. Micro-CT scanning procedure

Micro-CT imaging was performed at Department of Osteology & Biomechanics, University Medical Center Hamburg-Eppendorf, Hamburg, Germany.

Bone specimens were scanned by micro-computed tomography (Scanco Medical μCT 40; Switzerland). Each specimen was placed in a holder with a consistent cranio–caudal orientation and scanned in dry conditions. The specimens were foam padded to avoid any movement artifacts during scanning. Images were obtained at 55 kVp and 144 μA, at isotropic resolution of 10 μm, 2048×2048 pixels per slice. The integration time per each projection was 200 ms. In specimens that contained cortical and trabecular bone, both osseous compartments were scanned together.

Scanned bone volume in each specimen corresponded to the bone volume in the FE model in which stress was calculated. The vicinity of anatomical structures, such as tooth roots, infraorbital foramen, orbital rims, etc., was used to ensure a consistent site selection and co-registration of stress and micro-CT parameters. The majority of the selected sites over the mid-facial bones were distant from each other so that the inter-site overlapping was avoided.

4.4.2. Micro-CT evaluation procedure

Segmentation was carried out by manual marking of the contours of the region of interest (ROI) on scanned slices, which were interpolated to a stuck of all slices by Morph function of the micro-CT program to generate the volume of interest (VOI). In specimens that contained both cortical and trabecular bone, each compartment was manually separated on scanned slices. The segmentation parameters were set as follows: lower threshold 220, Gaus: sigma 0.8, and support 1.0.

Within the selected VOI of cortical and trabecular bone, microarchitecture was automatically evaluated using micro-CT evaluation program V6.5-1 with direct 3D morphometry.

The following microarchitectural parameters were evaluated for cortical bone (Table 3): cortical thickness (Ct.Th, mm), cortical porosity (Ct.Po, %), pore diameter (Po.Dm, mm), pore separation (Po.Sp, mm), total volume density (TV.Dn, mg HA/cm^3), and bone volume density (BV.Dn, mg HA/cm^3).

Table 3. *Microarchitectural parameters of cortical bone measured by micro-CT.*

Micro-CT parameter	Unit	Description
Cortical thickness (Ct.Th)	mm	Average thickness of cortical bone
Cortical porosity (Ct.Po)	%	Volume of pores in relation to the total volume of cortical bone
Pore diameter (Po.Dm)	mm	Average pore diameter
Pore separation (Po.Sp)	mm	Average distance between the pores
Total volume density (TV.Dn)	mg HA/cm^3	Density of all tissues within the volume of interest (VOI)
Bone volume density (BV.Dn)	mg HA/cm^3	Density of cortical bone material within the VOI

Table 4. *Microarchitectural parameters of trabecular bone measured by micro-CT.*

Micro-CT parameter	Unit	Description
Bone volume fraction (BV/TV)	%	Ratio between the mineralized bone volume and the total volume
Trabecular number (Tb.N)	1/mm	Average number of trabeculae per unit length
Trabecular thickness (Tb.Th)	mm	Average thickness of trabeculae
Trabecular separation (Tb.Sp)	mm	Average distance between trabeculae
Structure model index (SMI)	-	Relative presence of either plate-like or rod-like trabeculae. Ranges from 0 (ideal plate) to 3 (ideal rod). Negative values indicate concave trabecular surfaces [a].
Connectivity density (Conn.D)	$1/mm^3$	Degree of connectivity of trabeculae
Degree of anisotropy (DA)	-	Depicts trabecular orientation in a specific direction (higher DA = trabeculae have a preferred orientation; lower DA = trabeculae oriented evenly in all directions) [b,c,d]
Total volume density (TV.Dn)	$mg\ HA/cm^3$	Density of the all tissues within the VOI
Bone volume density (BV.Dn)	$mg\ HA/cm^3$	Density of trabecular bone material within the VOI

[a] – *Hildebrand and Rüegsigger, 1997;* [b] – *Ciarelli et al., 2000;* [c] – *Homminga et al., 2002;* [d] – *Djuric et al., 2010.*

Microarchitectural parameters measured for trabecular bone included (Table 4): bone volume fraction (BV/TV, %), trabecular number (Tb.N, 1/mm), trabecular thickness (Tb.Th, mm), trabecular separation (Tb.Sp, mm), structure model index (SMI, dimensionless), connectivity density (Conn.D, 1/mm3), degree of anisotropy (DA, dimensionless), total volume density (TV.Dn, mg HA/cm3), and bone volume density (BV.Dn, mg HA/cm3).

4.5. Statistical analysis

Shapiro-Wilk test was performed to assess whether the quantitative data of stress and bone microarchitectural parameters are consistent with a Gaussian (normal) distribution. A one-way analysis of variance (ANOVA) was used to determine differences in VMS and principal stress between the nasomaxillary, zygomaticomaxillary, and pterygomaxillary buttress. Stress magnitude in our model was compared to the stress from the study of Prado et al. (2013) by Student's t-test or appropriate non-parametric tests (Mann-Whitney test), depending on the normality of data distribution. The same statistical tests (Student's t-test or Mann-Whitney test) were used to assess the differences in micro-architectural parameters of cortical and trabecular bone between the investigated groups. Relationship between stress and micro-CT parameters of cortical and trabecular bone, as well as the relationship between the individual micro-architectural parameters was performed by Spearman's correlation analysis. Von Mises stress and principal stress measured during unilateral clenching were used in the correlation analysis.

Statistical analysis was performed in Statistical Package for the Social Sciences (SPSS) version 15.0. The statistical significance was evaluated at the level of $p \leq 0.05$.

5. RESULTS

5.1. Evaluation of stress distribution and displacement by finite element analysis

5.1.1. First molar biting

Figure 12 shows distribution of von Mises stress in the cortical and trabecular bone that corresponds to the routes of occlusal load transfer during the first molar loading. The highest stress was concentrated in the buccal and linqual cortical bone of the alveolar process just above the loaded tooth. High stress from this area distributed medially through the anterior cortical wall of the maxilla and upward around the piriform aperture and the frontal process corresponding to the area of the nasomaxillary buttress (Figure 12A,B).
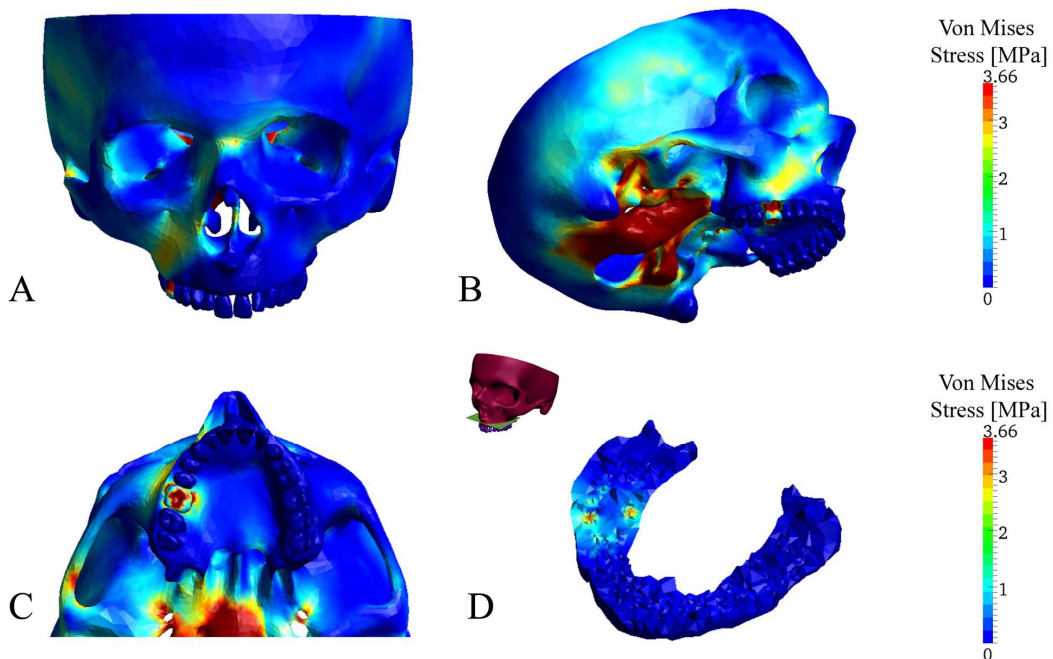
Figure 12. *Stress distribution in the cortical bone (**A** – anterior view, **B** – inferolateral view, **C** – inferior view) and trabecular bone (**D** – section through the alveolar process at the level of the tooth root) during the first molar loading.*

The parts of the zygomaticomaxillary buttress were also visualized by relatively high VMSs along the inferior border of the zygomatic bone and arch, and the lateral orbital margin (Figure 12B,C). Action of the masseter on the loaded side also contributed to the high stress along the temporal process of the zygomatic bone (Figure 12B,C). The anterior part of the nasal septum experienced the stress of the similar magnitude. In the region of the horizontal buttresses, moderate VMSs were observed in the medial part of the supraorbital margin on the unloaded side and at the infraorbital rim on the loaded side (Figure 12A,B). There was no significant stress in the area of the pterygomaxillary buttress and the hard palate. Moderate VMSs in the pterygoid process was due to action of the medial pterygoid muscle (Figure 12B).

In the trabecular bone of the alveolar process, VMS predominantly concentrated around the molar roots and distributed to both buccal and lingual cortical plates (Figure 12D). Trabecular bone of the zygoma showed no significant VMS during molar biting. There was no difference in the maximum value of VMSs registered in cortical and trabecular bone during the first molar biting.

5.1.2. Canine biting

A similar tendency toward the accumulation of VMSs in the buccal cortical plate adjacent to the loaded tooth was also observed during the canine biting (Figure 13A). From this area, high stress distributed upward around the piriform aperture along the nasomaxillary buttress (Figure 13A). Von Mises stress of the similar magnitude was also registered in the anterior part of the nasal septum and the nasofrontal junction (Figure 13A). There were no significant VMSs in the region of the horizontal buttresses, except relatively high stress in the temporal process of the zygomatic bone caused by masseter action (Figure 13B).

In the trabecular bone of the alveolar process, the highest stress was registered around the canine root and distributed predominantly toward the buccal cortical plate (Figure 13C). There was no significant stress in the trabecular compartment of the zygomatic bone. The maximum values of VMSs were similar in both cortical and trabecular bone.
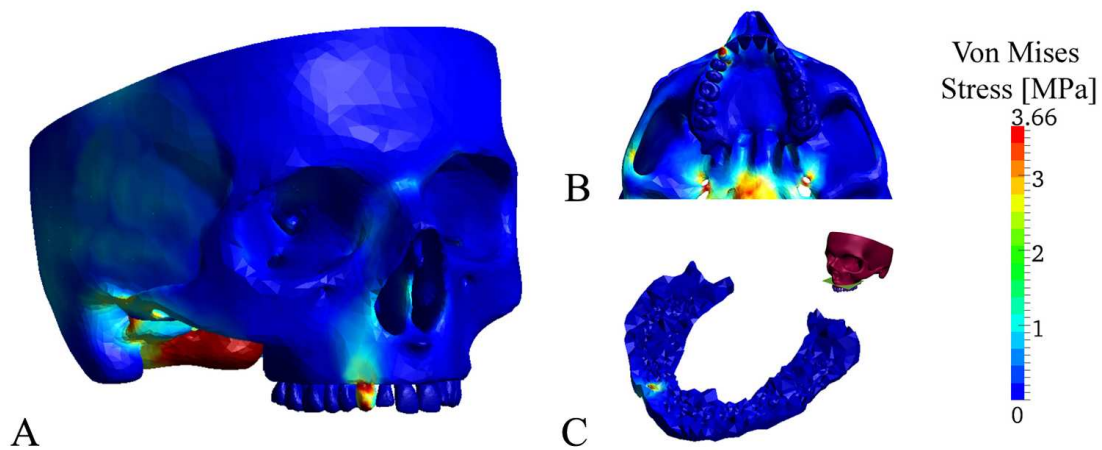
Figure 13. *Stress distribution in the cortical bone (**A** – anterolateral view, **B** – inferior view) and trabecular bone (**C** – section through the alveolar process at the level of the tooth root) during the canine loading.*

5.1.3. Unilateral clenching

Loading of the right half of the dental arch showed directions of occlusal stress distribution through the mid-facial skeleton more clearly. Von Mises stresses were distributed unevenly through both cortical and trabecular bone. The anterior cortical wall of the maxilla experienced the highest stress (Figure 14A,B). Medially, stress was distributed around the piriform aperture and along the frontal process of the maxilla reaching the medial orbital wall and the nasofrontal junction (Figure 14B). From this region, stress further dissipated over the opposite side of the skull along the supraorbital margin and the frontal bone with the gradual decrease in magnitude (Figure 14A). Relatively high stress was also noted in the walls of the nasal cavity on the loaded side. The highest VMSs in this area were registered in the lateral nasal wall and in the anterior half of the nasal septum (Figure 14D). Laterally, stress was distributed in the infrazygomatic crest ascending along the inferior border of the zygomatic bone and arch laterally, and along the lateral orbital rim superiorly (Figure 14D,E). Von Mises stresses in these regions were slightly lower when compared to stresses registered in the anterior maxilla. The area behind the infrazygomatic crest showed low VMS in the cortical bone

with the almost uniform distribution (Figure 14D). Higher stress in this region was observed only in the pterygoid process of the sphenoid bone that could be partially influenced by the action of the medial pterygoid muscle. There was no significant stress in the hard palate on the loaded side (Figure 14E).
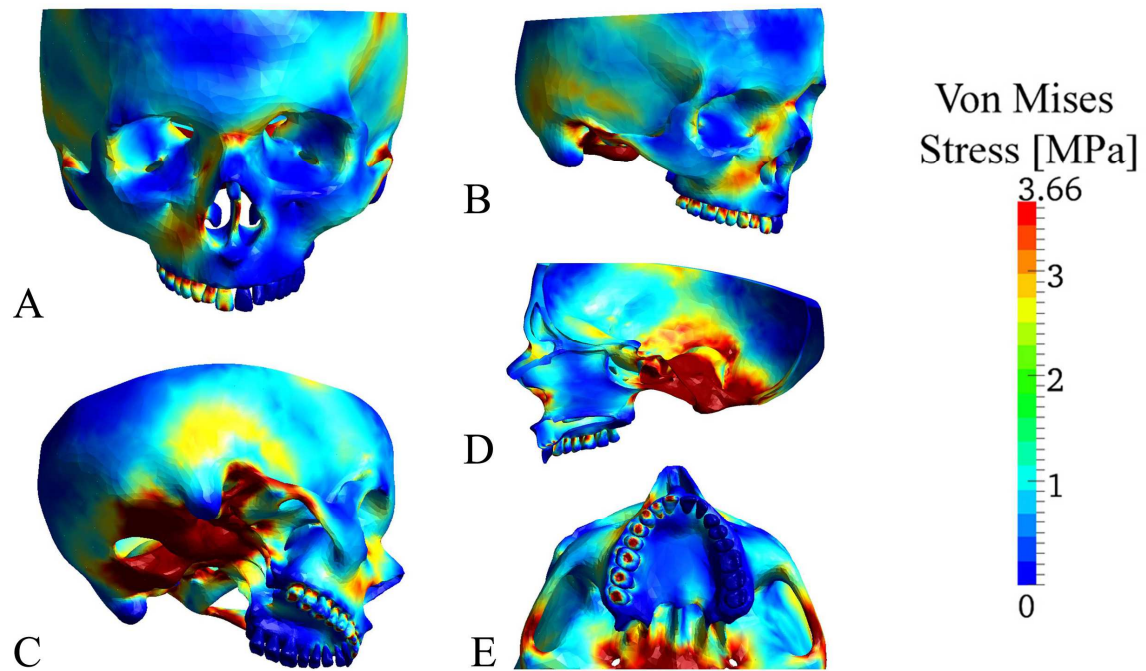
Figure 14. Distribution of von Mises stresses in the cortical bone of the mid-facial skeleton under unilateral clenching (A – anterior view, B – anterolateral view, C – inferolateral view, D – midsagittal section of the skull model, E – inferior view).

Similar pattern of the stress distribution was seen in the cortical bone on the unloaded side, but with significantly lower values. Only slight VMSs were observed around the piriform aperture, along the frontal process of the maxilla medially, and along the zygomatic and temporal processes of the zygomatic bone laterally (Figure 14A,E).

Analysis of principal stresses during unilateral clenching showed that high VMSs in the anterior cortical wall of the maxilla and along the area of the

nasomaxillary buttress corresponded mainly to compressive stress (Figure 15A,B), except a slight tensile stress in the cortex below the infraorbital foramen (Figure 15E,F).
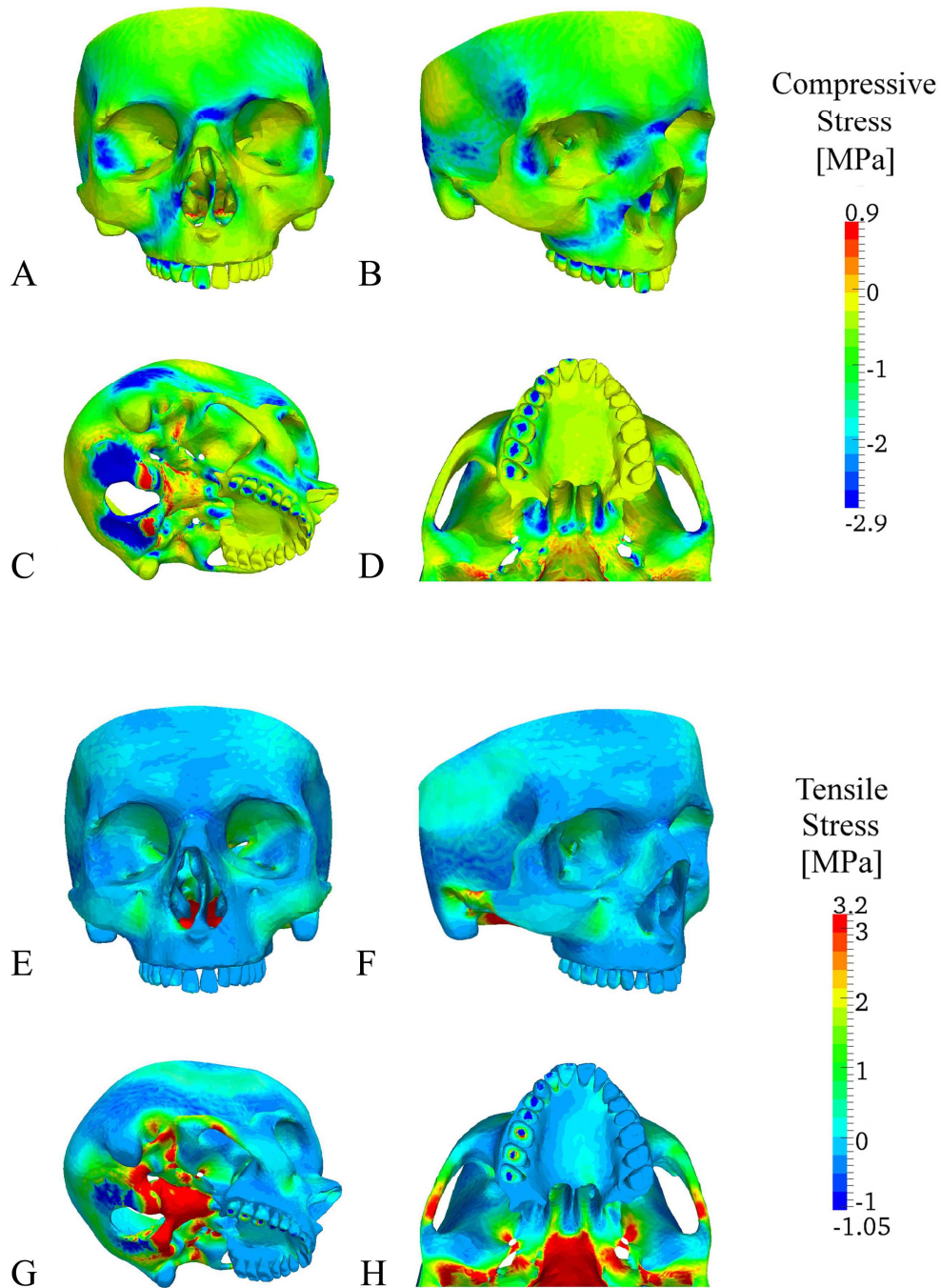
Figure 15. *Distribution of compressive (**A-D**) and tensile (**E-H**) stress in the cortical bone of the mid-facial skeleton under unilateral clenching.*

High VMSs registered in the anterior part of the nasal septum were due to compression (Figure 15A,B). In the region of the zygomaticomaxillary buttress, high VMSs in the infrazygomatic crest and along the lateral orbital rim were compressive in nature (Figure 15B,C). By contrast, VMSs along the inferior border of the zygomatic arch and the lateral aspect of the frontal process of the zygomatic bone were dominantly tensile (Figure 15F,G). The posterior maxillary wall behind the infrazygomatic crest that corresponds to the pterygomaxillary buttress was under slight compression (Figure 15C). Higher compressive stress in this area was registered only in the base of the pterygoid processes (Figure 15C,D), whereas the lateral pterygoid plate showed moderate tensile stress (Figure 15G,H). In the areas of the horizontal buttresses, relatively high compressive stresses were detected only in the supraorbital margin, particularly on the unloaded side (Figure 15A,B). Low tensile stress was registered in the medial aspect of the infraorbital margin (Figure 15A,B).

Von Mises stresses in the trabecular bone on the loaded side were also unevenly distributed (Figure 16A,B). In the trabecular bone of the alveolar process, the highest VMSs were concentrated around the tooth roots and distributed predominantly toward the buccal surface of the cortical bone (Figure 16A). Slightly lower stress was registered in the trabecular part of the zygomatic bone at the loaded side (Figure 16B).

Analysis of maximum principal stress showed that high VMSs in the alveolar process and the zygomatic bone were mainly compressive in nature (Figure 16C,D). There were no areas within the trabecular bone under significant tensile stress during unilateral clenching (Figure 16E,F).

Simulation of unilateral clenching also revealed different patterns of occlusal load distribution in the anterior vs. posterior maxilla. Stress registered in cortical bone anteriorly was significantly higher in magnitude showing the form of buttresses in contrast to lower stress and its nearly uniform distribution in the posterior maxilla (Figure 14A-C). There were no inter-site differences in the maximum VMS values in the trabecular bone along the alveolar process on the loaded side (Figure 16A). Analyzing the distribution of VMSs between cortical and trabecular bone in the anterior vs. posterior maxilla, it was observed that anterior cortical bone experiences almost twice as high stress as the trabecular bone, whereas both bony compartments in the posterior maxilla experienced the same stress.
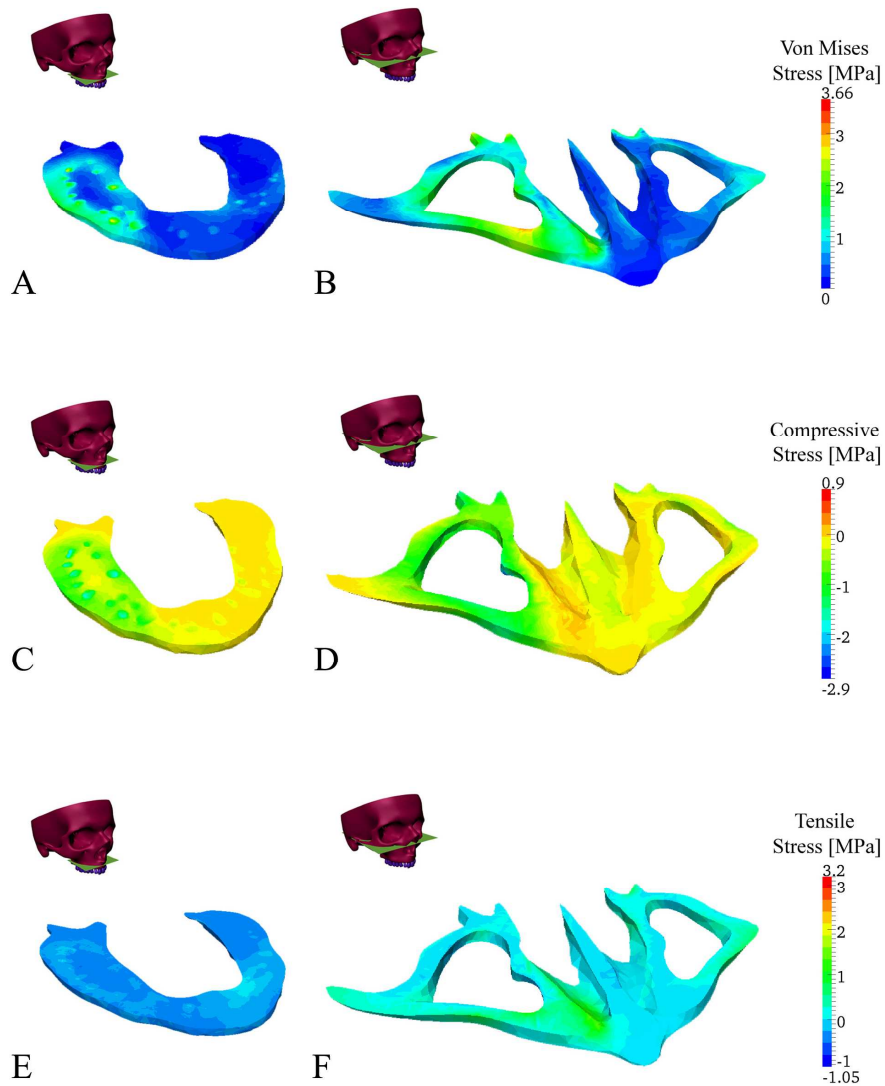
Figure 16. *Distribution of von Mises stresses (**A,B**) and the maximum principal stresses (**C-F**) in the trabecular bone of the alveolar process (**A,C,E**) and the zygomatic bone (**B,D,F**) during unilateral clenching.*

Figure 17 shows effective displacement of the mid-facial skeleton during unilateral clenching. The anterior segment of the facial skeleton, in which the highest VMSs were registered, displayed the largest upward displacement particularly in the region of the frontal process of the maxilla and nasofrontal junction. The same area including the frontal bone also showed more posterior displacement during clenching than other parts of the facial skeleton. There was no significant lateral displacement of the facial skeleton during unilateral clenching.
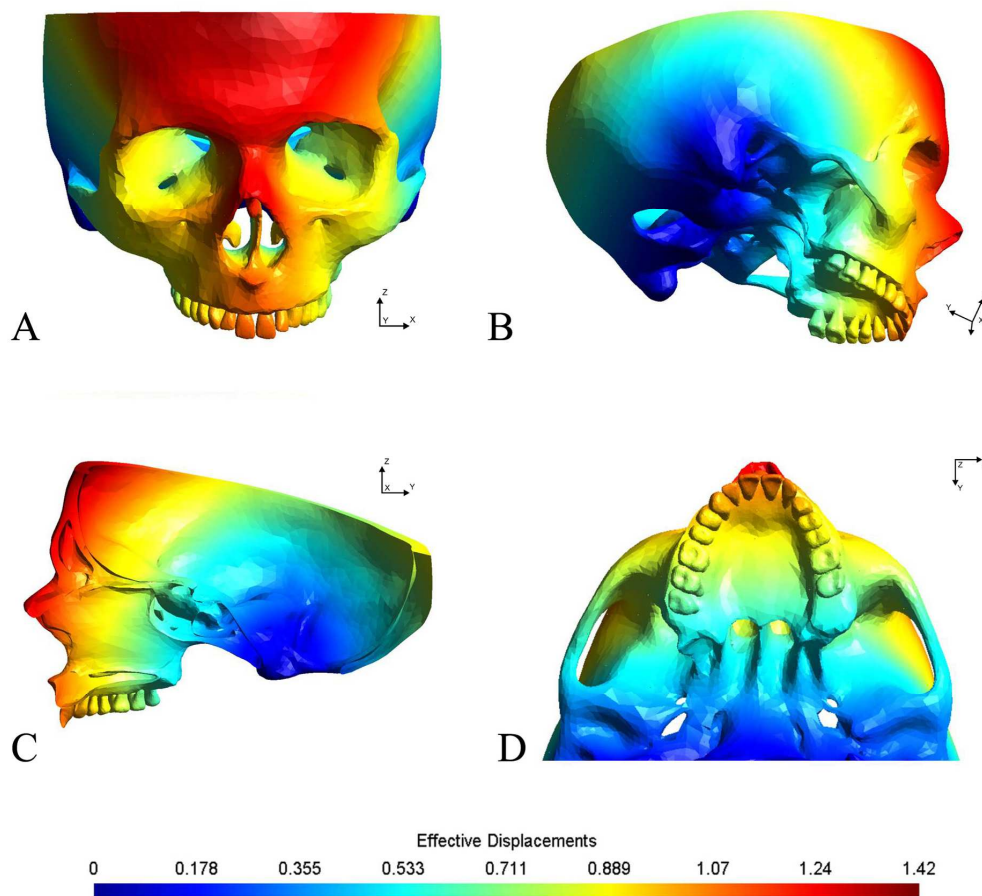
Figure 17. Effective displacement of the mid-facial skeleton during unilateral clenching (A – anterior view, B – lateral view, C – midsagittal section of the skull model, D – inferior view). Scale in mm.

5.1.4. Bilateral clenching

Von Mises stresses in the cortical bone were also unevenly distributed when the full dental arch was loaded simultaneously (Figure 18). The pattern of the VMS distribution on both sides was similar to that observed on the loaded side of the mid-facial skeleton during unilateral clenching, but the magnitude of VMS was slightly different. In the anterior maxilla stress was generally lower, except in the region of the nasofrontal junction and the nasal septum which showed no changes in VMS magnitude

(Figure 18A,C). From the region of the infrazygomatic crest, VMS distributed upward in the same direction, but over the broader area and with slightly increased magnitude (Figure 18B,D). Higher values of VMSs during bilateral clenching were also registered in the pterygoid processes of the sphenoid bone. Bilateral loading of the full dental arch caused no significant stress in the hard palate (Figure 18D).
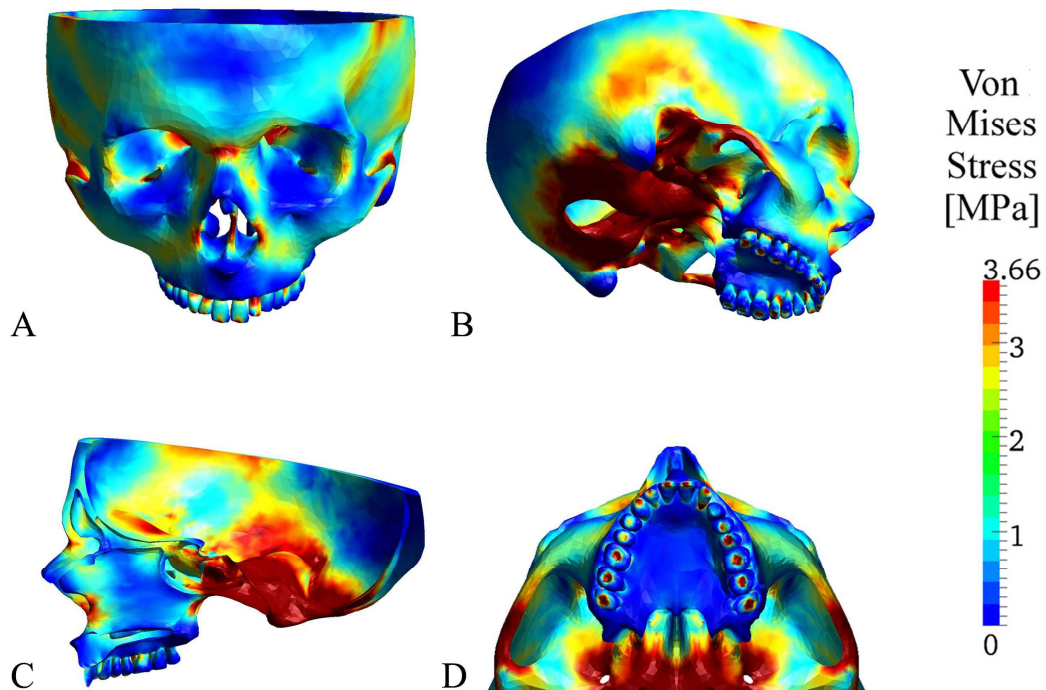
Figure 18. *Stress distribution in the cortical bone of the mid-facial skeleton during bilateral clenching (**A** – anterior view, **B** – anterolateral view, **C** – inferolateral view, **D** – midsagittal section of the skull model, **E** – inferior view).*

Trabecular bone of the alveolar process experienced the same magnitude of VMS as it was registered during unilateral loading accumulating predominantly around the tooth roots (Figure 19A). Low VMS was observed within the trabecular bone of the zygomatic bones (Figure 19B).
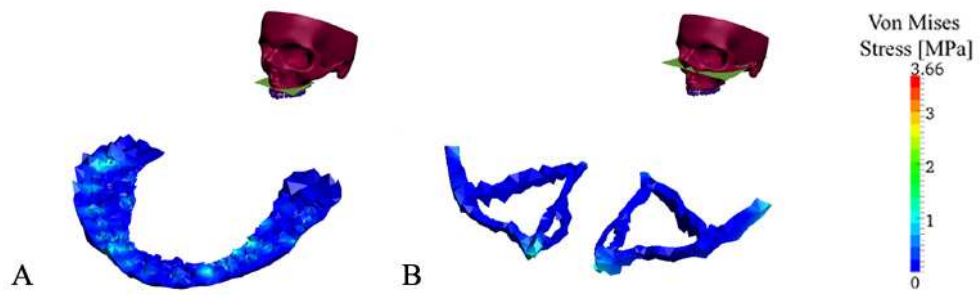
Figure 19. *Distribution of von Mises stress in the trabecular bone of the alveolar process (**A**) and zygomatic bone (**B**) during bilateral clenching.*
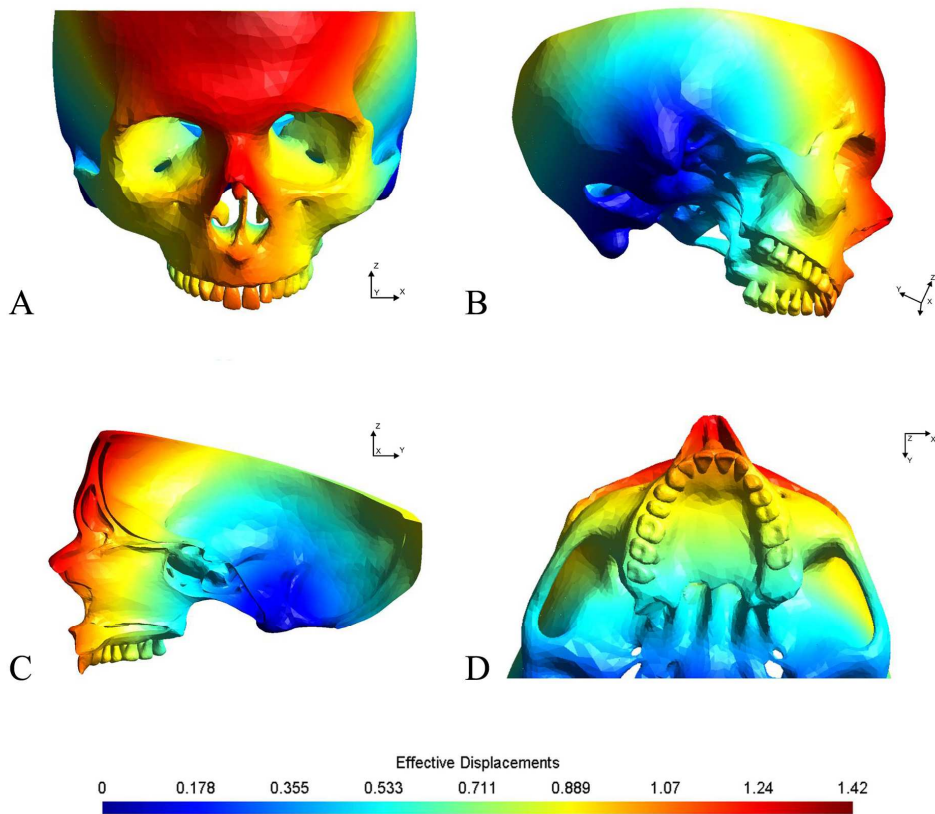
Figure 20. *Effective displacement of the mid-facial skeleton during bilateral clenching (**A** – anterior view, **B** – lateral view, **C** – sagittal section, **D** – inferior view). Scale in mm.*

Effective displacement of the mid-facial skeleton during full dental arch loading was also similar to that observed during unilateral clenching. Slightly higher upward and posterior displacement was evident in the anterior segment of the facial skeleton (Figure 20). Displacement in the lateral direction was no registered.

5.2. Quantitative analysis of stress by finite element analysis

5.2.1. Analysis of stress along the main vertical buttresses

Magnitude of VMS and compressive stress in the cortical bone along the nasomaxillary, zygomaticomaxillary, and pterygomaxillary buttress during unilateral clenching showed their different involvement in the distribution of occlusal loading. Table 5 and 6 displays magnitude of VMS and compressive stress along these vertical buttresses, respectively. The data are presented as mean values with a standard deviation (SD) and standard error (SE). Results of Shapiro-Wilk test showed normal distribution of the data (Table 5 and 6). Tensile stress was not measured due to its absence or extremely low values at the selected measurement sites along the buttresses.

Table 5. *Von Mises stress in the cortical bone along three main vertical buttresses during unilateral clenching.*

Buttress	Von Mises stress (MPa)			Shapiro-Wilk	*p*
	Mean	SD	SE	Z	value
Nasomaxillary	1.99	0.73	0.29	0.87	0.21
Zygomaticomaxillary	1.09	0.33	0.12	0.90	0.36
Pterygomaxillary	1.02	0.33	0.15	0.89	0.36

Table 6. *Compressive stress in the cortical bone along three main vertical buttresses during unilateral clenching.*

Buttress	Compressive stress (MPa)			Shapiro-Wilk	*p*
	Mean	**SD**	**SE**	**Z**	**value**
Nasomaxillary	-1.66	0.76	0.31	0.88	0.29
Zygomaticomaxillary	-0.80	0.39	0.15	0.90	0.35
Pterygomaxillary	-1.10	0.81	0.36	0.87	0.26

Table 7. *Comparative analysis of VMS and compressive stress along the main vertical buttresses assessed by ANOVA with Bonferroni's post-hoc test (NM – nasomaxilary buttress, ZM – zygomaticomaxillary buttress, PM – pterygomaxillary butress).*

Stress	Buttress		Mean Difference (I vs. II)	*p* value
	I	**II**		
Von Mises stress	*NM*	*ZM*	0.89*	0.02
		PM	0.96*	0.02
	ZM	*NM*	-0.89*	0.02
		PM	0.06	1.00
	PM	*NM*	-0.96*	0.02
		ZM	-0.06	1.00
Compressive stress	*NM*	*ZM*	-0.86	0.09
		PM	-0.55	0.56
	ZM	*NM*	0.86	0.09
		PM	0.31	1.00
	PM	*NM*	0.55	0.56
		ZM	-0.31	1.00

* – The mean difference is significant at the 0.05 level.

Cortical bone in the region of the nasomaxillary buttress experienced significantly higher VMS during unilateral clenching in comparison with the zygomaticomaxillary and pterygomaxillary buttress (Table 7). The nasomaxillary buttress also showed the highest compressive stress that did not reach the level of statistical significance. Cortical bone along the zygomaticomaxillary and pterygomaxillary buttress experienced similar VMS, while the slightly higher compressive stress was detected in the later (Table 7).

5.2.2. Comparative analysis of stress between our model and the model of Prado et al. (2013)

Table 8 shows mean value and standard deviation of VMS and maximum principal stress measured in cortical bone along the zygomaticomaxillary buttress in our model and in the FE model of Prado et al. (2013). Both studies provided similar distribution of VMSs (Chart 2A), but the values registered in our model were much lower (Table 8). However, the observed difference in the magnitude of VMS was not statistically significant (Table 8). Significant differences were found in the distribution (Chart 2B) and the magnitude of the maximum principal stress between the two studies (Table 8). Tensile stress at the attachment site of the masseter muscle was the only that completely matched, while other sites showed again lower values of the maximum principal stress in our study (Chart 2B).

Table 8. *Von Mises stress and the maximum principal stress in cortical bone of the zygomaticomaxillary buttress in our study and in the study of Prado et al. (2013).*

Stress	Our study	Prado et al., 2013	*p* value
Von Mises stress	1.54 (0.30)	6.04 (1.74)	0.06 [a]
Maximum principal stress	-0.10 (0.69)	2.26 (0.72)	0.04 [a]

[a] – *Student's t–test*
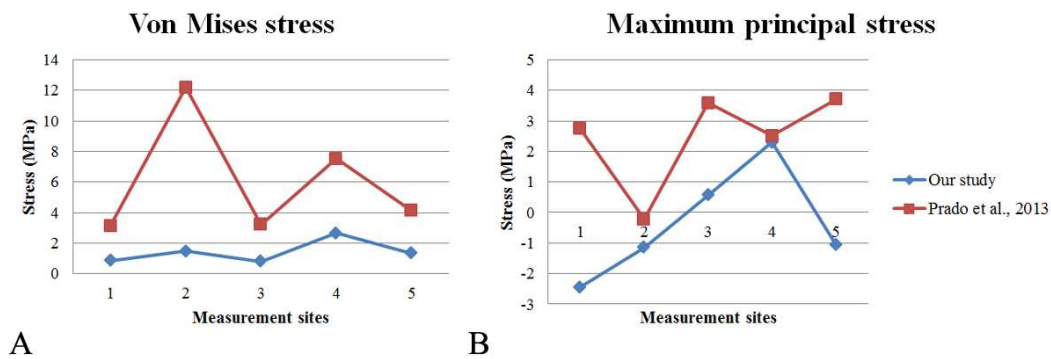
Chart 2. *Comparative analysis of VMS (**A**) and the maximum principal stress (**B**) measured along the zygomaticomaxillary buttress in our study and in the study by Prado et al. (2013).*

5.2.3. Analysis of stress in the high stress and low stress group

Table 9 summarizes an average values of VMS measured during unilateral clenching in cortical and trabecular bone from *high stress* and *low stress group*, respectively. Von Mises stress in the cortical bone from *high stress group* varied from 2.25 MPa to 2.75 MPa, whereas the *low stress group* experienced VMS between 0.65 MPa and 1.49 MPa. For the trabecular bone, VMS ranged from 0.49 to 1.67 MPa in the *high stress group*, whereas the *low stress group* experienced between 0.25 MPa and 0.46 MPa (Table 9).

Magnitude of compressive stress registered in cortical and trabecular bone from *high* and *low stress group* is displayed in Table 10. Tensile stress was not measured because the selected sites in the cortical and trabecular bone from both groups were mainly subjected to compression during unilateral clenching. Cortical and trabecular bone from *high stress group* experienced higher compressive stress than *low stress group* (Table 10).

Table 9. *Von Mises stress measured during unilateral clenching in cortical and trabecular bone from high stress and low stress group.*

Bone compartment (number of samples)	Von Mises stress (MPa)		
	Mean	SD [a]	SE [b]
Cortical bone			
High stress group (n=7)	2.53	0.19	0.07
Low stress group (n=18)	1.05	0.28	0.07
Trabecular bone			
High stress group (n=6)	0.95	0.56	0.23
Low stress group (n=7)	0.37	0.08	0.03

[a] – standard deviation; [b] – standard error.

Table 10. *Compressive stress registered during unilateral clenching in cortical and trabecular bone from high stress and low stress group.*

Bone compartment (number of samples)	Compressive stress (MPa)		
	Mean	SD [a]	SE [b]
Cortical bone			
High stress group (n=7)	-1.86	0.84	0.32
Low stress group (n=18)	-0.88	0.50	0.12
Trabecular bone			
High stress group (n=6)	-0.70	0.41	0.17
Low stress group (n=7)	-0.26	0.10	0.04

[a] – standard deviation; [b] – standard error.

5.3. Evaluation of the mid-facial bone microarchitecture in relation to occlusal stress

5.3.1. Analysis of cortical bone microarchitecture in relation to occlusal stress

Table 11 and 12 show microarchitectural parameters of cortical bone of the mid-facial skeleton assessed in *high stress* and *low stress group*, respectively. Each parameter is presented as mean value with a standard deviation (SD). All parameters in *high stress group* showed normal distribution (Table 11), while cortical thickness (Ct.Th) in the *low stress group* was the only parameter that was not normally distributed (Table 12).

Table 11. *Microarchitectural parameters of cortical bone from high stress group with Shapiro-Wilk test for normality of data distribution.*

Parameter	Mean	SD	Shapiro-Wilk Z	*p* value
Ct.Th	1.84	0.86	0.97	0.90
Ct.Po	8.67	3.58	0.93	0.57
Po.Dm	0.15	0.06	0.89	0.31
Po.Sp	0.41	0.04	0.95	0.69
TV.Dn	927.09	32.86	0.97	0.87
BV.Dn	1019.05	20.10	0.92	0.46

Table 12. *Microarchitectural parameters of cortical bone from low stress group with Shapiro-Wilk test for normality of data distribution.*

Parameter	Mean	SD	Shapiro-Wilk Z	*p* value
Ct.Th	1.55	0.65	0.89	0.04
Ct.Po	11.71	5.81	0.94	0.28
Po.Dm	0.14	0.03	0.96	0.51
Po.Sp	0.37	0.07	0.97	0.74
TV.Dn	883.04	90.61	0.97	0.74
BV.Dn	1000.29	48.37	0.95	0.39

Comparison of micro-architectural parameters of cortical bone between *high stress* and *low stress group* showed greater cortical thickness (Ct.Th) and slightly greater bone volume density (BV.Dn) in the regions where cortical bone was subject to high occlusal stress (Table 13). In the *high stress group*, cortical bone was less porous (Ct.Po) with increased distance between pores (Po.Sp) in comparison to the *low stress group* (Table 13). Similar diameter of pores (Po.Dm) was detected in both groups. However, observed differences in cortical bone microarchitecture between groups were not statistically significant. Representative cortical bone specimens from both groups are shown in Figure 21.

Table 13. *Microarchitectural parameters of cortical bone (reported as mean with standard error of mean) in the high stress group (HSG) and low stress group (LSG).*

Parameter	High stress group (n = 7)	Low stress group (n = 18)	HSG vs. LSG difference (%)	*p*
Ct.Th (mm)	1.84 (0.33)	1.55 (0.15)	-15.8	0.43[a]
Ct.Po (%)	8.67 (1.35)	11.71 (1.37)	25.9	0.21[b]
Po.Dm (mm)	0.15 (0.02)	0.14 (0.01)	-0.1	0.68[b]
Po.Sp (mm)	0.41 (0.02)	0.37 (0.02)	-9.8	0.25[b]
TV.Dn (mg HA/cm^3)	927.09 (12.42)	883.04 (21.36)	-4.7	0.09[b]
BV.Dn (mg HA/cm^3)	1019.05 (7.59)	1000.29 (11.40)	-1.9	0.18[b]

[a] *– Mann-Whitney test;* [b] *– Student's t-test*

Correlation analysis between microarchitectural parameters of cortical bone showed that increase in cortical thickness (Ct.Th) is accompanied by significant increase in bone volume tissue density (BV.Dn) and pore separation (Po.Sp) (Table 14). Other parameters, such as cortical porosity (Ct.Po), also showed a significant positive correlation with Po.Dm, whereas it correlated negatively with pore separation (Po.Sp) and cortical density (TV.Dn and BV.Dn).

Sample Nº 6
(VMS 2.56 MPa)

Sample Nº 21
(VMS 0.86 MPa)

Figure 21. *The 3D reconstruction image of cortical bone specimen from high stress (**A**) and low stress group (**B**) scanned by micro-CT. Von Mises stress experienced by each bone specimen was shown in brackets.*

Table 14. *Correlation analysis between stress and microarchitectural parameters of cortical bone (Spearman's correlation coefficient displayed in white cells, p value displayed in gray cells).*

Parameter	VMS	CS	Ct.Th	Ct.Po	Po.Dm	Po.Sp	TV.Dn	BV.Dn
VMS	1.000	-0.601**	0.179	-0.351	-0.075	0.378	0.375	0.290
CS	0.002	1.000	-0.136	-0.048	-0.077	-0.244	-0.025	-0.094
Ct.Th	0.391	0.516	1.000	-0.260	0.305	0.760**	0.551*	0.763**
Ct.Po	0.086	0.818	0.251	1.000	0.586**	-0.408**	-0.918**	-0.625**
Po.Dm	0.723	0.716	0.089	0.004	1.000	0.214	-0.395	-0.093
Po.Sp	0.062	0.240	<0.001	0.043	0.305	1.000	0.637**	0.755**
TV.Dn	0.065	0.906	<0.001	<0.001	0.108	0.001	1.000	0.860**
BV.Dn	0.160	0.654	<0.001	0.005	0.965	<0.001	<0.001	1.000

* Correlation is significant at the 0.05 level (2-tailed).

** Correlation is significant at the 0.01 level (2-tailed).

Although a significant correlation between VMS or compressive stress and particular microarchitectural parameter of cortical bone was not statistically detected (Table 14), we noticed differences in Ct.Po and Po.Dm between individual cortical bone samples of similar thickness and desity that experienced significantly different stresses during clenching. The greatest differences were detected between the cortex of the anterior wall of the maxilla below the infraorbital foramen and the posterior maxillary wall (Figure 22). Cortical bone from the posterior maxilla was three times more porous with two times greater pore diameter than the cortical bone from the anterior wall of the maxilla (Figure 22). Other cortical bone samples of similar Ct.Th and BV.Dn but different VMSs also showed similar variations in Ct.Po and Po.Dm, e.g., cortex of the zygomatic arch and the inferior orbital rim, with the two times greater Ct.Po in the latter.

Parameter	Sample 20	Sample 25
Ct.Th (mm)	0.71	0.77
Ct.Po (%)	0.04	0.12
Po.Dm (mm)	0.06	0.11
BV.Dn (mg HA/cm³ bone area)	984	977
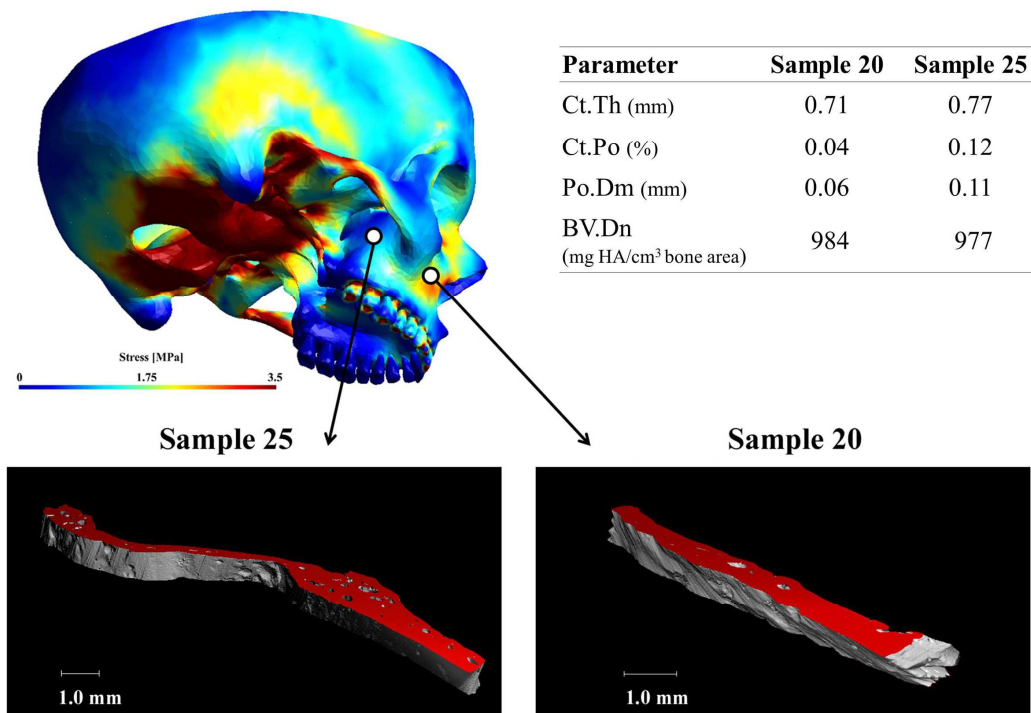
Figure 22. Differences in Ct.Po and Po.Dm between anterior and posterior cortical bone with similar thickness and density that experienced different stresses during clenching (sample No. 20 taken from the anterior maxillary wall; sample No. 25 harvested from the posterior maxillary wall).

5.3.2. Analysis of trabecular bone microarchitecture in relation to occlusal stress

Microarchitectural parameters of trabecular bone of the mid-facial skeleton in *high stress* and *low stress group* are summarized in Table 15 and 16, respectively. Results of Shapiro-Wilk test for normality of data distribution for both groups are also shown in the corresponding tables (Table 15 and 16). Only bone volume fraction (BV/TV), tissue volume density (TV.Dn), and bone volume density (BV.Dn) showed normal distribution in both groups (Table 15 and 16).

***Table 15**. Microarchitectural parameters of trabecular bone from high stress group with Shapiro-Wilk test for normality of data distribution.*

Parameter	Mean	SD	Shapiro-Wilk Z	*p* value
BV/TV	60.69	16.72	0.85	0.16
Tb.N	3.81	1.29	0.73	0.01
Tb.Th	0.32	0.04	0.71	0.01
Tb.Sp	0.35	0.13	0.79	0.04
SMI	-1.32	2.99	0.78	0.04
Conn.D	26.02	13.47	0.97	0.90
DA	1.91	0.77	0.78	0.04
TV.Dn	599.03	186.57	0.877	0.26
BV.Dn	993.07	13.45	0.837	0.12

Table 16. *Microarchitectural parameters of trabecular bone from low stress group with Shapiro-Wilk test for normality of data distribution.*

Parameter	Mean	SD	Shapiro-Wilk Z	*p* value
BV/TV	43.05	4.52	0.88	0.22
Tb.N	3.09	0.45	0.92	0.49
Tb.Th	0.25	0.05	0.91	0.36
Tb.Sp	0.42	0.08	0.91	0.41
SMI	0.09	0.94	0.76	0.02
Conn.D	35.49	23.12	0.79	0.03
DA	1.77	0.44	0.84	0.11
TV.Dn	394.37	67.96	0.94	0.63
BV.Dn	961.64	37.97	0.98	0.96

Sample Nº 12
(VMS 1.61 MPa)
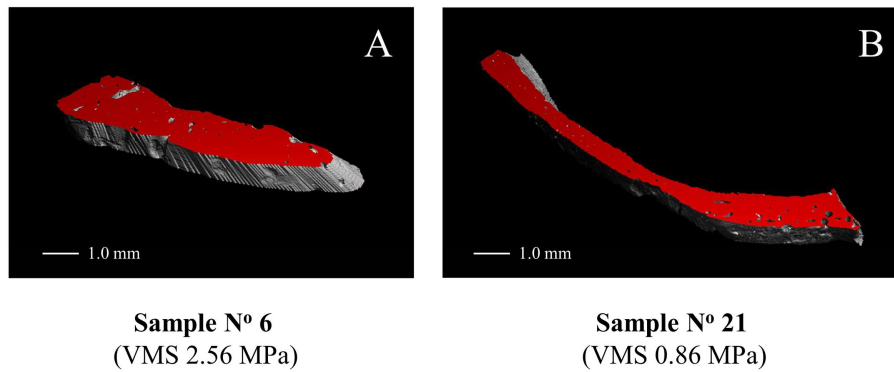
Sample Nº 3
(VMS 0.27 MPa)
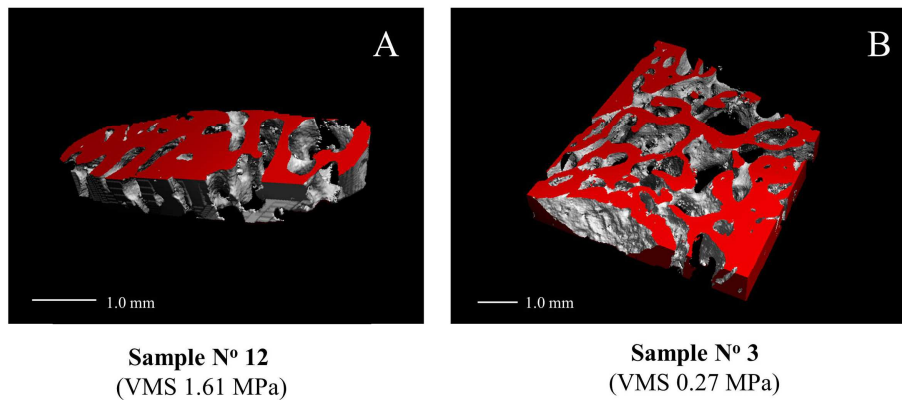
Figure 23. The 3D reconstruction image of trabecular bone specimen from high stress (A) and low stress group (B) scanned by micro-CT. Von Mises stress experienced by each bone specimen was shown in brackets.

There were differences in trabecular bone microarchitecture of the mid-facial bones between *high stress* and *low stress group* (Table 17). Trabecular bone that experienced high stress had significantly greater bone volume fraction (BV/TV), trabecular thickness (Tb.Th), and tissue volume density (TV.Dn) when compared to the *low stress group*. Trabecular number (Tb.N), degree of anisotropy (DA), and bone volume density (BV.Dn) were also greater in the *high stress group*. In the areas subjected to low stress, trabecualae were more separated (Tb.Sp) and more interconnected (Conn.D) than in the regions subjected to high stress. Trabeculae from both areas also differed in shape (SMI). Trabeculae from the *low stress group* showed plate-like shape, while trabeculae from *high stress group* had concave surfaces (negative SMI). However, these differences in trabecular bone microarchitecture between the groups did not reach the level of statistical significance. Representative trabecular bone specimens from both groups are shown in Figure 23.

Correlation analysis showed that an increase in VMS as well as compressive stress magnitude is accompanied by a significant increase in trabecular BV/TV and TV.Dn (Table 18). The statistically significant positive correlation was also noted between BV/TV and Tb.N (Table 18). Increase in BV/TV was also accompanied by a significant increase in both TV.Dn and BV.Dn. Trabecular number showed a significant negative correlation with Tb.Sp, whereas it correlated positively with Conn.D, TV.Dn and BV.Dn (Table 18).

Table 17. *Microarchitectural parameters of trabecular bone (reported as mean with standard error of mean) in high stress group (HSG) and low stress group (LSG).*

Parameter	High stress group (n = 6)	Low stress group (n = 7)	HSG vs. LSG difference (%)	p
BV/TV (%)	60.69 (6.83)	43.05 (1.71)	-29.1	0.02 [a]
Tb.N (1/mm)	3.81 (0.53)	3.09 (0.17)	-18.9	0.19 [b]
Tb.Th (mm)	0.32 (0.01)	0.25 (0.02)	-21.9	0.02 [b]
Tb.Sp (mm)	0.35 (0.05)	0.42 (0.03)	16.7	0.39 [b]
SMI	-1.32 (1.22)	0.09 (0.35)	-	0.25 [b]
Conn.D ($1/mm^3$)	26.02 (5.50)	35.49 (8.74)	26.7	0.57 [b]
DA	1.91 (0.31)	1.77 (0.17)	-7.3	0.89 [b]
TV.Dn (mg HA/cm^3)	599.03 (76.17)	394.37 (25.69)	-34.2	0.02 [a]
BV.Dn (mg HA/cm^3)	993.07 (5.49)	961.64 (14.35)	-3.1	0.08 [a]

[a] *– Student's t-test;* [b] *– Mann-Whitney test*

Table 18. *Correlation analysis between stress and microarchitectural parameters of trabecular bone (Spearman's correlation coefficient displayed in white cells, p value displayed in gray cells).*

Parameter	VMS	CS	BV/TV	Tb.N	Tb.Th	Tb.Sp	SMI	Conn.D	DA	TV.Dn	BV.Dn
VMS	1.000	-0.975**	0.609*	0.317	0.466	-0.303	-0.397	0.022	0.107	0.656*	0.355
CS	<0.001	1.000	-0.655*	-0.396	-0.421	0.355	0.393	-0.066	-0.168	-0.724**	-0.424
BV/TV	0.027	0.015	1.000	0.615*	0.346	-0.451	-0.451	0.055	0.478	0.956**	0.659*
Tb.N	0.292	0.180	0.025	1.000	-0.049	-0.819**	-0.291	0.599*	0.473	0.698**	0.698**
Tb.Th	0.109	0.152	0.247	0.873	1.000	0.132	-0.159	-0.505	-0.352	0.346	0.236
Tb.Sp	0.314	0.234	0.122	0.001	0.668	1.000	0.291	-0.582*	-0.549	-0.599*	-0.758**
SMI	0.180	0.184	0.122	0.334	0.603	0.334	1.000	-0.022	-0.220	-0.390	-0.187
Conn.D	0.943	0.830	0.859	0.031	0.078	0.037	0.943	1.000	0.269	0.137	0.275
DA	0.727	0.584	0.098	0.103	0.239	0.052	0.471	0.374	1.000	0.495	0.538
TV.Dn	0.015	0.005	<0.001	0.008	0.247	0.031	0.188	0.655	0.086	1.000	0.802**
BV.Dn	0.233	0.149	0.014	0.008	0.437	0.003	0.541	0.364	0.058	0.001	1.000

* Correlation is significant at the 0.05 level (2-tailed).

** Correlation is significant at the 0.01 level (2-tailed).

5.4. Evaluation of the facial bone microarchitecture in relation to Le Fort fracture lines

5.4.1. Analysis of cortical bone microarchitecture in relation to Le Fort fracture lines

Average values of microarchitectural parameters of cortical bone from *Le Fort* and *Non-Le Fort group* are shown in Table 19 and 20. The data are presented as mean value with a standard deviation (SD). All microarchitectural parameters showed normal distribution in both groups (Table 19 and 20).

Table 19. *Microarchitectural parameters of cortical bone from Le Fort group with Shapiro-Wilk test for normality of data distribution.*

Parameter	Mean	SD	Shapiro-Wilk Z	*p* value
Ct.Th	1.50	0.63	0.93	0.36
Ct.Po	11.48	5.67	0.88	0.08
Po.Dm	0.15	0.04	0.97	0.88
Po.Sp	0.38	0.08	0.89	0.10
TV.Dn	885.71	92.72	0.93	0.37
BV.Dn	1000.58	51.59	0.95	0.69

Table 20. *Microarchitectural parameters of cortical bone from Non-Le Fort group with Shapiro-Wilk test for normality of data distribution.*

Parameter	Mean	SD	Shapiro-Wilk Z	*p* value
Ct.Th	1.75	0.79	0.94	0.41
Ct.Po	10.28	5.28	0.94	0.41
Po.Dm	0.13	0.04	0.93	0.30
Po.Sp	0.39	0.05	0.98	0.97
TV.Dn	904.29	70.19	0.97	0.92
BV.Dn	1010.11	34.31	0.95	0.54

The greatest intergroup differences were detected in Ct.Th, Ct.Po and Po.Dm (Table 21). Cortical bone along the Le Fort fracture lines was thinner, more porous with larger pores when compared to the sites away from the fracture lines. Le Fort group also showed slightly lower bone density (TV.Dn and BV.Dn). However, none of the detected differences was statistically significant (Table 21).

Table 21. Microarchitectural parameters of cortical bone (reported as mean with a standard error of mean) in Le Fort group (LF) and non-Le Fort group (NLF).

Parameter	Le Fort group (n = 12)	Non-Le Fort group (n = 13)	LF vs. NLF difference (%)	p [a]
Ct.Th (mm)	1.50 (0.18)	1.75 (0.22)	16.6	0.39
Ct.Po (%)	11.48 (1.64)	10.28 (1.47)	-10.4	0.59
Po.Dm (mm)	0.15 (0.01)	0.13 (0.01)	-13.3	0.33
Po.Sp (mm)	0.38 (0.02)	0.39 (0.01)	2.6	0.63
TV.Dn (mg HA/cm^3)	885.71 (26.76)	904.29 (19.47)	2.1	0.58
BV.Dn (mg HA/cm^3)	1000.58 (14.89)	1010.11 (9.51)	0.9	0.59

[a] *– the difference between parameters assessed by Student's t-test*

5.4.2. Analysis of trabecular bone microarchitecture in relation to Le Fort fracture sites

Table 22 and 23 display microarchitectural parameters of trabecular bone in *Le Fort* and *Non-Le Fort group*, presented as mean value with a standard deviation (SD). The results of Shapiro-Wilk test demonstrated normal distribution of the following parameters in both groups: trabecular thickness (Tb.Th), trabecular separation (Tb.Sp), and bone volume density (BV.Dn).

Table 22. *Microarchitectural parameters of trabecular bone from Le Fort group with Shapiro-Wilk test for normality of data distribution.*

Parameter	Mean	SD	Shapiro-Wilk Z	*p* value
BV/TV	53.06	16.06	0.84	0.14
Tb.N	3.63	1.32	0.75	0.02
Tb.Th	0.28	0.06	0.83	0.11
Tb.Sp	0.37	0.13	0.89	0.29
SMI	-0.10	0.84	0.90	0.38
Conn.D	29.00	23.47	0.79	0.05
DA	2.14	0.69	0.86	0.19
TV.Dn	514.94	185.00	0.88	0.28
BV.Dn	986.16	17.38	0.92	0.50

Table 23. *Microarchitectural parameters of trabecular bone from Non-Le Fort group with Shapiro-Wilk test for normality of data distribution.*

Parameter	Mean	SD	Shapiro-Wilk Z	*p* value
BV/TV	49.58	14.13	0.73	0.01
Tb.N	3.24	0.59	0.86	0.16
Tb.Th	0.29	0.05	0.89	0.27
Tb.Sp	0.40	0.09	0.88	0.23
SMI	-0.94	2.91	0.74	0.01
Conn.D	32.92	16.32	0.85	0.11
DA	1.58	0.34	0.73	0.01
TV.Dn	466.45	162.46	0.80	0.05
BV.Dn	967.57	41.06	0.94	0.67

Comparison of microarchitectural parameters of trabecular bone between the groups showed the differences in structure model index (SMI), degree of anisotropy (DA), connectivity density (Conn.D), and tissue volume density (TV.Dn) (Table 24). However, only the difference in DA was statistically significant. Trabecular bone from Le Fort fracture sites showed minor differences in other microarchitectural parameters when compared to the *Non-Le Fort group* (Table 24).

Table 24. *Microarchitectural parameters of trabecular bone (reported as mean with a standard error of mean) in Le Fort group (LF) and non-Le Fort group (NLF).*

Parameter	Le Fort group (n = 6)	Non-Le Fort group (n = 7)	LF vs. NLF difference (%)	*p*
BV/TV (%)	53.06 (6.56)	49.58 (5.34)	-7.02	0.47 [a]
Tb.N (1/mm)	3.63 (0.54)	3.24 (0.22)	-2.04	0.78 [a]
Tb.Th (mm)	0.28 (0.03)	0.29 (0.02)	3.57	0.89 [b]
Tb.Sp (mm)	0.37 (0.05)	0.40 (0.03)	8.11	0.65 [b]
SMI	-0.10 (0.34)	-0.94 (1.10)	-	0.87 [a]
Conn.D (1/mm^3)	29.00 (9.58)	32.92 (6.17)	13.52	0.25 [a]
DA	2.14 (0.28)	1.58 (0.13)	-35.44	0.02 [a]
TV.Dn (mg HA/cm^3)	514.94 (75.53)	466.45 (61.41)	-10.39	0.48 [a]
BV.Dn (mg HA/cm^3)	986.16 (7.09)	967.57 (15.52)	-1.92	0.31 [b]

[a] - *Mann-Whitney test;* [b] - *Student's t-test.*

6. DISCUSSION

6.1. Distribution of occlusal forces through the mid-facial skeleton: insight from finite element analysis

6.1.1. Both cortical and trabecular bone transfer occlusal forces through the mid-facial skeleton

The pattern of occlusal load distribution through the mid-facial skeleton observed in our study was partially consistent with the classical theory of buttresses. Areas of the nasomaxillary and zygomaticomaxillary buttresses were clearly seen in the cortical bone with the higher stress registered in the former. These sites also exhibited the highest strains in dry human skulls during artificial tooth loading (Endo, 1965). The distribution of compressive and tensile stresses along the two buttresses in our model was in line with the reported strain gauge data (Endo, 1965). Similar to Endo's findings (1970), we also demonstrated that the action of the masseter and the temporalis muscle contribute to the tensile stresses in the zygomatic arch and the lateral part of the frontal process of the zygomatic bone. In contrast to the cortical bone, significantly lower stress in the trabecular bone of the anterior maxilla during clenching indicates that cortical bone, particularly the buccal plate, bears most of the occlusal load anteriorly. This finding is corroborated by the study of Peterson et al. (2006), who found the greatest cortical thickness and density in the region of the nasomaxillary and the zygomaticomaxillary buttresses. These authors suggested that such structural properties in combination with greater cortical stiffness may ensure that anterior maxilla withstands relatively high occlusal loads (Peterson et al., 2006). Furthermore, the mechanical competence of the cortical bone along the two buttresses was also confirmed in clinical practice. Their importance for the maintenance of the masticatory function is supported by the fact that surgical reconstruction and reinforcement of these buttresses after trauma are essential in the treatment of the mid-facial fractures (Miloro et al., 2004; Erkmen et al., 2009; Pollock, 2012).

Interestingly, we observed relatively high stress in the anterior cortical wall of the maxilla placed between the buttresses (Figure 14). This contrasts with the classical

belief that this part of the maxilla is not involved in the occlusal load dissipation due to its thin cortical bone structure (Cryer, 1916). Although we noticed that the stress distribution in the previous FE studies (Gross et al., 2001; Cattaneo et al., 2003; Prado et al., 2013) were similar to our finding, there were no comments about the importance of this region in the overall load transfer. Only Peterson et al. (2006) in the study that was not based on FE analysis proposed that, regardless of the thickness, greater density of cortical bone in this area could be due to its involvement in the occlusal load transfer. Additionally, lower cortical bone porosity and pore diameter detected in our study also support this hypothesis (Figure 22).

Our results do not support the classic proposal that occlusal load transfer in the posterior maxilla follows the route of the pterigomaxillary buttress. This area had been occasionally analyzed in the previous strain gauge and FE studies. Only Endo (1965) found much lower strain values in the cortical bone in the posterior vs. anterior maxilla, which led him to conclude that "the human facial skeleton may be more adapted to chew with posterior teeth". Concerning the fact that stress in cortical and trabecular bone of the posterior maxilla in our model were of the similar magnitude, it is likely that both osseous compartments are equally involved in the occlusal load dissipation. This could also explain why the posterior maxillary cortex showed lower occlusal stress in comparison with the anterior cortex. However, there are divided opinions over the relative involvement of cortical and trabecular bone in the occlusal load transfer in this region, based on the FE analyses of dental implants. Some authors have suggested that cortical bone is more important in the load transfer, because thicker cortex and/or larger contact area between cortical bone and implant may reduce stress to the surrounding bone and thus prevent complications associated with an implant overloading (Akca et al., 2008; Qian et al., 2009; Alikhasi et al., 2014). Other authors have emphasized that trabecular bone also plays a significant role in the occlusal load buffering and transferring to the adjacent cortical bone (Nomoto et al., 2006; Ohashi et al., 2010). The posterior maxilla contains more voluminous trabecular bone, while the cortical bone is thinner and less dense then anteriorly (Cryer, 1916; Standring, 2005; Peterson et al., 2006). The stiffness of cortical bone is also much lower in this region (Peterson et al., 2006), which could limit its ability to resist high loads from molar biting if trabecular bone do not participate in the transfer of occlusal loads. Some authors also underlined the structural analogy between the posterior maxilla and the epiphyses of the long bones, which had been described to distribute the load over a broader area (Peterson et

al., 2006). Numerous tooth roots and greater surface area of the periodontal ligament in the molars could also provide more effective transfer of occlusal forces from the teeth to the bone in the posterior maxilla.

6.1.2. The role of the nasal septum in the occlusal load transfer

The classical theory assumed the nasal septum as supporting buttress (Cryer, 1916), but recent studies suggest that it might be of the same importance for the dissipation of occlusal forces to the anterior skull base like vertical buttresses (Hilloowala and Kanth, 2007; Pollock, 2012). Our results also support the direct involvement of the septum in the occlusal load transfer. Although thin, the bones of the nasal septum were considered mechanically stable since they contain no penetrations of blood vessels or nerves that might compromise their structure (Pollock, 2012). However, little experimental work has been done to examine the biomechanics of the septum in humans. A few studies on animals showed that the main function of the septal cartilage and associated soft tissues is to ensure the structural integrity of the septum by absorbing the forces generated during mastication (Kim et al., 2005; Al Dayeh et al., 2009; Lee et al., 2010), while the role of the bony septum was not discussed.

6.1.3. The role of cortical bone along horizontal buttresses in the occlusal load transfer

It has been reported recently that cortical bone in the region of the horizontal buttresses in animals may adapt its structure in response to increased occlusal loading (He and Kiliaridis, 2003; Menegaz et al., 2009; Dechow et al., 2010). Additionally, the thickness of the hard palate was recognized as a significant masticatory related characteristic important for hominid phylogeny (Strait et al., 2007). The results of our study support the involvement of the frontal and zygomatic buttress in masticatory mechanics of the mid-face, whereas there was no evidence of the direct involvement of the hard palate in performing the same function. In previous FE analyses, the functional significance of the horizontal buttresses in humans received little scientific attention. Studies of bone strain in the supraorbital and infraorbital region in both human and non-

human primate skulls were consistent in suggestions that the two buttresses participate in the transfer of occlusal forces, but the level of stress and strain transmitted to these buttresses differed significantly from study to study (Endo, 1965; Endo, 1970; Hylander et al., 1991a,b). Based on the low in vivo strains and disproportionately greater bone mass in the supraorbital region of the non-human primates, Hylander et al. (1991a, 1991b) gave priority to the protective role of the frontal buttress against mechanical forces. This role has traditionally been attributed to all horizontal buttresses in the human mid-facial skeleton (Rowe and Williams, 1985; Pollock, 2012). Considering the fact that the effect of vertically directed masticatory loads was analyzed in majority of FE studies, this could be the possible reason why they failed to provide stronger evidence about the involvement of the circumorbital region and the hard palate in the mid-facial biomechanics.

In finite element studies, some necessary simplifications could potentially limit the interpretation of the results. The assumption of bone anisotropy would seem more reliable instead bone homogeneity and isotropy. However, this procedure may also influence the results negatively (Strait et al., 2005), particularly when the material has a complex geometry with many curved surfaces like the facial skeleton. In that case, assumption of bone isotropy and linear elasticity is considered accurate for both qualitative and quantitative analyses, but only if the elastic properties of the skeletal element being modeled are assigned, like in our study (Strait et al., 2005). The fact that occlusal loading was simplified to only vertical forces might be considered as a limitation because teeth are normally subjected to oblique and horizontal forces during mastication as well. However, the presence and/or predominance of the single components of occlusal forces depend on the phase of the chewing cycle. At the position of the maximum intercuspation that we simulated, vertically directed occlusal forces are the most dominant (Ingervall, 1972; Lundeen and Gibbs, 1982; Mohamed and Christensen, 1985).

6.2. The importance of trabecular bone modeling for finite element studies of mastication

Previous FEA analyses of occlusal load distribution through the mid-facial skeleton were performed on skull models composed only of cortical bone (Gross et al., 2001; Prado et al., 2012; Prado et al., 2013). By including trabecular bone in the model, we observed that its presence may influence the distribution and magnitude of von Mises stress and principal stress in the cortical bone. The results of comparative stress analysis with the FE model of Prado et al. (2013) suggested that both quantitative and qualitative analysis of the maximum principal stress may be significantly changed if trabecular bone is included in the model (Chart 2). Given that the differences in bone elastic properties and loading conditions between these two studies might partially contribute to the observed differences in the distribution and magnitude of stress, it would be beneficial to address the partial effect of trabecular bone modeling to the stress analysis in the future FE studies.

6.3. Microstructural properties reflect functional bone adaptation of the mid-facial skeleton to occlusal loading

Although the concept of buttresses in the mid-facial skeleton has been extensively studied as well as the principle of structural bone adaptation to functional loading (Wolff, 1870; Skedros and Baucom, 2007), there has been no study to link microstructure of the mid-facial bones to the distribution of occlusal loading. Only Peterson et al. (2006) pointed out an influence of occlusal loading to regional heterogeneity in the facial bone structure, but the authors limited their analysis only to the cortical thickness and density. Nevertheless, biomechanical adaptation of bone in the limited parts of the mid-facial skeleton received more scientific attention. In the alveolar process, reduced occlusal loading in growing animals frequently led to cortical bone thinning (Bresin et al., 1994), decreased mineralization in cortical and trabecular bone (Tanaka et al., 2007), and reduction in trabecular BV/TV and Tb.Th (Bresin et al., 1994; Mavropoulos et al., 2004; Mavropoulos et al., 2005; Odman et al., 2008). Similar deterioration in bone microstructure due to tooth loss was detected even at the sites

distant from the alveolar process, such as the zygomatic and frontal bones (Yoshino et al., 2007; Dechow et al., 2010; Williams and Slice, 2014).

6.3.1. Cortical bone increases thickness and density in response to higher occlusal stress

In our study of the complete mid-facial skeleton, cortical bone showed a tendency toward greater thickness (Ct.Th) and density (BV.Dn) in the areas experiencing high occlusal stress. This finding was in line with the study of Menegaz et al. (2009), who described thickening of cortical bone in the hard palate of growing rabbits as a reaction to occlusal overloading. Similar adaptive response of cortical bone to functional loading was frequently observed in the postcranial skeletal sites (Lambers et al., 2013). Unlike Peterson et al. (2006), who reported an inverse relationship between cortical thickness and density within the maxilla, we found a positive correlation between these two parameters. Such discrepancy may be due to different measurement techniques and/or larger number of cortical bone samples analyzed in our study.

However, the differences in Ct.Th and BV.Dn between the high stress and low stress groups were not significant. This might suggest that, besides occlusal stress, more factors are included in the determination of the cortical bone thickness and density in the mid-facial skeleton. Similar assumption was made by Thongudomporn et al. (2009), who found that the maximum bite force accounts for only 10-20% of the cortical thickness heterogeneity in the alveolar bone. There are also studies emphasizing the role of genetic factors in the development of the facial skeleton in terms of internal architecture (Harris and Johnson, 1991; Cassidy et al., 1998; Johannsdottir et al., 2005; Mulder et al., 2006a). The most illustrative among them is the study of Mulder et al. (2006a) that reported the presence of regional variations in cortical thickness in a pig mandible during fetal period in the absence of occlusal loading.

Cortical porosity is also important microarchitectural characteristic due to its ability to predict bone strength (McCalden et al., 1993; Wachter et al., 2002; Basillais et al., 2007). In our study, cortical bone that was less engaged in the occlusal load dissipation showed tendency toward greater porosity. The correlation analysis suggests that increased pore size could indicate increased cortical porosity in the mid-facial

bones, which is in line with the studies performed on the femoral cortex (Stein et al., 1999; Thomas et al., 2006; Milovanovic et al., 2014).

6.3.2. Trabecular bone shows significant increase in BV/TV and Tb.Th in response to higher occlusal stress

More obvious regional differences in microarchitecture between the sites experiencing high and low occlusal stress were observed in trabecular bone. The greatest stress-related differences between the groups were detected in bone volume fraction (BV/TV) and trabecular thickness (Tb.Th) (Table 17). Bearing in mind that BV/TV and Tb.Th are usually the first to change during the alteration of occlusal loading (Mavropoulos et al., 2004; Mavropoulos et al., 2005; Tanaka et al., 2007; Odman et al., 2008; Kingsmill et al., 2010; Yeh and Popowics, 2011), our results support high sensitivity of these two parameters to the influence of occlusal stress. Trabecular bone volume fraction could also reflect the inter-site differences in bone mechanical properties since BV/TV was recognized as a major single determinant of the Young's modulus and bone stiffness in some postcranial skeletal sites (Stauber et al., 2006). A weak correlation between BV/TV and Tb.Th found in our study and in the study of Arisaka et al. (2009) contrasts with the finding of Gonzalez-Garcia and Monje (2013a), who reported that trabecular thickening of the alveolar bone is mainly responsible for increased BV/TV in edentulous jaws. Changes of Tb.Th in response to occlusal forces were also detected in the alveolar bone of growing animals after tooth eruption (Yeh and Popowics, 2011). It was suggested that the mechanism by which fine trabecular network in pig mandibles adapts to the onset of occlusal loading is to reduce Tb.N and to increase Tb.Sp and thickness of the remaining trabeculae (Yeh and Popowics, 2011). However, our results that considered the whole mid-facial skeleton of a mature human individual suggest that trabecular bone is reinforced by more numerous and less separated trabeculae in the areas under high occlusal stress. Many authors also reported that higher BV/TV in the alveolar bone is usually accompanied by a significant increase in trabecular number (Tb.N) and bone mineral density (BMD) (Mavropoulos et al., 2004; Arisaka et al., 2009; Gonzalez-Garcia and Monje, 2013b; Kim and Henkin, 2013). This pattern of trabecular organization had been described as a common adaptive response to functional loading in postcranial skeletal sites (Barak et al., 2011).

Trabeculae in our study showed more concave surfaces (negative SMI) in the regions subjected to high occlusal stress when compared to more plate-like trabeculae in the low stress group. Similarly, Mulder et al. (2006b) and Yeh and Popowics (2011) found more concave trabeculae around the erupted tooth in growing animals after the achievement of occlusal contacts. In addition, Gonzalez-Garcia and Monje (2013a) also reported that areas of human jaws with higher bone volume fraction usually contain concave trabeculae.

Our results corroborate recent experimental studies that suggested occlusal loading as an important determinant of the facial bone microarchitecture (Bresin et al., 1999; Kato et al., 2004; Mavropoulos et al., 2004; Mavropoulos et al., 2005; Tanaka et al., 2007; Yoshino et al., 2007; Odman et al., 2008; Dechow et al., 2010; Kingsmill et al., 2010). We also demonstrated that differences in occlusal stress may be responsible for the regional variations in bone micro-structure in the adult male dentate skull, particularly in the trabecular bone. Given that stress measured during one phase of the chewing cycle was considered for correlation analysis, bone areas of interest may possibly experience greater or lower stresses during other chewing phases, e.g. during biting and/or chewing of the hard food that requires higher occlusal forces to be squashed (Stanisic-Sinobad, 2001). This could partially explain why we fail to detect stronger correlation between stress and microarchitecture, particularly in cortical bone. By performing FEA and micro-CT analysis of the same skull, the influence of sex and age-related differences in the facial bone structure and morphology were avoided as well as the influence of dentate status. Therefore, our findings might be not representative for other bone specimens. Further studies are needed to explore if the relationship between occlusal stress and facial bone microstructure differs in skulls of different sex, age and dental status. This would be of a special clinical importance, particularly to oral implantologists, because bone microstructure has a great influence on the primary stability of the dental implants and their clinical success rate (Nkenke et al., 2003; Miyamoto et al., 2005; Akca et al., 2006; Roze et al., 2009).

6.4. Fractures of the mid-facial skeleton

Like every material subjected to external loading, bone will break when the applied load exceeds its strength (Brandi, 2009). In general, the ability of bone to resist fracture is dependent on both injury-related factors and bone properties (Brandi, 2009). In the facial skeleton, the mechanism of injury and bone fracture tolerance were recognized up to date to determine the facial bone strength to fracture (Dempster, 1967).

6.4.1. The role of injury-related factors in the Le Fort fracture development

The facial skeleton is adapted to receive and distribute occlusal forces resulted from habitual masticatory activities that are predominantly vertical in direction, but it is significantly less tolerable to horizontally directed impacts (Le Fort, 1901; Rowe and Williams, 1985; Pollock, 2012). Bearing in mind that the bones generally have much higher compressive strength than tensile strength (Dempster and Liddicoat, 1952), the facial bones are more likely to be fractured under tensile forces. Our results confirmed that the mid-facial skeleton at the microstructural level is well adapted to compressive occlusal stress in contrast to negligible levels of tensile stress registered during biting and clenching.

After Le Fort's experiments, numerous biomechanical studies identified injury-related factors behind observed regularity in the pattern of the mid-facial fractures. Impact acting directly on a large surface of the midface will result in Le Fort fractures (Rowe and Williams, 1985; Hardt and Kuttenberger, 2010). Frontally and laterally directed impacts to the lower third of the midface cause Le Fort I fractures, while a blunt force acting on the middle and the upper part of the midface result in Le Fort II and Le Fort III fracture, respectively (Rowe and Williams, 1985; Hardt and Kuttenberger, 2010). Beside the importance of the impactor size (Hodgson, 1967; Rowe and Williams, 1985) and impact point (Rowe and Williams, 1985; Hardt and Kuttenberger, 2010), many authors also outlined the role of the magnitude of kinetic energy applied to the face (Hodgson, 1967; Nahum et al., 1968; Nahum, 1977; Rowe and Williams, 1985; Nyquist et al., 1986; Hardt and Kuttenberger, 2010) and impact duration (Hodgson, 1967) in the pattern of the mid-facial fracture development. The strong relationship between injury mechanism and the mid-facial fractures was supported by recent epidemiological studies. Along with an increase in the incidence of

high-velocity impacts in last few decades, e.g. during traffic accidents, there was a corresponding decrease in the number of patients sustaining typical Le Fort fractures (Steidler et al., 1980; Kahnberg and Göthberg, 1987; Haug et al., 1990; Lim et al., 1993; Rakocevic, 1993; Gopalakrishna et al., 1998; Hogg et al., 2000; Iida et al., 2001; Venugopal et al., 2010). Different authors reported that 3-57.5% of all facial fractures could be classified according to the Le Fort's scheme (Steidler et al., 1980; Kahnberg and Göthberg, 1987; Rakocevic, 1993; Alvi et al., 2003; Lee, 2009; Venugopal et al., 2010).

6.4.2. Bone fracture tolerance

For a long time, bone fracture tolerance was used as an indicator of the facial bone strength (Hampson, 1995). Although the authors were consistent in reporting the differences in fracture tolerances between the facial bones, there was a large variability in the fracture tolerance of a single bone between the studies. These variations were frequently interpreted to result from gender- and age-related differences in bone strength. Gadd et al. (1968) found that facial bones in females are significantly less tolerable to impact than in males. Yamada and Evans (1970) also stated that there is a decline in the facial bone strength during aging. These authors found 20-30% lower bone strength in cadavers over 70 years when compared to individuals aged between 20-30 years (Yamada and Evans, 1970).

6.4.3. Microstructural basis of bone fracture: insight from postcranial skeletal sites

Numerous studies that investigated bone microstructure in elderly individuals with hip and/or vertebral fractures revealed that age-related deterioration of both cortical and trabecular bone microarchitecture decreases bone strength and consequently increases bone fragility (Barth et al., 1992; McCalden et al., 1993; Bell et al., 1999; Stein et al., 1999; Djuric et al., 2010; Djonic et al., 2011; Milovanovic et al., 2012). Cortical thinning, increased porosity, and larger pore diameter of cortical bone had been commonly detected in individuals with hip fracture (Barth et al., 1992; Bell et al., 1999; Stein et al., 1999; Djonic et al., 2011; Milovanovic et al., 2012). Cortical porosity as well as other bone histomorphometric features has been reported to affect significantly bone's ability to withstand fracture, a property known as bone toughness (Barth et al.,

1992; Squillante and Williams, 1993; Yeni et al., 1997; Wang and Puram, 2004). Cortical bone containing numerous and smaller osteons with smaller Haversian canals had been suggested to be more effective in preventing fracture (Moyle et al., 1978; Barth et al., 1992; Squillante and Williams, 1993; Wang and Puram, 2004). Microstuctural properties of trabecular bone that were frequently reported in individuals with hip fracture include: decreased BV/TV, reduced Tb.N and Tb.Th, increased Tb.Sp, loss of trabecular connectivity, and predominance of rod-like trabeculae (SMI) (Goldstein et al., 1993; Hildebrand and Rüegsigger, 1997; Ciarelli et al., 2000; Legrand et al., 2000; Passi and Gefen, 2005; Djuric et al., 2010; Milovanovic et al., 2012).

However, comparative analysis with these studies could not be made because increased bone fragility that they investigated was based on age-related bone loss and corresponding deterioration in bone micro-architecture (Beck et al., 2000; Busse et al., 2010; Djuric et al., 2010; Djonic et al., 2011; Milovanovic et al., 2012; Milovanovic et al., 2014). By contrast, we are dealing with a site-specific bone fragility in the mid-facial skeleton of a young adult individual, whose bone micro-architecture is not affected by aging process.

6.4.4. Le Fort fractures: is there any association with bone microarchitecture?

Bone microstructural heterogeneity, similar to that detected in our study, has been frequently linked to the regional variability in bone quality and bone strength at the postcranial skeletal sites (Burr et al., 1997; Ciarelli et al., 2000; Legrand et al., 2000; Homminga et al., 2002; Robling et al., 2002; Warden et al., 2005; Ruff et al., 2006; Stauber and Müller, 2006; Hulme et al., 2007; Djuric et al., 2010; Wegrzyn et al., 2010; Milovanovic et al., 2012). In the femoral neck and vertebrae, such microstructural heterogeneity had been suggested to induce region-specific differences in bone fragility (Bell et al., 1999; Gong et al., 2005; Eckstein et al., 2007; Djuric et al., 2010; Milovanovic et al., 2012). In our study, however, there was no clear evidence of weaker micro-architecture of cortical and trabecular bone in biomechanical terms along Le Fort fracture lines.

Cortical bone showed slightly lower thickness and porosity with a larger pore diameter at the Le Fort fracture sites that were not statistically significant. Similarly, majority of the micro-architectural parameters of trabecular bone displayed only minor differences between the study groups (Table 24). Degree of anisotropy (DA) was the

only parameter that showed significantly greater values at the Le Fort fracture lines, which indicate that trabeculae are oriented along the direction of the principle loading. Such trabecular network could withstand forces applied along the trabecular axis, but it may be relatively weak against forces applied from other directions. Similar changes of DA have been reported to contribute to the region specific bone fragility in the postcranial skeletal sites (Ciarelli et al., 2000; Homminga et al., 2002; Djuric et al., 2010; Milovanovic et al., 2012). Milovanovic et al. (2012) proposed DA as an independent determinant of the increased fragility of the superolateral femoral neck that is less loaded during daily activities in contrast to the more loaded inferomedial neck that contains more anisotropic trabeculae (Kalmey and Lovejoy, 2002; Rudman et al., 2006; Djuric et al., 2010; Milovanovic et al., 2011). According to the analogy with the femoral neck, it seems that trabecular bone along Le Fort fracture lines is well adapted to habitual masticatory loads, whereas it is significantly less tolerable to the forces applied from other directions including horizontal impacts that are responsible for the mid-facial fracture development (Rowe and Williams, 1985; Hardt and Kuttenberger, 2010).

Although statistically non-significant, the highest absolute difference between Le Fort and Non-Le Fort group was noticed in the trabecular shape. Trabeculae away from the Le Fort fracture sites showed tendency toward more concave surfaces, that we also detected in trabecular bone subjected to high occlusal stress. Such shape might signify mechanical competence of trabecular bone, considering that its predominance over plate-like trabeculae coincides also with teeth eruption and the onset of occlusal loading (Mulder et al., 2006b; Yeh and Popowics, 2011; Gonzalez-Garcia and Monje, 2013b).

Although some properties of cortical and trabecular bone microarchitecture at the Le Fort fracture lines were similar to those found in postcranial skeletal sites, comparative analysis with these studies should be made with caution. Knowing that one of the major reasons behind increased bone fragility in the femoral neck and vertebrae is region-specific deterioration of bone micro-architecture (Beck et al., 2000; Busse et al., 2010; Djonic et al., 2011; Milovanovic et al., 2012; Milovanovic et al., 2014), results from these studies could not be simply extrapolated to our case. Regional variability in bone micro-architecture in our study is more likely to result from development and adaptation process to habitual masticatory activities. In addition to the limitations

resulting from cross sectional study design, our study is also limited by the fact that we analyzed bone micro-architecture in the single male skull without Le Fort fractures. Knowing that the fracture tolerance of the facial bones is age- and sex-dependent (Gadd et al., 1968; Yamada and Evans, 1970), it would be beneficial to explore the role of bone microarchitecture in increased fracture susceptibility in females and in the elderly.

7. CONCLUSIONS

The finite element analysis performed in this study demonstrated that both cortical and trabecular bone are involved in the occlusal load transfer through the mid-facial skeleton.

The pattern of stress distribution through the cortical bone in our model supports direct involvement of the nasomaxillary and zygomaticomaxillary buttresses in the occlusal load transfer during habitual masticatory activities. These two buttresses were subjected to the highest occlusal stress that was dominantly compressive in nature. Our results also support previous suggestions of the direct involvement of the nasal septum in the occlusal load transfer. Concerning horizontal buttresses, cortical bone was loaded along the frontal and zygomatic buttresses during clenching, whereas there was no clear evidence of the occlusal stress distribution through the cortical bone of the hard palate.

In the trabecular bone, distribution of occlusal stress was detected along the alveolar process of the maxilla, while minor stress was registered in the trabecular compartment of the zygomatic bone.

Our analysis revealed different involvement of cortical and trabecular bone in the occlusal load distribution through the anterior vs. posterior maxilla. We found that cortical bone in the anterior maxilla has a priority in the distribution of occlusal loads, whereas both cortical and trabecular bone in the posterior maxilla are equally involved in performing this task.

Comparative analysis of stress with the FE study of Prado et al. (2013) showed that qualitative and quantitative assessment of von Mises stress and principal stress in the cortical bone may be affected if the mid-facial skeleton is modeled without trabecular bone. Thus, we suggest that future FE models of mastication should include both cortical and trabecular bone.

Our study is the first to link microarchitecture of the mid-facial bones to occlusal stress in a mature dentate individual. We demonstrated that cortical and trabecular bone of the mid-facial skeleton exhibit regional variations in microarchitecture that could be a consequence of different occlusal stress.

In the areas subjected to high stress, cortical bone showed a tendency toward greater thickness and density, lower porosity, and greater pore separation. Changes in cortical thickness correlated positively with changes in bone density. The correlative

analysis also showed that the enlargement of pores and increased distance between the pores could be the mechanism by which cortical bone of the mid-facial skeleton increases its porosity.

Stress-related differences in microstructure were more pronounced in trabecular bone, which showed significantly greater bone volume fraction (BV/TV) and trabecular thickness (Tb.Th) in the areas under high occlusal stress. Trabecular network in these regions was consisted of more numerous and less separated trabeculae with concave surfaces, and greater mineral density. Correlation analysis between occlusal stress and microarchitectural parameters suggested that trabecular bone responds to higher occlusal stress by increasing BV/TV. This analysis also indicated that greater trabecular number is mainly responsible for greater trabecular bone volume in the regions subjected to high stress.

Micro-CT analysis showed no clear evidence of weaker bone microarchitecture in biomechanical terms in the mid-facial skeleton along Le Fort fracture lines.

Common fracture sites in the mid-facial skeleton were composed of slightly thinner and more porous cortical bone with larger pores, while trabeculae at the same sites had different shape and connectivity density that were not statistically significant. Significantly higher degree of anisotropy of trabecular bone detected along the Le Fort lines may partially explain the involvement of these sites in the facial bone fractures. Given that trabeculae oriented along the axis of principle loading could withstand forces resulting from habitual masticatory activities, it could be relatively weak against the forces applied from other directions, e.g. horizontal impacts that result in the Le Fort fractures.

8. REFERENCES

1. Akca K, Chang TL, Tekdemir I, Fanuscu MI. Biomechanical aspects of initial intraosseous stability and implant design: a quantitative micro-morphometric analysis. Clinical Oral Implants Research 2006; 17: 465–472.

2. Akca K, Fanuscu MI, Caputo AA. Effect of compromised cortical bone on implant load distribution. Journal of Prosthodontics 2008; 17: 616–620.

3. Al Dayeh AA, Rafferty KL, Egbert M, Herring SW. Deformation of nasal septal cartilage during mastication. Journal of Morphology 2009; 270(10): 1209–1218.

4. Al-Khafagy HH. Influence of cancellous bone rigidity on stress distribution in bone around dental implant: a finite element study. Journal of International Dental & Medical Research 2010; 3(1): 11–14.

5. Alexandridis C, Caputo AA, Thanos CE. Distribution of stresses in the human skull. Journal of Oral Rehabilitation 1985; 12(6): 499–507.

6. Alexandridis C, Thanos CE, Caputo AA. Distribution of stress patterns in the human zygomatic arch and bone. Journal of Oral Rehabilitation 1981; 8(6): 495–505.

7. Alikhasi M, Siadat H, Geramy A, Hassan-Ahangari A. Stress distribution around maxillary anterior implants as a factor of labial bone thickness and occlusal load angles: A 3-dimensional finite element analysis. Journal of Oral Implantology 2014; 40(1): 37–42.

8. Allsop DL, Warner CY, Wille MG, Schneider DC, Nahum AM. Facial impact response–a comparison of the Hybrid III dummy and human cadaver. In Proceedings of the 32nd Stapp Car Crash Conference, Atlanta, Georgia, 1988.

9. Alvi A, Doherty T, Lewen G. Facial fractures and concomitant injuries in trauma patients. The Laryngoscope 2003; 113(1): 102–106.

10. Arisaka R, Matsuo A, Chiba H, Takahashi H, Takeuchi S, Watanabe M, Hojo S. Preliminary Clinical Study to Evaluate the Relationship between Systemic Bone Turnover and the Microstructure of the Alveolar Bone. Oral Science International 2009; 6: 27–35.

11. Bakke M. Bite force and occlusion. Seminars in Orthodontics 2006; 12(2): 120–126.

12. Barak MM, Lieberman DE, Hublin JJ. A Wolff in sheep's clothing: Trabecular bone adaptation in response to changes in joint loading orientation. Bone 2011; 49: 1141–1151.

13. Barth R, Williams J, Kaplan F. Osteon morphometry in females with femoral neck fractures. Clinical Orthopaedics and Related Research 1992; (283): 178–186.

14. Basillais A, Bensamoun S, Chappard C, Brunet-Imbault B, Lemineur G, Ilharreborde B, Tho MCHB, Benhamou CL. Three-dimensional characterization of cortical bone microstructure by microcomputed tomography: validation with ultrasonic and microscopic measurements. Journal of Orthopaedic Science 2007; 12: 141–148.

15. Beck TJ, Looker AC, Ruff CB, Sievanen H, Wahner HW. Structural trends in the aging femoral neck and proximal shaft: analysis of the Third National Health and Nutrition Examination Survey dual-energy X-ray absorptiometry data. Journal of Bone and Mineral Research 2000; 15: 2297–2304.

16. Beck TJ, Ruff CB, Warden KE, Scott WW Jr, Rao GU. Predicting femoral neck strength from bone mineral data. A structural approach. Investigative Radiology 1990; 25: 6–18.

17. Bell KL, Loveridge N, Power J, Garrahan N, Stanton M, Lunt M, Meggitt BF, Reeve J. Structure of the femoral neck in hip fracture: Cortical bone loss in the inferoanterior to superoposterior axis. Journal of Bone and Mineral Research 1999; 14(1): 111–119.

18. Bernhard A, Milovanovic P, Zimmermann EA, Hahn M, Djonic D, Krause M, Breer S, Pueschel K, Djuric M, Amling M, Busse B. Micro-morphological properties of osteons reveal changes in cortical bone stability during aging, osteoporosis, and bisphosphonate treatment in women. Osteoporosis International 2013; 24(10): 2671–2680.

19. Bouxsein ML, Boyd SK, Christiansen BA, Guldberg RE, Jepsen KJ, Müller R. Guidelines for assessment of bone microstructure in rodents using micro-computed tomography. Journal of Bone and Mineral Research 2010; 25(7): 1468–1486.

20. Brandi ML. Microarchitecture, the key to bone quality. Rheumatology 2009; 48 (Suppl. 4): 3–8.

21. Bresin A, Johansson C, Kiliaridis S. Effects of occlusal strain on the development of the dentoalveolar process in the growing rat. A morphometric study. European Journal of Musculoskeletal Research 1994; 3: 112–122.

22.   Bresin A, Kiliaridis S, Strid KG. Effect of masticatory function on the internal bone structure in the mandible of the growing rat. European Journal of Oral Sciences 1999; 107: 35–44.

23.   Burr DB, Forwood MR, Fyhrie DP, Martin RB, Schaffler MB, Turner CH. Bone microdamage and skeletal fragility in osteoporotic and stress fractures. Journal of Bone and Mineral Research 1997; 12: 6–15.

24.   Busse B, Djonic D, Milovanovic P, Hahn M, Püschel K, Ritchie RO, Djuric M, Amling M. Decrease in the osteocyte lacunar density accompanied by hypermineralized lacunar occlusion reveals failure and delay of remodeling in aged human bone. Aging Cell 2010; 9: 1065–1075.

25.   Cassidy KM, Harris EF, Tolley EA, Keim RG. Genetic influence on dental arch form in orthodontic patients. The Angle Orthodontist 1998; 68: 445–454.

26.   Cattaneo PM, Dalstra M, Melsen B. The transfer of occlusal forces through the maxillary molars: A finite element study. American Journal of Orthodontics and Dentofacial Orthopedics 2003; 123(4): 367–373.

27.   Chen H, Zhou X, Shoumura S, Emura S, Bunai Y. Age- and gender-dependent changes in three-dimensional microstructure of cortical and trabecular bone at the human femoral neck. Osteoporosis International 2010; 21: 627–636.

28.   Ciarelli TE, Fyhrie DP, Schaffler MB, Goldstein SA. Variations in three-dimensional cancellous bone architecture of the proximal femur in female hip fractures and in controls. Journal of Bone and Mineral Research 2000; 15: 32–40.

29.   Cormier J, Manoogian S, Bisplinghoff J, Rowson S, Santago A, McNally C, Duma S, Bolte Iv J. The tolerance of the nasal bone to blunt impact. Annals of Advances in Automotive Medicine 2010; 54: 3–14.

30.   Cryer MH. The Internal Anatomy of the Face. Philadelphia: Lea &Febiger; 1916.

31.   Cui WQ, Won YY, Baek MH, Lee DH, Chung YS, Hur JH, Ma YZ. Age- and region-dependent changes in three-dimensional microstructural properties of proximal femoral trabeculae. Osteoporosis International 2008; 19: 1579–1587.

32.   Dechow PC, Wang Q, Peterson J. Edentulation alters material properties of cortical bone in the human craniofacial skeleton: functional implications for craniofacial structure in primate evolution. The Anatomical Record 2010; 293: 618–629.

33.   Dempster WT. Correlation of types of cortical grain structure with architectural features of the human skull. American Journal of Anatomy 1967; 120(1): 7–31.

34. Dempster WT, Liddicoat RT. Compact bone as a non-isotropic material. American Journal of Anatomy, 1952; 91: 331–362.

35. Dimitroulis G, Eyre J. A 7-year review of maxillofacial trauma in a central London hospital. British Dental Journal 1991; 170(8): 300–302.

36. Djonic D, Milovanovic P, Djuric M. Basis of Bone Strength vs. Bone Fragility: A Review of Determinants of Age-Related Hip Fracture Risk. Srpski arhiv za celokupno lekarstvo 2013; 141(7-8): 548–552.

37. Djonic D, Milovanovic P, Nikolic S, Ivovic M, Marinkovic J, Beck T, Djuric M. Inter-sex differences in structural properties of aging femora: implications on differential bone fragility: a cadaver study. Journal of Bone and Mineral Metabolism 2011; 29(4): 449–457.

38. Djuric M, Djonic D, Milovanovic P, Nikolic S, Marshall R, Marinkovic J, Hahn M. Region-Specific Sex-Dependent Pattern of Age-Related Changes of Proximal Femoral Cancellous Bone and Its Implications on Differential Bone Fragility. Calcified Tissue International 2010; 86: 192–201.

39. Duboeuf F, Hans D, Schott AM, Kotzki PO, Favier F, Marcelli C, Meunier PJ, Delmas PD. Different morphometric and densitometric parameters predict cervical and trochanteric hip fracture: The EPIDOS Study. Journal of Bone and Mineral Research 1997; 12(11): 1895–1902.

40. Eckstein F, Matsuura M, Kuhn V, Priemel M, Mueller R, Link TM, Lochmueller EM. Sex differences of human trabecular bone microstructure in aging are site-dependent. Journal of Bone and Mineral Research 2007; 22: 817–824.

41. Endo B. Distribution of stress and strain produced in the human facial skeleton by the masticatory force. Journal of the Anthropological Society of Nippon 1965; 73(4): 123–136.

42. Endo B. Experimental studies on the mechanical significance of the form of the human facial skeleton. Journal of the Faculty of Science, the University of Tokyo 1966; 3: 1–106.

43. Endo B. Analysis of stress around the orbit due to masseter and temporalis muscles respectively. Journal of the Anthropological Society of Nippon 1970; 78(4): 251–266.

44. Erkmen E, Atac MS, Yucel E, Kurt A. Comparison of biomechanical behavior of maxilla following Le Fort I osteotomy with 2- versus 4-plate fixation using 3D-FEA. International Journal of Oral Maxillofacial Surgery 2009; 38: 173–179.

45. Ferrario VF, Sforza C, Serrao G, Dellavia C, Tartaglia GM. Single tooth bite forces in healthy young adults. Journal of Oral Rehabilitation 2004; 31: 18–22.

46. Gadd CW, Nahum AM, Gatts J, Danford JP. A study of head and facial bone impact tolerances. In Proceedings, General Motors Corporation, Safety Research and Development Laboratory, 1968, p. 1–9.

47. Gassner R, Tuli T, Hächl O, Rudisch A, Ulmer H. Cranio-maxillofacial trauma: a 10 year review of 9543 cases with 21067 injuries. Journal of Craniomaxillofacial Surgery 2003; 31(1): 51–61.

48. Gnudi S, Malavolta N, Testi D, Viceconti M. Differences in proximal femur geometry distinguish vertebral from femoral neck fractures in osteoporotic women. British Journal of Radiology 2004; 77(915): 219–223.

49. Goldstein SA, Goulet R, McCubbrey D. Measurement and significance of three-dimensional architecture to the mechanical integrity of trabecular bone. Calcified Tissue International 1993; 53: S127–S33.

50. Gong H, Zhang M, Yeung HY, Qin L. Regional variations in microstructural properties of vertebral trabeculae with aging. Journal of Bone and Mineral Metabolism 2005; 23: 174–180.

51. Gonzalez-Garcia R, Monje F. Is micro-computed tomography reliable to determine the microstructure of the maxillary alveolar bone? Clinical Oral Implants Research 2013a; 24: 730–737.

52. Gonzalez-Garcia R, Monje F. The reliability of cone-beam computed tomography to assess bone density at dental implant recipient sites: a histomorphometric analysis by micro-CT. Clinical Oral Implants Research 2013b; 24: 871–879.

53. Gopalakrishna G, Peek-Asa C, Kraus JF. Epidemiologic features of facial injuries among motorcyclists. Annals of Emergency Medicine 1998; 32: 425–430.

54. Gross MD, Arbel G, Hershkovitz I. Three-dimensional finite element analysis of the facial skeleton on simulated occlusal loading. Journal of Oral Rehabilitation 2001; 28: 684–694.

55. Gröning F, Fagan M, O'Higgins P. Modeling the human mandible under masticatory loads: which input variables are important? The Anatomical Record 2012; 295: 853–863.

56. Haug RH, Prather J, Indressano T. An epidemiologic survey of facial fractures and concomitant injuries. Journal of Oral and Maxillofacial Surgery 1990; 48: 926–932.

57.   Hampson D. Facial injury: a review of biomechanical studies and test procedures for facial injury assessment. Journal of Biomechanics 1995; 28(1): 1–7.

58.   Hardt N, Kuttenberger J. Mechanism of craniofacial fractures. In: Hardt N, Kuttenberger J, editors. Craniofacial trauma: diagnosis and management. Berlin: Springer; 2010, p. 55–61.

59.   Harris EF, Johnson MG. Heritability of craniometric and occlusal variables: a longitudinal sib analysis. American Journal of Orthodontics and Dentofacial Orthopedics 1991; 99: 258–268.

60.   He T, Kiliaridis S. Effects of masticatory muscle function on craniofacial morphology on growing ferrets (Mustela putorius furo). European Journal of Oral Sciences 2003; 11: 510–517.

61.   Hildebrand T, Rüegsigger P. Quantification of Bone Microarchitecture with the Structure Model Index. Computer Methods in Biomechanics and Biomedical Engineering 1997; 1: 15–23.

62.   Hilloowala R, Kanth H. The transmission of masticatory forces and nasal septum: structural comparison of the human skull and Gothic cathedral. Journal of Craniomandibular Practice 2007; 25(3): 166–171.

63.   Hodgson VR. Tolerance of the facial bones to impact. American Journal of Anatomy 1967; 120(1): 113–122.

64.   Hogg NJ, Stewart TC, Armstrong JE, Girotti MJ. Epidemiology of maxillofacial injuries at trauma hospitals in Ontario, Canada between 1992 and 1997. Journal of Trauma 2000; 49: 425–432.

65.   Homminga J, McCreadie BR, Ciarelli TE, Weinans H, Goldstein SA, Huiskes R. Cancellous bone mechanical properties from normals and patients with hip fractures differ on the structure level, not on the bone hard tissue level. Bone 2002; 30: 759–764.

66.   Hsu ML, Chang CL. Application of finite element analysis in dentistry. In: Moratal D, editor. Finite Element Analysis. Rijeka: Sciyo; 2010, p. 43–60.

67.   Hulme PA, Boyd SK, Ferguson SJ. Regional variation in vertebral bone morphology and its contribution to vertebral fracture strength. Bone 2007; 41: 946–957.

68.   Hylander WL, Picq PG, Johnson KR. Masticatory-stress hypotheses and the supraorbital region of primates. American Journal of Physical Anthropology 1991a; 86: 1–36.

69.   Hylander WL, Picq PG, Johnson KR. Function of the supraorbital region of primates. Archives of Oral Biology 1991b; 36: 273–281.

70. Iida S, Kogo M, Sugiura T, Mima T, Matsuya T. Retrospective analysis of 1502 patients with facial fractures. International Journal of Oral and Maxillofacial Surgery 2001; 30: 286–290.

71. Ingervall B. Range of the sagittal movement of the mandibular condyles and inclination of the condyle path in children and adults. Acta Odontologica Scandinavica 1972; 30: 67–75.

72. Johannsdottir B, Thorarinsson F, Thordarson A, Magnusson TE. Heritability of craniofacial characteristics between parents and offspring estimated from lateral cephalograms. American Journal of Orthodontics and Dentofacial Orthopedics 2005; 127: 200–207.

73. Kahnberg KE, Göthberg KA. Le Fort fractures (I). A study of frequency, etiology and treatment. International Journal of Oral and Maxillofacial Surgery 1987; 16(2): 154–159.

74. Kalmey JK, Lovejoy CO. Collagen fiber orientation in the femoral necks of apes and humans: do their histological structures reflect differences in locomotor loading? Bone 2002; 31: 327–332.

75. Kaptoge S, Beck TJ, Reeve J, Stone KL, Hillier TA, Cauley JA, Cummings SR. Prediction of incident hip fracture risk by femur geometry variables measured by hip structural analysis in the study of osteoporotic fractures. Journal of Bone and Mineral Research 2008; 23(12): 1892–1904.

76. Kato Y, Kizu Y, Tonogi M, Ide Y, Yamane G. Observation of the internal structure of the zygomatic bone by micro-computed tomography. Journal of Oral Biosciences 2004; 46: 523–529.

77. Kim DW, Egan KK, O'Grady K, Toriumi DM. Biomechanical strength of human nasal septal lining: comparison of the constituent layers. The Laryngoscope 2005; 115(8): 1451–1453.

78. Kim YJ, Henkin J. Micro-computed tomography assessment of human alveolar bone: bone density and three-dimensional micro-architecture. Clinical Implant Dentistry and Related Research 2013; 9: *Article in press*, DOI: 10.1111/cid.12109.

79. Kingsmill VJ, Boyde A, Davis GR, Howell PGT, Rawlinson SCF. Changes in bone mineral and matrix in response to a soft diet. Journal of Dental Research 2010; 89: 510–514.

80. Kojic M, Mijailovic S, Zdravkovic N. Modelling of muscle behaviour by the finite element method using Hill's three-element model. International Journal for Numerical Methods in Engineering 1998; 43(5): 941–953.

81. Korioth TWP, Hannam AG. Deformation of the human mandible during simulated tooth clenching. Journal of Dental Research 1994; 73(1): 56–66.

82. Kumagai H, Suzuki T, Hamada T, Sondang P, Fujitani M, Nikawa H. Occlusal force distribution on the dental arch during various levels of clenching. Journal of Oral Rehabilitation 1999; 26: 932–935.

83. Lambers FM, Koch K, Kuhn G, Ruffoni D, Weigt C, Schulte FA, Müller R. Trabecular bone adapts to long-term cyclic loading by increasing stiffness and normalization of dynamic morphometric rates. Bone 2013; 55(2): 325–334.

84. Le Fort R. Etude experimental sur les fractures de la machoire superieure. Revue chirurgie de Paris 1901; 23: 208-227, 360–379.

85. Lee KH. Interpersonal violence and facial fractures. Journal of Oral and Maxillofacial Surgery 2009; 67(9): 1878–1883.

86. Lee SJ, Liong K, Lee HP. Deformation of Nasal Septum during Nasal Trauma. The Laryngoscope 2010; 120(10): 1931–1939.

87. Legrand E, Chappard D, Pascaretti C, Duquenne M, Krebs S, Rohmer V, Basle MF, Audran M. Trabecular bone microarchitecture, bone mineral density, and vertebral fractures in male osteoporosis. Journal of Bone and Mineral Research 2000; 15: 13–19.

88. Lim LH, Lam LK, Moore MH, Trott JA, David DJ. Associated injuries in facial fractures: review of 839 patients. British Journal of Plastic Surgery 1993; 46: 635–638.

89. Lundeen H, Gibbs CH. Jaw Movements and Forces during chewing and swallowing and their clinical significance. In: Lundeen HC, Gibbs CH, editors. Advances in occlusion. Littleton: John Wright, PSC Inc; 1982.

90. Lundeen GA, Vajda EG, Bloebaum RD. Age-related cancellous bone loss in the proximal femur of caucasian females. Osteoporosis International 2000; 11: 505–511.

91. Mavropoulos A, Ammann P, Bresin A, Kiliaridis S. Masticatory demands induce region-specific changes in mandibular bone density in growing rats. Angle Orthodontics 2005; 75: 625–630.

92. Mavropoulos A, Kiliaridis S, Bresin A, Ammann P. Effect of different masticatory functional and mechanical demands on the structural adaptation of the mandibular alveolar bone in young growing rats. Bone 2004; 35: 191–197.

93. McCalden RW, McGeough JA, Barker MB, Court-Brown CM. Age-related changes in the tensile properties of cortical bone: the relative importance of changes in porosity, mineralization, and microstructure. Journal of Bone and Joint Surgery. American Volume 1993; 75: 1193–1205.

94. Menegaz RA, Sublett SV, Figueroa SD, Hoffman TJ, Ravosa MJ. Phenotypic plasticity and function of the hard palate in growing rabbits. The Anatomical Record 2009; 292: 277–284.

95. Michelotti J, Clark J. Femoral Neck Length and Hip Fracture Risk. Journal of Bone and Mineral Research 1999; 14: 1714–1720.

96. Miloro M, Ghali GE, Larsen PE, Waite P. Peterson's principles of oral and maxillofacial surgery, Hamilton: BC Decker Inc; 2004.

97. Milovanovic P, Djonic D, Marshall RP, Hahn M, Nikolic S, Zivkovic V, Amling M, Djuric M. Micro-structural basis for particular vulnerability of the superolateral neck trabecular bone in the postmenopausal women with hip fractures. Bone 2012; 50: 63–68.

98. Milovanovic P, Potocnik J, Stoiljkovic M, Djonic D, Nikolic S, Neskovic O, Djuric M, Rakocevic Z. Nanostructure and mineral composition of trabecular bone in the lateral femoral neck: Implications for bone fragility in elderly women. Acta Biomaterialia 2011; 7(9): 3446–3451.

99. Milovanovic P, Rakocevic Z, Djonic D, Zivkovic V, Hahn M, Nikolic S, Amling M, Busse B, Djuric M. Nano-structural, compositional and micro-architectural signs of cortical bone fragility at the superolateral femoral neck in elderly hip fracture patients vs. healthy aged controls. Experimental Gerontology 2014; 55: 19–28.

100. Miyamoto I, Tsuboi Y, Wada E, Suwa H, Iizuka T. Influence of cortical bone thickness and implant length on implant stability at the time of surgery–clinical, prospective, biomechanical, and imaging study. Bone 2005; 37: 776–780.

101. Mohamed SE, Christensen LV. Mandibular reference positions. Journal of Oral Rehabilitation 1985; 12: 355–367.

102. Moyle DD, Welborn IIIJW, Cooke FW. Work to fracture of canine femoral bone. Journal of Biomechanics 1978; 11(10-12): 435–440.

103. Mulder L, Koolstra JH, de Jonge HW, van Eijden TMGJ. Architecture and mineralization of developing cortical and trabecular bone of the mandible. Anatomy and Embryology 2006a; 211: 71–78.

104. Mulder L, van Groningen LB, Potgieser YA, Koolstra JH, van Eijden TMGJ. Regional differences in architecture and mineralization of developing mandibular bone. The Anatomical Record 2006b; 288A: 954–961.

105. Nahum AM, Gatts JD, Gadd CW, Danforth J. Impact tolerance of the skull and face. In Proceedings of the 12th Stapp Car Crash Conference, Detroit, USA, 1968.

106. Nahum AM. The prediction of maxillofacial trauma. Transactions. Section on Otolaryngology. Americal Academy of Ophthalmology and Otolaryngology 1977; 84(5): 932–933.

107. Nahum IS. The biomechanics of maxillofacial trauma. Clinics in Plastic Surgery 1975; 2(1): 59–64.

108. Nakamura T, Turner CH, Yoshikawa T, Slemenda CW, Peacock M, Burr DB, Mizuno Y, Orimo H, Ouchi Y, Johnston CC. Do variations in hip geometry explain differences in hip fracture risk between Japanese and white Americans? Journal of Bone and Mineral Research 1994; 9: 1071–1076.

109. Nkenke E, Hahn M, Weinzierl K, Radespiel-Tröger M, Neukam FW, Engelke K. Implant stability and histomorphometry: a correlation study in human cadavers using stepped cylinder implants. Clinical Oral Implants Research 2003; 14: 601–609.

110. Nomoto S, Matsunaga S, Ide Y, Abe S, Takahashi T, Saito F, Sato T. Stress distribution in maxillary alveolar ridge according to finite element analysis using micro-CT. The Bulletin of Tokyo Dental College 2006; 47(4): 149–156.

111. Nyquist GW, Cavanaugh JM, Goldberg SJ, King AI. Impact Tolerance and Response of the Face. In Proceedings of the Advances in Bioengineering Conference, 1986, p. 75–81.

112. Odman A, Mavropoulos A, Kiliaridis S. Do masticatory functional change influence the mandibular morphology in adult rats. Archives of Oral Biology 2008; 53: 1149–1154.

113. Ohashi T, Matsunaga S, Nakahara K, Abe S, Ide Y, Tamatsu Y, Takano N. Biomechanical role of peri-implant trabecular structures during vertical loading. Clinical Oral Investigations 2010; 14: 507–513.

114. Park HS, Lee ZJ, Jeong SH, Kwon TG. Density of the alveolar bone and basal bones of the maxilla and the mandible. American Journal of Orthodontics and Dentofacial Orthopedics 2008; 133: 30–37.

115. Partanen J, Jamsa T, Jalovaara P. Influence of the upper femur and pelvic geometry on the risk and type of hip fractures. Journal of Bone and Mineral Research 2001; 16(8): 1540–1546.

116. Passi N, Gefen A. Trabecular bone contributes to strength of the proximal femur under mediolateral impact in the avian. Journal of Biomechanical Engineering 2005; 127(1): 198–203.

117. Peterson J, Dechow PC. Material properties of the human cranial vault and zygoma. The Anatomical Record A 2003; 274: 785–797.

118. Peterson J, Wang Q, Dechow PC. Material properties of the dentate maxilla. The Anatomical Record Part A: Discoveries in Molecular, Cellular, and Evolutionary Biology 2006; 288(9): 962–972.

119. Pollock RA. Craniomaxillofacial buttresses: anatomy and operative repair. New York: Thieme Medical Publishers; 2012.

120. Prado FB, Freire AR, Rossi AC, Caria PHF. Finite element analysis of the three support pillars in human craniofacial skeleton. Journal of Biomechanics 2012; 45(1): 179.

121. Prado FB, Noritomi PY, Freire AR, Rossi AC, Neto FH, Caria PHF. Stress distribution in human zygomatic pillar using three-dimensional finite element analysis. International Journal of Morphology 2013; 31(4): 1386–1392.

122. Pulkkinen P, Eckstein F, Lochmüller EM, Kuhn V, Jämsä T. Association of geometric factors and failure load level with the distribution of cervical vs. trochanteric hip fractures. Journal of Bone and Mineral Research 2006; 21(6): 895–901.

123. Qian L, Todo M, Matsushita Y, Koyano K. Effects of implant diameter, insertion depth, and loading angle on stress/strain fields in implant/jawbone systems: finite element analysis. International Journal of Oral Maxillofacial Implants 2009; 24(5): 877–886.

124. Rakocevic Z. Komparativna analiza vrednosti rendgenografskih metoda u dijagnostici povreda maksilofacijalne regije, Doktorska disertacija, Univerzitet u Beogradu; 1993.

125. Robling AG, Hinant FM, Burr DB, Turner CH. Improved bone structure and strength after long-term mechanical loading is greatest if loading is separated into short bouts. Journal of Bone and Mineral Research 2002; 17: 1545–1554.

126. Roze J, Babu S, Saffarzadeh A, Gayet-Delacroix M, Hoornaert A, Layrolle P. Correlating implant stability to bone structure. Clinical Oral Implants Research 2009; 20: 1140–1145.

127. Rowe NL, Williams JL. Maxillofacial injuries (vol I). Edinburgh: Churchill Livingstone; 1985.

128. Rudman K, Aspden R, Meakin J. Compression or tension? The stress distribution in the proximal femur. Biomedical Engineering OnLine 2006; 5: 12.

129. Ruff C, Holt B, Trinkaus E. Who's afraid of the big bad Wolff?:"Wolff's law" and bone functional adaptation. American Journal of Physical Anthropology 2006; 129: 484–498.

130. Schneider DC, Nahum AM. Impact Studies of Facial Bones and Skull. Proceedings of the 16th Stapp Car Crash Conference, Detroit, USA, 1972.

131. Sicher H, Tandler J. Anatomie Fur Zahnartzte. Berlin: Springer; 1928.

132. Skedros JG, Baucom SL. Mathematical analysis of trabecular 'trajectories' in apparent trajectorial structures: The unfortunate historical emphasis on the human proximal femur. Journal of Theoretical Biology 2007; 244: 15–45.

133. Shiau YY, Wang JS. The effects of dental condition on hand strength and maximum bite force. Cranio: The Journal of Craniomandibular Practice 1993; 11: 48–54.

134. Squillante RG, Williams JL. Videodensitometry of osteons in females with femoral neck fractures. Calcified Tissue International 1993; 52(4): 273–277.

135. Standring S. Gray's anatomy: The anatomical basis of clinical practice, fortieths edition. New York: Churchill Livingstone; 2005.

136. Stanisic-Sinobad D. Osnovi gnatologije. Beograd: Univerzitet u Beogradu, Stomatoloski fakultet; 2001.

137. Stauber M, Müller R. Age-related changes in trabecular bone micro-structures: global and local morphometry. Osteoporosis International 2006; 17: 616–626.

138. Stauber M, Rapillard L, van Lenthe GH, Zysset P, Müller R. Importance of individual rods and plates in the assessment of bone quality and their contribution to bone stiffness. Journal of Bone and Mineral Research 2006; 21: 586–595.

139. Steidler NE, Cook RM, Reade PC. Incidence and management of major middle third facial fractures at the Royal Melbourne Hospital. A retrospective study. International Journal of Oral Surgery 1980; 9(2): 92–98.

140. Stein MS, Feik SA, Thomas CDL, Clement JG, Wark JD. An automated analysis of intracortical porosity in human femoral bone across age. Journal of Bone and Mineral Research 1999; 14: 624–632.

141. Stojanovic B. Generalization of Hill's phenomenological model in order to investigate muscle fatigue, Ph.D. Thesis, CIMSI, University of Kragujevac, Serbia; 2007.

142. Stojanovic B, Kojic M, Rosic M, Tsui CP, Tang CY. An extension of Hill's three-component model to include different fiber types in finite element modeling of muscle. International Journal for Numerical Methods in Engineering 2007; 71(7): 801–817.

143. Strait DS, Richmond BG, Spencer MA, Ross CF, Dechow PC, Wood BA. Masticatory biomechanics and its relevance to early hominid phylogeny: an examination of palatal thickness using finite-element analysis. Journal of Human Evolution 2007; 52(5): 585–599.

144. Strait DS, Wang Q, Dechow PC, Ross CF, Richmond BG, Spencer MA, Patel BA. Modeling elastic properties in finite-element analysis: how much precision is needed to produce an accurate model? The Anatomical Record A 2005; 283: 275–287.

145. Swearingen JJ. Tolerances of the human face to crash impact. Federal Aviation Agency, Civil Aeromedical Research Institute, Oklahoma City, USA; 1965, p. 1–24.

146. Tanaka E, Sano R, Kawai N, Langenbach GE, Brugman P, Tanne K, van Eijden TM. Effect of food consistency on the degree of mineralization in the rat mandible. Annals of Biomedical Engineering 2007; 35: 1617–1621.

147. Tanne K, Miyasaka J, Yamagata Y, Sachdeva R, Tsutsumi S, Sakuda M. Three-dimensional model of the human craniofacial skeleton: method and preliminary results using finite element analysis. Journal of Biomedical Engineering 1988; 10(3): 246–252.

148. Testut JL. Traite d'Anatomie Humanie, 2nd ed. Paris: Doin; 1911.

149. Thomas CDL, Feik SA, Clement JG. Increase in pore area, and not pore density is the main determinant in the development of porosity in human cortical bone. Journal of Anatomy 2006; 209: 219–230.

150. Thongudomporn U, Chongsuvivatwong V, Geater AF. The effect of maximum bite force on alveolar bone morphology. Orthodontics and Craniofacial Research 2009; 12: 1–8.

151. Tortopidis D, Lyons MF, Baxendale RH, Gilmour WH. The variability of bite force measurement between sessions, in different positions within the dental arch. Journal of Oral Rehabilitation 1998; 25(9): 681–686.

152. Van Eijden TM, Korfage JA, Brugman P. Architecture of the human jaw-closing and jaw-opening muscles. The Anatomical Record 1997; 248(3): 464–474.

153. Wachter NJ, Krischak GD, Mentzel M, Sarkar MR, Ebinger T, Kinzl L, Claes L, Augat P. Correlation of bone mineral density with strength and microstructural parameters of cortical bone in vitro. Bone 2002; 31(1): 90–95.

154. Venugopal MMG, Sinha CR, Menon CPS, Chattopadhyay CPK, Chowdhury CSKR. Fractures in the maxillofacial region: A four year retrospective study. Medical Journal Armed Forces India 2010; 66(1): 14–17.

155. Wang X, Puram S. The Toughness of Cortical Bone and Its Relationship with Age. Annals of Biomedical Engineering 2004, 32(1): 123–135.

156. Warden SJ, Hurst JA, Sanders MS, Turner CH, Burr DB, Li J. Bone adaptation to a mechanical loading program significantly increases skeletal fatigue resistance. Journal of Bone and Mineral Research 2005; 20: 809–816.

157. Wegrzyn J, Roux JP, Arlot ME, Boutroy S, Vilayphiou N, Guyen O, Delmas PD, Chapurlat R, Bouxsein ML. Role of trabecular microarchitecture and its heterogeneity parameters in the mechanical behavior of ex vivo human L3 vertebrae. Journal of Bone and Mineral Research 2010; 25(11): 2324–2331.

158. Williams SE, Slice DE. Influence of edentulism on human orbit and zygomatic arch shape. Clinical Anatomy 2014; 27(3): 408–416.

159. Wolff J. Uber die innere architektur der knochen und ihre bedeutung fuer die frage vom knochenwachstum. Archiv s. pathologische Anatomie und Physiologie und für klinische Medizin 1870; 50: 389–453.

160. Wood SA, Strait DS, Dumont ER, Ross CF, Grosse IR. The effects of modeling simplifications on craniofacial finite element models: The alveoli (tooth sockets) and periodontal ligaments. Journal of Biomechanics 2011; 44(7): 1831–1838.

161. Yamada H. Strength of the biological materials. Baltimore: Williams & Wilkins; 1970.

162. Yamada H, Evans FG. Ratios for age changes in the mechanical properties of human organs and tissues. In Evans FG, editor. *Strength of Biological Materials*, Baltimore: Williams and Wilkins; 1970, p. 255–280.

163. Yeh KD, Popowics TE. The impact of occlusal function on structural adaptation in alveolar bone of the growing pig, Sus Scrofa. Archives of Oral Biology 2011; 56: 79–89.

164. Yeni YN, Brown CU, Wang Z, Norman TL. The influence of bone morphology on fracture toughness of the human femur and tibia. Bone 1997; 5: 453–459.

165. Yoganandan N, Fintar F, Sances A. Biodynamics of steering wheel induced facial trauma. Journal of Safety Research 1991; 22(4): 179–190.

166. Yoshino M, Kato Y, Kizu Y, Tonogi M, Abe S, Ide Y, Yamane GY. Study on internal structure of zygomatic bone using micro-finite element analysis model - differences between dentulous and edentulous dentition in Japanese cadavers. The Bulletin of Tokyo Dental College 2007; 48: 129–134.

167. Zandi M, Saleh M, Seyed Hoseini SR. Are facial injuries caused by stumbling different from other kinds of fall accidents? The Journal of Craniofacial Surgery 2011; 22(6): 2388–2292.

Curriculum Vitae

Dr. Aleksa Janović was born on October 29th 1983 in Priboj. He finished elementary school "Vuk Karadžić" in 1998, and Gymnasium in Priboj in 2002. He was enrolled in University of Belgrade - School of Medicine in 2002, graduated in 2008 with GPA 9.17/10. He was enrolled in Doctoral Studies (course: Skeletal biology) at University of Belgrade - School of Medicine in 2009/2010. Since 2004, he has been participating in research projects within the Laboratory for Anthropology, Institute of Anatomy, University of Belgrade - School of Medicine, under guidance of Prof. Dr. Marija Djurić. Since 2011, he has been working as a research fellow on the project III45005 funded by Ministry of Education and Science of the Republic of Serbia. He is an author or co-author of 7 papers published in peer reviewed international journals indexed in Journal Citation Report list. In May 2012, he was appointed to the position of an assistant professor at the Department of Radiology, University of Belgrade - School of Dentistry. He was enrolled in residency in diagnostic radiology at the University of Belgrade - School of Medicine in 2013.

Биографија кандидата

Др Алекса Јановић је рођен 29. октобра 1983. године у Прибоју. Основну школу „Вук Караџић“ завршио је 1998. године, а 2002. године и Гимназију (природно-математички смер) у Прибоју. На Медицински факултет у Београду уписао се 2002. године. Димпломирао је 2008. године са просечном оценом 9,17 (девет, седамнаест). Докторске студије – смер Биологија скелета (на енглеском језику) уписао је 2009. године на Медицинском факултету у Београду. Од 2004. године је члан истраживачког тима Лабораторије за антропологију Института за анатомију Медицинског факултета у Београду, којом руководи проф. др Марија Ђурић. Од 2011. године ради као сарадник на пројекту III45005 који финансира Министарство просвете и науке Републике Србије. Аутор је или коаутор 7 радова штампаних у целини у часописима индексираним у JCR листи. У мају 2012. године, изабран је у звање асистента на предмету Основи клиничке радиологије на Стоматолошком факултету Универзитета у Београду. Специјализацију из Радиологије на Медицинском факултету у Београду започео је 2013. године.

Прилог 1.

Изјава о ауторству

Потписани: Алекса М. Јановић

Изјављујем

да је докторска дисертација под насловом

„Микроструктурна адаптација коштаног ткива фацијалног скелета на дистрибуцију оклузалног оптерећења код особа са пуним зубним низом и њена улога у настанку прелома фацијалног скелета"

- резултат сопственог истраживачког рада,
- да предложена дисертација у целини ни у деловима није била предложена за добијање било које дипломе према студијским програмима других високошколских установа,
- да су резултати коректно наведени и
- да нисам кршио ауторска права и користио интелектуалну својину других лица.

Потпис докторанда

У Београду, 16.12.2014. године

Прилог 2.

Изјава о истоветности штампане и електронске верзије докторског рада

Име и презиме аутора: Алекса М. Јановић

Студијски програм: биологија скелета

Наслов рада: Микроструктурна адаптација коштаног ткива фацијалног скелета на дистрибуцију оклузалног оптерећења код особа са пуним зубним низом и њена улога у настанку прелома фацијалног скелета.

Ментор: проф. др Марија Ђурић

изјављујем да је штампана верзија мог докторског рада истоветна електронској верзији коју сам предао за објављивање на порталу **Дигиталног репозиторијума Универзитета у Београду.**

Дозвољавам да се објаве моји лични подаци везани за добијање академског звања доктора наука, као што су име и презиме, година и место рођења и датум одбране рада.

Ови лични подаци могу се објавити на мрежним страницама дигиталне библиотеке, у електронском каталогу и у публикацијама Универзитета у Београду.

Потпис докторанда

У Београду, 16.12.2014. године

др Алекса М. Јановић

Прилог 3.

Изјава о коришћењу

Овлашћујем Универзитетску библиотеку „Светозар Марковић" да у Дигитални репозиторијум Универзитета у Београду унесе моју докторску дисертацију под насловом:

„Микроструктурна адаптација коштаног ткива фацијалног скелета на дистрибуцију оклузалног оптерећења код особа са пуним зубним низом и њена улога у настанку прелома фацијалног скелета"

која је моје ауторско дело.

Дисертацију са свим прилозима предао/ла сам у електронском формату погодном за трајно архивирање.

Моју докторску дисертацију похрањену у Дигитални репозиторијум Универзитета у Београду могу да користе сви који поштују одредбе садржане у одабраном типу лиценце Креативне заједнице (Creative Commons) за коју сам се одлучио.

1. Ауторство
2. Ауторство - некомерцијално
3. Ауторство – некомерцијално – без прераде
4. Ауторство – некомерцијално – делити под истим условима
5. Ауторство – без прераде
6. Ауторство – делити под истим условима

(Молимо да заокружите само једну од шест понуђених лиценци, кратак опис лиценци дат је на полеђини листа).

Потпис докторанда

У Београду, 16.12.2014. године